PHOTOAFFINITY LABELLING OF ALPHA-SYNUCLEIN USING DIAZIRINE-FUNCTIONALIZED CAFFEINE, NICOTINE, AND 1-AMINOINDAN

A thesis submitted to the
College of Graduate and Postdoctoral Studies
In Partial Fufillment of the Requirements
For the degree of Master of Science
In the College of Pharmacy and Nutrition
University of Saskatchewan
Saskatoon

By

BRIGITTE MOSER

PERMISSION TO USE

By submitting this thesis in partial fulfillment of the requirements for a Postgraduate degree from the University of Saskatchewan, I agree that the University of Saskatchewan libraries may make this thesis available for inspection. I agree that permission for copying this thesis in any manner, in whole or in part, for scholarly purposes may be granted by the professors who supervised this work, or in their absence, by the head of the department or dean of the college in which this work was completed. It is understood that any copying or publication or use of this thesis or parts of the thesis for financial gain is not allowed without my written consent. It is understood that recognition shall be given to me and the University of Saskatchewan in any scholarly use which may be made of any material in this thesis.

Requests for permission to copy or use this document in part or in full should be addressed to:

Head of the College of Pharmacy and Nutrition
105 Wiggins Road
University of Saskatchewan
Saskatoon, Saskatchewan S7N 5E5 Canada

OR

Dean
College of Graduate and Postdoctoral Studies
University of Saskatchewan
116 Thorvaldson Building, 110 Science Place
Saskatoon, Saskatchewan S7N 5C9 Canada

ABSTRACT

Alpha-synuclein aggregation is a hallmark pathological feature of Parkinson's disease, and as such, it is thought to be a contributing factor to the disease. In the past, our group identified several compounds (1-aminoindan, nicotine, caffeine) capable of interacting with alpha-synuclein. These compounds were combined into bifunctional agents, such that caffeine was linked to one of 1-aminoindan, nicotine, or caffeine by a six-carbon chain. The nicotine and 1-aminoindan bifunctional agents were able to interact with alpha-synuclein *in vitro* and rescue cell growth in a yeast cell model overexpressing alpha-synuclein. However, the specifics of this protein-ligand interaction are unknown as alpha-synuclein is intrinsically disordered. To gain insight into possible binding regions on alpha-synuclein, we propose to use diazirine photoaffinity labelling to identify these sites. Our approach toward creating the diazirine probes was to link a four-carbon chain containing a diazirine to the amines of theophylline, nornicotine, and 1-aminoindan. We began by converting the ketone moiety of 4-hydroxy-2-butanone to a diazirine ring in three steps. The linker was then either tosylated or iodinated at the alcohol position. At this stage, the tosylated linker can be used to alkylate the N7-position of theophylline, and the iodinated linker can be used to alkylate the primary amine of 1-aminoindan, the secondary amine of nornicotine, or the bifunctional compounds to complete the synthesis of the diazirine probes. Isothermal titration calorimetry was used to determine all compounds binding affinity for alpha-synuclein; however, the methodology was unable to produce reliable binding data. Characterization of the diazirine probe's activity toward alpha-synuclein aggregation was carried out using a Thioflavin T assay. The results from these studies were compared to the unlabelled compounds to determine the probe's ability to inhibit alpha-synuclein aggregation relative to the original compounds. No direct anti-aggregation activity was observed for any diazirine-functionalized probes or unfunctionalized compounds. To investigate the binding interactions between alpha-synuclein and the photoaffinity probe, the probe was incubated with alpha-synuclein and irradiated with UVA for 30 minutes prior to trypsin digestion and analysis by electrospray mass spectrometry or tandem mass spectrometry. This final step resulted in labelling of alpha-synuclein by the caffeine-diazirine derivative at the glutamic acid 28 and tyrosine 39 amino acid positions. Labelling was not observed for the 1-aminoindan, nicotine, or caffeine six carbon linked caffeine diazirine compounds in the given conditions.

ACKNOWLEDGEMENTS

First, I would like to thank my supervisors Drs. Ed Krol and Jeremy Lee for their wisdom and support throughout my journey. I am truly privileged to have had you as supervisors. Your passion for science was always motivating, and the learning environment you provided allowed me to both grow and enjoy myself.

I would like to thank my committee members: Dr. David Sanders, Dr. Kate Dadachova. Your support and suggestions were invaluable. I am grateful for your insights and outside opinions.

I would like to thank my former and current lab members. Working with you and learning from you made my days in the lab a pleasure.

I would like to thank Dr. Paulos Chumala from Dr. George Katselis' mass spectrometry laboratory in the College of Medicine, for completing the LC-MS/MS and data analyses. The effort put into ensuring this work was completed properly was very reassuring and did not go unnoticed.

I would like to thank Dr. Haixia Zhang for training me, teaching me about protein mass spectrometry, and consulting on our methodology. Your knowledge helped bridge the gap between many areas of my work.

I would like to thank Dr. Michal Bonecki and the PCCF for training me and allowing me to use their space and instruments.

Finally, I would like to thank the College of Pharmacy and Nutrition, the College of Medicine, and the Natural Science and Engineering Research Council of Canada (NSERC) for providing me funding for this work and allowing me to pursue this degree.

DEDICATION

I would like to dedicate this thesis to my parents (Joanne and Rob) and my brother (Robert Jr.).

TABLE OF CONTENTS

LIST OF FIGURES

LIST OF TABLES

LIST OF ABBREVIATIONS

Abbreviation	Definition
ABC	Ammonium bicarbonate buffer
ACN	Acetonitrile
AD	1-aminoindan-diazirine; 9
AS	Alpha-synuclein
C_2D_2	C_8-6-C_8 Diazirine; 12
C_8-6- C_8	Caffeine six-carbon linked caffeine
C_8-6-I	Caffeine six-carbon linked 1-aminoindan
C_8-6-N	Caffeine six-carbon linked nicotine
CD	Caffeine-diazirine; 6
cNDGA	Cyclized nordihydroguaiaretic acid
DAD	Diode array detector
DCM	Dichloromethane
DIPEA	N,N-Diisopropylethylamine
DLB	Dementia with Lewy bodies
DMSO	Dimethyl sulfoxide
EDTA	Ethylenediaminetetraacetic acid
EtOAc	Ethyl acetate
FA	Formic acid
HOSA	Hydroxylamine-*O*-sulfonic acid
HPLC	High-performance liquid chromatography
ITC	Isothermal titration calorimetry
LP	Lewy pathology
MS	Mass spectrometry
MS/MS	Tandem mass spectrometry
MSA	Multiple system atrophy
NAC	non-amyloid-β component
ND	Nicotine-diazirine; 10
NMR	Nuclear magnetic resonance
PAL	Photoaffinity labelling
PBS	Phosphate-buffered saline
PD	Parkinson's disease
PDD	Parkinson's disease dementia
QTOF	Quadrupole time of flight
SNpc	Substantia nigra pars compacta
TFE	Trifluoroethanol
THF	Tetrahydrofuran

ThT	Thioflavin T
TLC	Thin layer chromatography
UV	Ultraviolet

INTRODUCTION

1.1 Introduction

Parkinson's disease is a common neurodegenerative disease characterized by two main pathological features.[1] The aggregation of protein into intracytoplasmic inclusions known as Lewy pathology is one of these pathological features. While many proteins make up these inclusions, alpha-synuclein is their primary component. [2,3]

Alpha-synuclein is an intrinsically disordered protein thought to have a role in vesicular trafficking and cell signalling.[4,5] It is commonly divided into three main sections: the N-terminus, the non-amyloid-β component region, and the C-terminus. However, it is prone to aggregation under certain conditions.[6] This aggregation leads to cellular dysfunction such as the production of reactive oxygen species, mitochondrial dysfunction, and cell death.[7] As such, alpha-synuclein has become a primary target for treatment development in Parkinson's disease as Parkinson's disease treatments are not curative to date.

Several chemicals (caffeine, nicotine, and 1-aminoindan) have demonstrated a somewhat weak ability to interact with alpha-synuclein in previous work.[8,9] To improve their capacity to interact with the protein, they were linked in different combinations with a six-carbon chain to produce bifunctional agents.[10] These agents were caffeine six-carbon linked caffeine, caffeine linked 1-aminoindan, and caffeine linked nicotine. Two of these compounds, caffeine linked 1-aminoindan, and caffeine linked nicotine, were capable of rescuing yeast cell growth in a cell model with excess alpha-synuclein, indicating potential suitability to being Parkinson's disease drug candidates. The way the new bifunctional agents interacted with alpha-synuclein was not well understood.

Therefore, this work will focus on improving this understanding through three steps. The first step is through the synthesis of diazirine photoaffinity labelling probes, which are molecular probes activated by light to covalently link to the nearest molecule.[11] Second, the probes will be characterized using biological assays such as the Thioflavin T assay which detects alpha-synuclein aggregation.[12] Finally, photoaffinity labelling probes will be used in labelling studies to identify the amino acids to which the drugs bind.

1.2 Parkinson's Disease

Parkinson's disease (PD) is the second most common neurodegenerative disease.[13–15] In North America, the prevalence is estimated to be 572 per 100,000 people above 45 years of age.[13]

It is rare for people below the age of 50 to be affected by the disease.[14,15] However, the prevalence of PD only increases with age, reaching an estimated 3 to 4% within the population of those who are 80 years of age or older.

PD is best known for its three cardinal symptoms: bradykinesia, rest tremor, and rigidity.[1,14,16] Postural instability was considered a cardinal feature in the past but has since been removed as it is considered to occur later in the progression of the disease. [16,17] To classify someone as having parkinsonism, bradykinesia – the slowness of movement – is required as well as either one *or* both of the remaining symptoms. [1,14,16] Once parkinsonism has been identified, the remaining inclusion and exclusion criteria can be applied for a formal diagnosis of either clinically established PD or clinically probable PD (for a more comprehensive explanation of criteria see [16]).[14,16] While the majority of PD symptoms appear to be motor related, non-motor symptoms are also part of the inclusion criteria. [1,14,16] Non-motor symptoms of PD include sleep disturbances (e.g. rapid eye movement sleep behaviour disorder), hyposomnia, autonomic dysfunction (e.g. constipation), and psychiatric dysfunction (e.g. depression), all of which can significantly impair one's quality of life. [16] Recently, evidence suggests that certain non-motor symptoms, such as rapid eye movement sleep behaviour disorder and olfactory loss, are some of the first indicators of the prodromal stage of the disease.[18–20]

To be diagnosed with PD, clinical diagnosis by a specialist during life is considered the gold standard. [16] Post-mortem, the diagnosis can be confirmed through pathological testing for the hallmark traits of PD, the first of which is the degeneration and death of dopaminergic cells in the substantia nigra pars compacta (SNpc).[2,21,22] Neurodegeneration of dopaminergic neurons happens preferentially in the ventrolateral region of the SNpc, sparing the other regions. Evidence suggests that cell death in this region results in the motor features of parkinsonism.[2] The second hallmark of PD is Lewy pathology (LP). In general, LP is defined as intracellular inclusions predominantly composed of aggregated α-synuclein (AS) protein.[1–3,14] However, the intracellular protein inclusions are also composed of approximately 90 other types of molecules.[1] LP can be separated into two categories, Lewy bodies and Lewy neurites, both of which are primarily AS protein. [2,3] Lewy bodies differ from Lewy neurites in that Lewy bodies are intracytoplasmic inclusions whereas Lewy neurites are found in neurites. Unfortunately, both pathological features of the disease are not completely selective markers of PD. [2] SNpc dopaminergic cell degeneration and LP

are seen in other neurodegenerative diseases. Some guidelines are detailed in the literature to aid in proper pathological identification of PD; however, they require validation.

Given the primary pathological features, it should come as no surprise that many PD treatments are centered around dopamine. The first treatment for PD was levodopa, a dopamine precursor that functions by supplementing the brain with dopamine. [23] Levodopa continues to be the standard for PD treatment of motor symptoms to date. [24] Subsequently, additional treatments for motor symptoms have been developed which include dopamine agonists, catechol-o-methyltransferase inhibitors, monoamine oxidase-b inhibitors, and surgical interventions. [24,25] These treatments are generally dopamine-oriented, like levodopa. Treatments for PD non-motor symptoms exist as well. [26] They are generally not universal, rather they are targeted towards individual symptoms of the disease. None of these treatments, motor or non-motor, have been able to delay or cure the disease, indicating that the underlying cause for PD must lie elsewhere. [25]

In 1997, the first genetic mutation associated with PD was identified as an alanine to threonine substitution at the 53 position of AS protein in the SNCA gene. [27] This discovery was monumental as it was the first to implicate both a monogenic and AS cause for PD. In the years that followed, many other SNCA mutations, including whole locus multiplications, as well as other genetic loci aside from the SNCA gene were discovered that have a role in PD. [28,29] To date, over twenty genetic loci have been associated with PD as well as certain genetic risk factors. Most cases, however, are sporadic in nature and only a small percentage, roughly 5 to 10%, are familial. [28]

Regardless, the information garnered from such studies has led to the identification of potential PD treatment targets. Aside from AS, leucine rich repeat kinase 2, VPS35, and parkin RBR E3 ubiquitin ligase are among the most studied. [28] Proteins such as these are involved in vesicular trafficking, protein degradation, and protein transportation, which appear to be some of the overarching themes on the molecular level. Despite this, much is still uncertain as to how these definitively result in PD. However, much of the pathogenesis is suspected to rely on the protein alpha-synuclein.

1.3 Alpha-Synuclein (AS)

Alpha-synuclein is a 140 amino acid long protein weighing 14 460 Da. AS is known for existing in an intrinsically disordered state in solution and in the intracellular environment. [4,30] However, there are conflicting reports that AS exists as a helically folded tetramer. [31] In reality, both conformations may exist in a dynamic equilibrium. Native AS will also transition into an

alpha-helical form when interacting with phospholipid bilayers, preferring acidic phospholipids to net neutral vesicles. [32] Unsurprisingly, it is abundant in the nervous system, but AS can also be found in other tissues, including red blood cells. [33,34]

AS is predominantly localized to the pre-synaptic terminals of neurons and synaptic vesicles due to its preference for surfaces with high curvature. [5,35] It appears to have a synaptic regulatory function. There are multiple claims of AS activity which include protein interactions, lipid interaction and modulation, chaperone activity, dopamine regulation, and many more. [36] Other than that, it is thought to have a role in the function of the mitochondria. [37] Ultimately, alpha-synuclein's physiological function is not completely understood despite years of study.

Alpha-synuclein is divided into three sections (Figure 1.1): the N-terminal region, the non-amyloid-β component (NAC) region, and the C-terminal region. The N-terminal region ranges from residues 1 to 60. Interestingly, most of the known genetic mutations in the SNCA gene reside in this region: A30P, E46K, H50Q, G51D, A53E, and A53T. [28] The NAC region runs from residues 61 to 95. This region was first discovered in the study of Alzheimer's disease and amyloid deposition, hence its name. [38] It is a hydrophobic region thought to be highly involved in misfolding and aggregation of protein. Both the N-terminal region and NAC region confer AS the ability to bind charged lipids due to the seven 11-mer repeats and consensus sequence which makes it form a three-turn, amphipathic alpha helix. [35] Finally, there is the C-terminal region from residues 96 onward. The C-terminal region is acidic and largely unstructured even when bound to micelles. [39] Aggregation regulation is thought to occur because of this region. [40] Finally, a chaperone-mediated autophagy sequence from residues 95 to 99 assists with protein degradation. [41]

Figure 1.1 AS protein: all three regions and the amino acid residues which define them. Red (left) is the N-terminal region which goes from residues 1 to 60. Blue (middle) is the NAC region from residues 61 to 95. Light green (right) represents the C-terminus from residues 96 to 140.

Rather than being in disordered or alpha-helical form, AS can also form aggregates with beta-sheet structures like other amyloid diseases.[6] (Figure 1.2). In this first step of the aggregation process, the free, monomer AS forms soluble oligomers.[42] Evidence suggests that even at this stage AS oligomers can disrupt cell functions.[43–45] These oligomers then go on to form insoluble amyloid fibrils which will become Lewy pathology.[42] Lewy pathology and AS fibrils are thought to result in reactive oxygen species, mitochondrial dysfunction, and degeneration of dopaminergic neurons.[7]

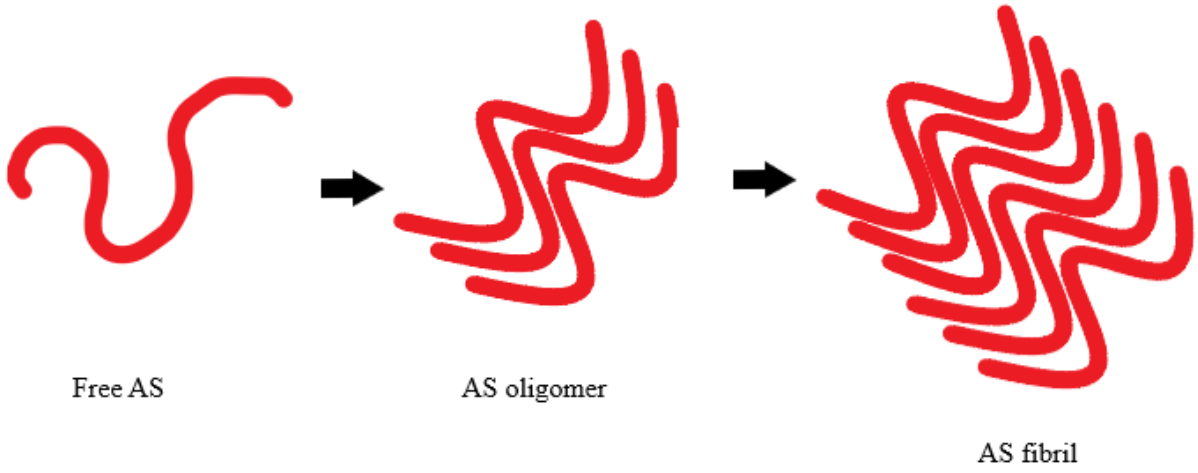

Figure 1.2 Illustration of AS progression into fibrils. Free AS first transitions to oligomers and then into fibrils.

There are many factors influencing alpha-synuclein's aggregation which include, but are not limited to, the following. Phosphorylation of serine-129 is thought to contribute to aggregation, possibly by increasing the rate of aggregation.[46,47] As previously noted, mutations in the SNCA gene are linked to PD.[28] *In vitro* evidence suggests these mutations play a role in the rate of aggregation as well as elongation.[48] Lipid vesicles and the solution pH were also contributing factors to aggregation. As with the current understanding of alpha-synuclein's physiological function, the precise cause and mechanism of alpha-synucleinopathy initiation are not yet completely understood.

The most concerning property of AS is its prion-like infectiousness. Seeded aggregation is the mechanism by which this is thought to occur. Through seeded aggregation, fibril fragments leave infected cells and initiate fibrillization in uninfected cells.[49] Evidence shows that AS seeds can act as fibrillization sites for free AS.[48,50] Several studies have documented support for cell to

cell transmission of AS aggregates and Lewy pathology as well. This was first confirmed when neural tissue grafts demonstrated Lewy pathology post-mortem following transplantation into PD patients.[51] In mouse models, AS pathology was found in the central nervous system following intramuscular injection of AS seeds, implying retrograde transport and propagation of disease.[52] Further work with the same model demonstrated this transmission occurs in other peripheral sites.[53]

To study the formation of these AS aggregates *in vitro,* the gold standard approach for fibril detection is the thioflavin T (ThT) assay. Thioflavin T specifically interacts with amyloid fibrils and protofibrils *in vitro* due to their beta sheet character and does not interact with other unfolded, folded, or oligomeric proteins.[12] ThT may be performed in cells; however, it is less specific as ThT may interact with other cellular components.[54]

To perform the assay *in vitro*, monomeric proteins are solubilized in buffer and allowed to aggregate although specific experimental conditions vary.[12] It is most desirable to have monomeric proteins present at the start of the assay and not oligomeric proteins as this will affect growth rates. Adding ThT will allow visualization of aggregation via a blue shift in fluorescence emission from 510 nm to 480 nm.[12,55] Excitation of ThT occurs around a 450 nm maximum.[55] More fluorescence from the solution implies more aggregation; thus, ThT may be used to observe the effects small molecules may have on protein aggregates.

Two experimental protocols are typically used to measure fibril formation. In the first, ThT is present in the protein mixture and measurements are taken over time.[12] Less protein is required in these assays, making kinetics-based assays more affordable. This method receives criticism from the fact that ThT may interfere with fibril formation and small molecule binding.[56] The second protocol does not have ThT present, and samples are extracted from the mixture which are then read with ThT.[12] More protein is necessary in these experiments, but the aggregation mixture is simpler.

1.4 Other AS diseases

PD is not the only disease afflicted by the aggregation of AS. Dementia with Lewy bodies (DLB), Parkinson's disease dementia (PDD), and multiple system atrophy (MSA) also exhibit AS

pathology. Along with PD, these illnesses are termed alpha-synucleinopathies because they share AS proteinaceous inclusions.

DLB and PDD share a considerable amount of overlap. Both diseases consist of fluctuating cognition, cognitive impairment, rapid eye movement sleep behaviour disorder, parkinsonism, and visual hallucinations. [57–59] However, DLB and PDD are differentiated temporally. [57] DLB may present first as dementia followed by parkinsonism, or dementia and PD symptoms may appear concurrently. For PDD on the other hand, the PD precedes the development of dementia by twelve months, making PDD a subtype of PD. Due to their similarities, it is debated as to whether they are distinct diseases and should be qualified as such. [57,58] Pathologically, there is not a distinction based on current international pathological staging systems. [59]

MSA on the other hand is quite different from PDD and DLB. MSA presents with progressive autonomic failure as well as parkinsonian, pyramidal, and cerebellar features. [60,61] Like DLB and PD, MSA also has proteinaceous AS inclusions. However, they are oligodendroglial cytoplasmic inclusions called Papp-Lantos bodies, as opposed to PD and DLB where AS accumulation is seen in neurons.

All three diseases exhibit similarities with respect to the presence of alpha-synuclein. PD likely receives more attention due to its prevalence as compared to these diseases, but it is possible these three diseases would benefit from a better understanding of AS. Also, treatments targeted toward AS may be beneficial for the broader category of alpha-synucleinopathies.

1.5 Previous Work

A common practice in the field of biochemistry is to turn toward epidemiological studies for potential drug candidates. Reviewing such literature in the field of PD and AS indicated to Dr. Lee that there were three likely drug candidates for PD treatment. [8,9]

Genetics are not the only contributing factor to Parkinson's disease. Environmental factors influence one's likelihood of developing PD as well. Studies have found cigarette smoking to be inversely related to the incidence of PD, which implies that the primary constituent – nicotine – may act as the active ingredient. [62–64] Caffeine, another natural product, also has an inverse relationship to the incidence of PD. [65,66] Finally, 1-aminoindan, a metabolite of rasagiline, was selected for further study as there was evidence to suggest that it may have neuroprotective effects. [67,68]

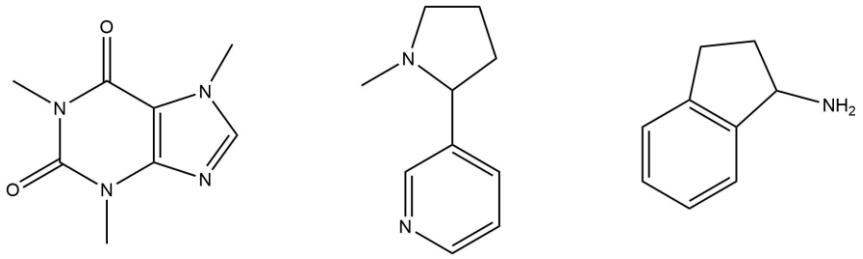

Figure 1.3 Potential drug hits for PD therapies. Left to right: caffeine, nicotine, 1-aminoindan.

Given the evidence from the aforementioned studies, caffeine, nicotine, and 1-aminoindan (Figure 1.3) were tested for the ability to interact with AS. [8,9] These three molecules possessed the ability to interact with AS as evidenced by nanopore analysis, circular dichroism, nuclear magnetic resonance (NMR), and/or isothermal titration calorimetry (ITC). Within these studies, nicotine was studied in more detail. Nanopore and NMR suggested that nicotine preferentially interacted with the C- and N-terminal regions of AS. [8] The interaction is thought to result in AS adopting a loop conformation (Figure 1.4), as ITC data suggests a 1:1 ratio of drug to protein.

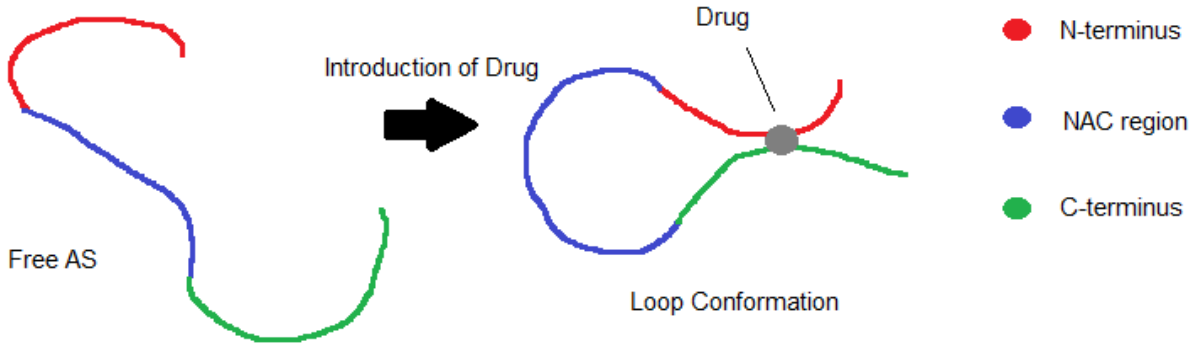

Figure 1.4 Hypothesized mechanism of interaction for neuroprotective compounds.

Given the ability of these molecules to interact with AS, it was hypothesized that by combining two of these molecules into one larger molecule that two possible effects could be observed. First, the strength of the interaction between the combined molecule and the protein will be stronger than that of the individual molecules. Second, the bifunctional compounds would have increased activity because they bring two active components in proximity, and the second binding event could follow the first binding event more easily.

Therefore, work was carried out to synthesize a variety of bifunctional agents which linked caffeine to 1-aminoindan, caffeine, or nicotine with a six carbon chain (Figure 1.5). [10] When assessed for their ability to bind to AS, there was little improvement in the strength of interaction

as one might have expected given the previous hypothesis. Notably, caffeine six carbon linked caffeine (C_8-6-C_8) was an exception to this finding as its K_d was far greater than caffeine, its monomer. To evaluate the second half of the hypothesis, the compounds were tested in a yeast cell model overexpressing AS. Two compounds, caffeine linked 1-aminoindan (C_8-6-I) and caffeine linked nicotine (C_8-6-N), were able to rescue cell growth more effectively than the monomer compounds, other bifunctional compounds, or combinations of monomer compounds. This evidence could suggest that C_8-6-I and C_8-6-N interact with AS to rescue cell growth, but given their lower binding constants, other cellular mechanisms may help rescue cell growth as well.

Regardless, additional study and experimentation could offer more insight toward solving the discrepancy between ITC results and yeast cell results. It is not understood where the bifunctional and monomer compounds interact with AS protein. As the different regions of AS are responsible for different effects on aggregation, this information could guide drug development for PD as well as aid in understanding AS aggregation itself. For intrinsically disordered proteins, crystal structures may be ideal to visualize the protein-ligand interaction, but to date have been unobtainable for AS. Thus, there exists the need to employ alternative methods to understand how the drugs interact with AS.

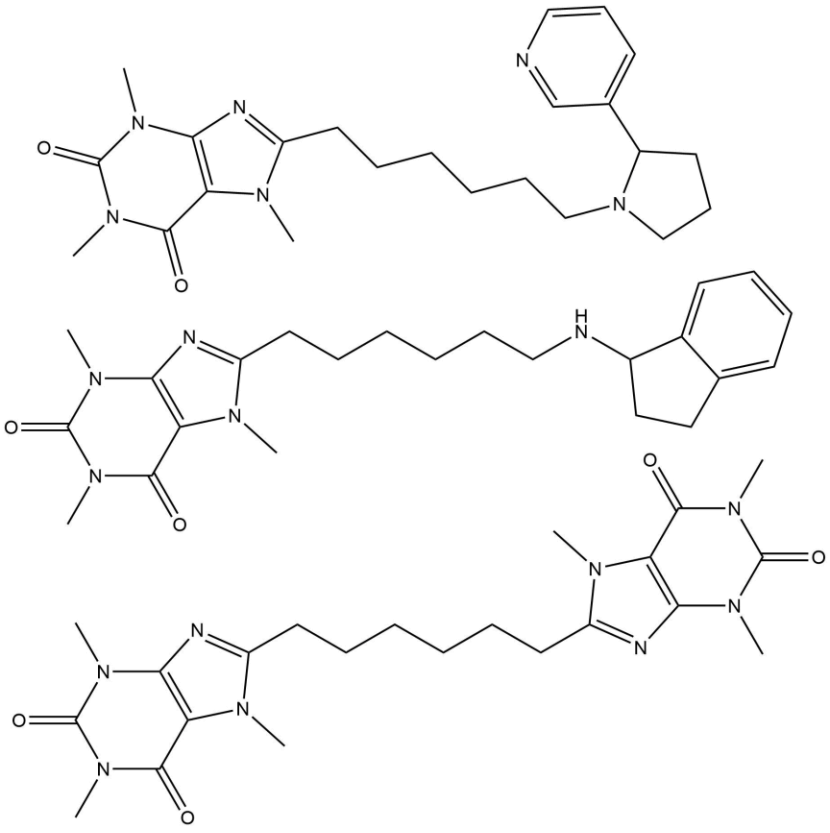

Figure 1.5 Bifunctional compounds of interest in the present study. Compounds are as follows: C_8-6-N (top), C_8-6-I (middle), C_8-6-C_8 (bottom).

1.6 Photoaffinity Labelling

Photoaffinity labelling (PAL) is a chemical biology technique that allows insight into the interaction of a probe and a biomolecule.[69] To perform PAL, a molecular probe is first synthesized which contains both the photophore and the structural motif of interest. The structural motif's purpose is to mimic the ligand of interest, whereas the photophore's purpose is to be activated by light and form a covalent bond where the motif interacts. This molecular probe is then incubated in the target system and allowed to interact with biomolecules in the location it prefers (Figure 1.6). Photoirradiation in the ultraviolet (UV) range activates the photophore, forming a covalent bond between the probe and its target. This probe-biomolecule complex is then analyzed, and conclusions are drawn regarding the probe's ability to interact. PAL can be applied to study protein-protein interactions.[11] However, most work in the field focuses on biomolecule-ligand interactions.

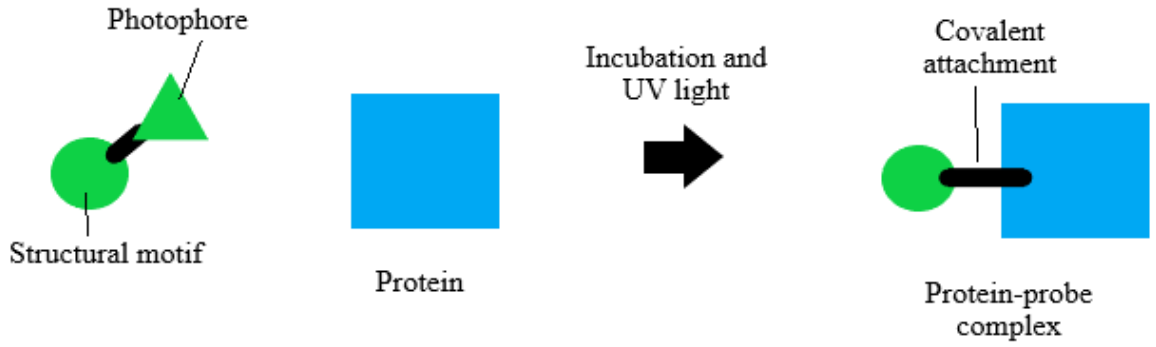

Figure 1.6 Illustration of the process of photoaffinity labelling. The green circle represents the structural motif that is attached to a photophore (green triangle) used for labelling. Once incubated with the protein (blue square) and UV light, the protein-probe complex forms via the formation of a covalent bond due to activation of the photophore.

PAL is used for two major applications. The first is *in situ* which provides the probe exposure to a wide range of potential targets. Overall, *in situ* labelling is particularly useful in drug discovery for identifying a more complete range of targets a drug may have in a cell system. Depending upon the experiment, the probe will have another functional group, referred to as a tag. There are many potential tags that could be introduced to the probe which include, but are not limited to, biotin, isotopes, fluorophores, or reactive groups (e.g. a terminal alkyne).[69–71] Biotin is used in studies as it can be isolated with affinity chromatography, allowing labelled biomolecules

to be isolated. Isotopes and fluorophores are used as tags for visualization of labelled proteins or proteins subunits. Reactive groups are used as tags because they are smaller and modify the chemical structure of the probe less, allowing cell permeation. Also, they can be chemically linked to other tags in subsequent steps, allowing for the benefits of different tags while minimizing changes to the probe's structure during labelling.

The second application of PAL is far simpler. In this case, PAL may be performed *in vitro*. This is generally completed for the purpose of binding site identification. *In vitro* PAL is ideal for providing insight into the binding sites of a molecule on a protein, identification of allosteric sites, and potentially even identification of protein conformation.

Following labelling, the probe-biomolecule complex must be analyzed. High performance liquid chromatography (HPLC) coupled to mass spectrometry (MS) is frequently used for analysis of the labelled biomolecules. [72] HPLC separates the components in solution and MS identifies the number of probes attached to the protein. Enzymatic digestion is then performed following the PAL procedure to break proteins down into shorter peptide sequences. Tandem mass spectrometry (MS/MS) following HPLC separation of the peptide digest allows for more precise identification of the labelling sites. Under ideal conditions, MS/MS can fragment the labelled peptides such that the modified amino acid can be determined. HPLC-MS or HPLC-MS/MS can be applied for the identification of biomolecules from *in situ* experiments as well, but additional purification is typically employed before analysis. The cells are lysed, tagged, purified with affinity chromatography, and analyzed by sodium dodecyl sulfate polyacrylamide gel electrophoresis before HPLC or enzymatic digestion. However, advances in proteomics are making purification before analysis less of a requirement. [73]

When designing a PAL experiment, probe design requires consideration. First, the photophore should be stable to the system conditions. [70,72,74] Decomposition of the photophore in the system may result in a false negative. The photophore should also be activated by light in a range that does not negatively affect the system. As well, the by-products of probe activation should not negatively affect the system. Essentially, negatively affecting the system may impact the results in a way that may not be an accurate representation of probe binding. Next, the probe should be as similar as possible to the molecule it is trying to mimic. Biochemical assays or *in silico* testing can be performed to evaluate the similarity between the probe and the molecule. Finally, the bond between the probe and target must be stable enough that analysis can be completed without being

concerned about decomposition. Given these criteria, benzophenones, aryl azides, and diazirines are the most applied photophores in PAL literature.

There are many advantages for the use of benzophenones in PAL. Benzophenones are activated by UVA light in the range of 350-365 nm, a long enough range that biomolecules should not be affected. Irradiation causes the benzophenone to convert to a triplet diradical state (Figure 1.7). The activated photophore can exist in this state for up to 120 μs before relaxing to ground state if it remains unreacted. [69] The triplet diradical reacts in a long understood, two-step mechanism, hydrogen abstraction followed by recombination. The active species prefers to react with O-H and C-H bonds, meaning it can react with all amino acids. The active state is essentially inert to water because the reacted product will convert back to the ketone via dehydration shortly after reacting with water. [69,71] Synthesis of the benzophenone is also easy as starting materials are commercially available.

Certain drawbacks exist as well. Benzophenones are relatively large and bulky photophores, as such they may not be the most appropriate for all PAL studies because of their impact on probe activity. [69,71,72] Furthermore, longer irradiation times (more than 30 minutes) are required for benzophenones which may lead to substantial non-specific binding. Finally, while able to react with all amino acids, certain locations are preferred.

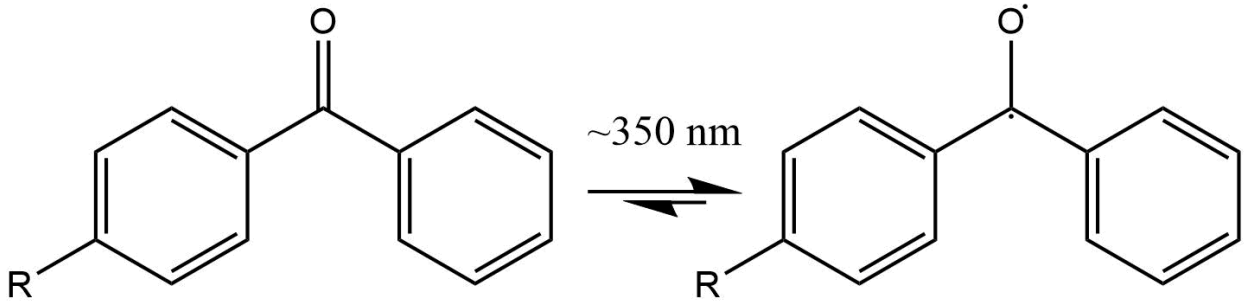

Figure 1.7 Benzophenone activation scheme. Benzophenone (left) is converted into diradical (right).

Aryl azides are the second of the three commonly used photophores in PAL. They are activated by relatively short range light (250-350 nm). [72] The azide becomes a singlet nitrene once it is activated (Figure 1.8), losing inert N_2 gas. [69] The singlet nitrene can relax to a less energetic triplet state if it remains unreacted during its 0.1 ms lifetime. Both species will insert into C-H bonds through different, long established mechanisms. The singlet species reacts via insertion, and the triplet species reacts via hydrogen abstraction followed by recombination. Ultimately, the products from both the singlet and triplet species are the same. The major benefits to using aryl

azides in PAL are their size and the ease of synthesis. [69,72] Beginning from their respective amine, azides can be synthesized in either one or two steps. [75,76] The loss of nitrogen gas during activation can also be considered relatively beneficial as nitrogen gas should not affect biological systems.

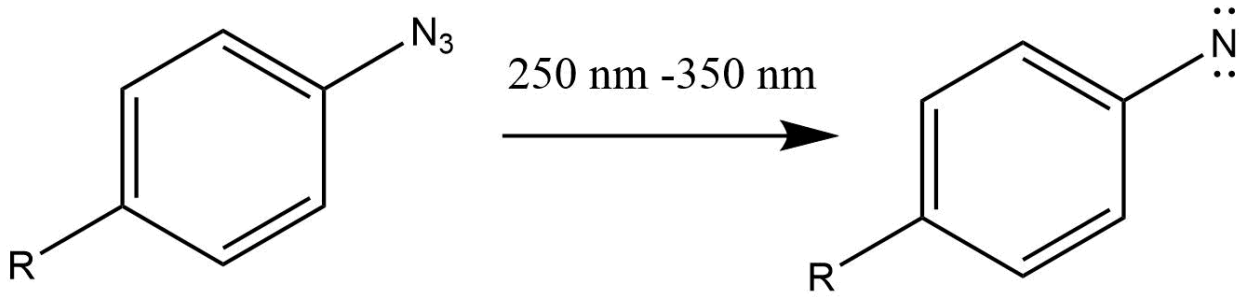

Figure 1.8 Aryl azide activation scheme. Aryl azide depicted on the left and nitrene on the right.

The major drawback of aryl azides in PAL is their activation. Activation occurs in a range that is harmful toward biomolecules. [69,72] While the loss of nitrogen gas in their activation should not impact biological systems, the wavelength of light required for activation renders this benefit questionable. The final major disadvantage of aryl azides is their propensity to undergo side reactions. [69] The singlet species can be converted to benzazirines and dehydroazepines, which will react with nucleophiles. The triplet species can be oxidized to the nitro species. The azide itself can also be reduced back to the amine form. All these reactions can result in difficulties achieving high labelling yields.

The third and final of the common PAL photophores are diazirines. Diazirines are small photophores that are activated by light in the 350 to 380 nm UVA range. [69,72] Once activated, the diazirine loses nitrogen gas and becomes a singlet carbene (Figure 1.9) with a half-life in the nanosecond range. Such a brief half-life is excellent for reducing non-specific labelling of biomolecules. This carbene species can insert into O-H, C-H, and N-H bonds. The mechanisms of diazirine reactions have been understood for many years. It can convert into a triplet carbene state capable of reacting with C-H bonds though a diradical mechanism. When activated by light, the diazirine may convert into a diazoisomer instead of the singlet carbene. However, the diazoisomer

is still capable of converting to the singlet carbene state. Diazirines are also stable to a wide range of conditions, which is beneficial during both the synthesis and labelling.

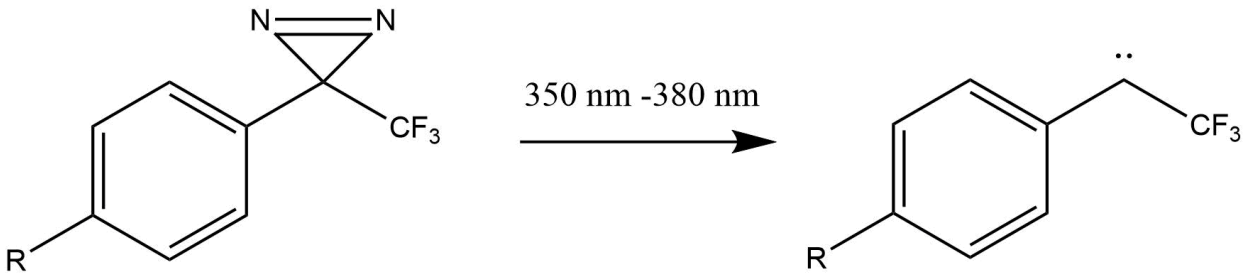

Figure 1.9 Activation of aryl diazirine (left) to a carbene (right).

Due to the short half-life, quenching of the carbene by solvent frequently occurs, resulting in lower labelling yields. [69] Another aspect affecting labelling yields is the conversion of the diazoisomer to the singlet carbene state. The conversion takes a long time which can again lead to difficulties with labelling efficiency and potentially non-specific labelling. The triplet state carbene may be oxidized, again limiting labelling. As well, diazirines are typically divided into two groups: alkyl diazirines and aryl diazirines, each with its own flaws. In the case of alkyl diazirines, a hydride shift can occur converting the carbene to a double bond and further reducing labelling yields. Finally, synthesis of diazirines is relatively difficult, particularly for aryl diazirines.

Clearly, there are benefits and drawbacks to all the most used photoactivatable groups in PAL. Comparing benzophenones, aryl azides, and diazirines solely based upon such information may be misleading as labelling efficiency is also dependant upon the target. [77] Comparing photophores based upon *in silico* modelling may be an appropriate approach toward selecting the optimal photophore with which to modify the drug. However, AS is the target protein and most of the studies have been performed with unfibrillated, free in solution AS. [8–10,78] Although examples in the Protein Data Bank (PDB) report crystal structures of AS fibrils or AS segments bound to other peptides, to date, there is no structure in the PDB of unbound, monomeric AS which would be sufficient for *in silico* testing of free AS. Therefore, the selection of photophore must be based upon what is synthetically possible. Caffeine is the most troublesome of all the compounds as it is small and limited in its ability to be modified with a photophore. For this reason, the addition of a short alkyl diazirine linker to the N7 position of theophylline was chosen. This linker will be far

smaller than benzophenones, aryl azides, or aryl diazirines. For consistency, this linker will be used for all other compounds.

PAL of AS has not been published frequently in literature. To date, there is only one study that has performed PAL on AS which was published in 2018. [79] Several major differences exist between the current work and what was published. Most notably, labelling was performed on pre-fibrillated AS using aryl azide photophores on completely different drugs. The success of the 2018 study suggests PAL may be viable for unfibrillated AS while the limited number of studies suggest work in the area is still novel.

1.7 Diazirines

To perform this study, both the monomer compounds and bifunctional agents must have diazirines. Considering the ways diazirines can be incorporated onto these molecules, creating a diazirine linker that could be used to alkylate nitrogen atoms is the simplest course of action. Given the size of aryl diazirines, it would be better to use a small alkyl diazirine chain. Ideally, this chain would be as small as possible (e.g. hydroxyacetone could be used as a starting material). However, synthesis of a diazirine from this compound in our lab was unsuccessful (M. Pirlot, personal communication). Therefore, synthesis of a four-carbon chain diazirine linker was chosen. Many researchers were able to successfully convert 4-hydroxy-2-butanone into 3-(2-hydroxyethyl)-3-methyl-3H-diazirine in the literature. Often, the hydroxyl group is subsequently converted to a different leaving group. The resulting compound is used in alkylation reactions, just as desired for this work.

Synthesis of 3-(2-hydroxyethyl)-3-methyl-3H-diazirine is completed in three steps (Figure 1.10). The most common synthetic strategy to produce this diazirine linker is as follows. [80–85] First, liquid ammonia is condensed into a flask containing 4-hydroxy-2-butanone and allowed to react for approximately 5 hours, sometimes refluxing at around -30 °C. This results in conversion of the ketone to an imine which is then transformed into a diaziridine with the addition of hydroxylamine-*O*-sulfonic acid in methanol. The length of step two varies considerably in the literature; typically, it occurs overnight. The reaction is brought to room temperature during this time and followed by filtration and concentration in the morning. The diaziridine is converted finally to a diazirine in the third step. Iodine is added to the compound and triethylamine on ice until the colour of iodine persists. This step typically takes two hours to complete, but again there is a wide range in the literature from ten minutes to five hours. The reaction is extracted and purified by column

chromatography. The overall yield for the conversion of 4-hydroxy-2-butanone to 3-(2-hydroxyethyl)-3-methyl-3H-diazirine in the literature ranges from 30-51%. [80–84] However, one patent reported a 3% yield for this reaction. [85]

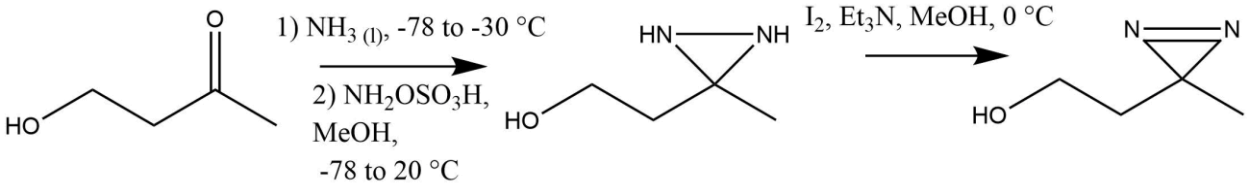

Figure 1.10 Synthetic scheme of diazirine linker depicting a typical synthetic route.

Several alternatives to this pathway exist. One alternative is the replacement of liquid ammonia in the first step of Figure 1.10 with ammonia in methanol. [86,87] This substitution may be particularly useful as ammonia in methanol can be purchased commercially in small quantities. If large scale synthesis is not the goal, this may be more ideal. However, the yield appears to suffer as a result of this alteration, excluding the patent which reports a 3% yield. [85] When everything in the reaction is kept consistent, literature yields were 20% and 28%. [86,87]

Other studies have focused more on the reagents used in the conversion of the diaziridine to a diazirine. One study reports the use of tBuOK to perform the final transformation. [88] The yield for this reaction was 62% conversion from the ketone to the diazirine, 11% higher than the next best yield. At first glance, this appears to be an effective way to increase the yield from a relatively low yielding reaction. However, there were several major changes to the standard protocol for this reaction that do not allow for a direct comparison. Most notably, the reaction makes use of a sealed metal tube capable of withstanding high pressures (10 MPa). The study does not control for the use of the sealed tube. Therefore, it is possible that the tube may have the biggest impact in the first or second step, and the use of tBuOK is not the determining factor for the observed increase. Regardless, this was one of the higher yielding reactions for this compound.

Another study by the same group compared the use of different bases for the dehydrogenation of the diaziridine. [89] This study made use of the same one-pot, sealed tube synthesis as the previous study to test ten different bases that are typically cheaper and easier to handle than tBuOK. All bases were compared using levulinic acid, and the highest yielding base (KOH) was then applied to create diazirines of several other compounds. It is possible the most effective base for levulinic acid may not be the same for all other compounds, but the study

demonstrated an increased yield for 3-(2-hydroxyethyl)-3-methyl-3H-diazirine (75% yield) as compared to the tBuOK reaction. [88,89] To the best of my knowledge, this is the highest yield for this diazirine compound.

For the general category of alkyl diazirine synthesis, there is another common approach to diaziridine transformation into diazirines. Silver oxide (Ag_2O) may be used to oxidize diaziridines. [90,91] However, the process tends to be low yielding and require additional filtration due to the silver salts.

Finally, there is one last interesting alternative for the oxidation of diaziridines: NaClO. Sodium hypochlorite, or bleach, has been used to obtain high yields for the oxidation of diaziridines to diazirines on certain molecules. [92] A 6% w/v solution of bleach was used to convert adamantanone diaziridine to adamantanone diazirine (Figure 1.11) resulting in a 99% yield in this step. The article hints at the synthesis of other alkyl diazirines being less than favourable, but the comment lacks clarity surrounding whether or not 6% bleach was used in the synthesis of other alkyl diazirines. Given the cost-effectiveness and availability of bleach, this may be the best departure point for the synthesis of diazirines.

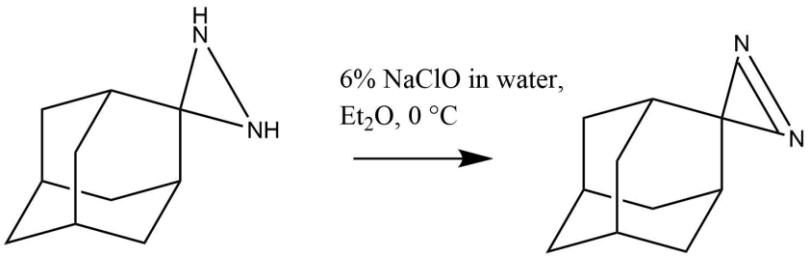

Figure 1.11 Conditions for conversion of adamantanone diaziridine to adamantanone diazirine.

1.8 Hypothesis

1. The diazirine-functionalized probes will interact with AS the same way that the drugs from which they are derived interact with AS.
2. The diazirine-functionalized probes will preferentially label the N- and C- terminal regions of AS.

1.9 Objectives

a. To synthesize photoaffinity labelling probes of all molecules being studied.

This study will focus on both the monomer and bifunctional compounds. Caffeine, 1-aminoindan, nicotine, C_8-6-C_8, C_8-6-I, and C_8-6-N diazirine probes will be synthesized.

b. To characterize the activity and binding affinity of the probes and compare them to the original drugs.

All diazirine labelled probes and the drugs upon which they are based will be subjected to isothermal titration calorimetry to determine binding affinity. The same compounds AS aggregation inhibition activity will be determined by Thioflavin T assays. The data from each of the probes will be compared to their respective drug to determine the impact of the linker.

c. To perform photoaffinity labelling and mass spectrometric proteomics with the characterized probes.

Photoaffinity labelling will be performed using a simple *in vitro* design. This will be followed by tryptic digestion of the protein and HPLC-MS or MS/MS. Digestion, mass spectrometry, as well as data analysis and validation will be performed by collaborators. Collaborators for this step are George Katselis, Paulos Chumala, and Haixia Zhang.

METHODS

2.1 Ethical Considerations

This project does not involve either animals or humans. Therefore, no ethical approval is required.

2.2 Reagents

All chemicals were obtained commercially, mainly from either Sigma-Aldrich or Alfa Aesar. Alpha -synuclein was purchased from rPeptide.

2.3 Compound Synthesis

2.3.1 3-(2-hydroxyethyl)-3-methyl-3H-diazirine

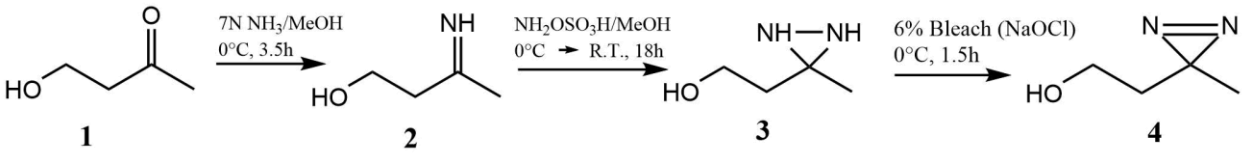

1 2 3 4

51% crude yield in three steps

4-hydroxy-2-butanone (1 eq, 5.67 mmol) was put under nitrogen and on ice. The ketone was dissolved in 7N ammonia in methanol (5.67 mL) and reacted for 3.5 hours. Hydroxylamine-*O*-sulfonic acid (1.1 eq, 6.24 mmol) dissolved in methanol was added to the mixture, allowing the reaction to come to room temperature overnight. The precipitate was filtered off and the filtrate was concentrated *in vacuo*, resulting in a thick, yellow oil. The oil was returned to ice after drying. A minimal amount of ice was added to the flask, followed by diethyl ether (15 mL) and 6% bleach (NaOCl, 35 mL). The resulting solution was stirred for 1.5 hours, adding ice chips throughout. The reaction mixture was then extracted with 3 x 20 mL diethyl ether. The organic layers were combined and dried over $MgSO_4$. The mixture was then concentrated *in vacuo* at 22 °C and 370 mbar without further purification, resulting in a yellow, watery oil (51% crude yield in three steps, 0.297 g). ^{1}H NMR ($CDCl_3$, 500 MHz, 22 °C): δ 3.53 (t, J = 6.3 Hz, 2H), 1.64 (t, J = 6.3 Hz, 2H), 1.08 (s, 3H).

2.3.2 2-(3-methyl-3H-diaziren-3-yl)ethyl 4-methylbenzenesulfonate

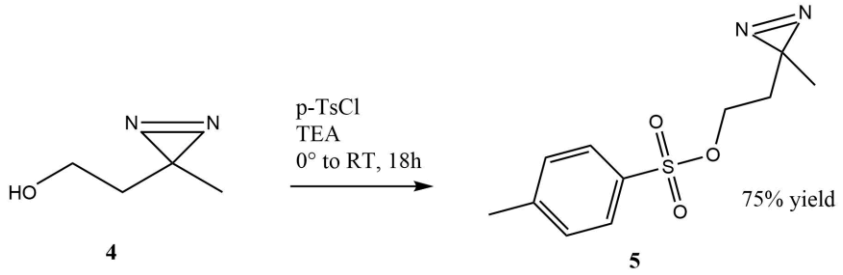

4 5

3-(2-hydroxyethyl)-3-methyl-3H-diazirine (1 eq, 0.718 mmol) was dissolved in anhydrous dichloromethane under nitrogen on an ice bath. Triethylamine (2 eq, 1.437 mmol) was added and stirred for ten minutes. p-Toluenesulfonyl chloride (1.4 eq, 1.006 mmol) was dissolved in anhydrous dichloromethane and then added dropwise to the reaction. The solution was stirred overnight, allowing the reaction to come to room temperature. Pyridine (2 mL) was added to the mixture. After ten minutes, the reaction mixture was washed with 20 mL 1 M HCl, then 20 mL saturated sodium bicarbonate, and finally, 20 mL brine. The organic phase was dried over $MgSO_4$, filtered, and dried *in vacuo*. Purification by column chromatography (1:1 DCM:Hexanes) yielded a pale yellow oil (75% yield, 0.136 g). ^{1}H NMR ($CDCl_3$, 500 MHz, 22 °C): δ 7.81 (d, *J* = 8.3 Hz, 2H), 7.37 (d, *J* = 8.0 Hz, 2H), 3.95 (t, *J* = 6.4 Hz, 2H), 2.54 (s, 3H), 1.67 (t, *J* = 6.4 Hz, 2H), 1.00 (s, 3H).

2.3.3 Caffeine diazirine

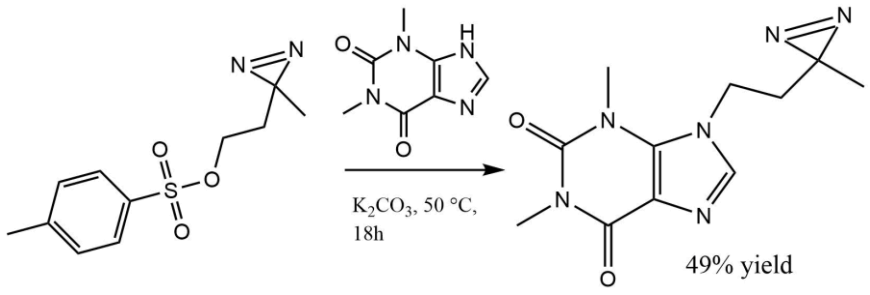

5 6

Theophylline (1.5 eq, 1.07 mmol) and K_2CO_3 (10.5 eq, 7.54 mmol) were placed under nitrogen and dissolved in DMSO. 2-(3-methyl-3H-diaziren-3-yl)ethyl 4-methylbenzenesulfonate (1 eq, 0.72 mmol) was dissolved in anhydrous tetrahydrofuran and added dropwise to the theophylline solution. The mixture was heated to 50 °C and reacted overnight. The reaction was poured into 30 mL water and extracted with 3 x 40 mL DCM. The organic layers were combined and washed with 3 x 25 mL water. Finally, the organic layers were dried ($MgSO_4$) and concentrated

in vacuo. Purification by column chromatography (EtOAc: Hexanes 8:2) yielded a lightly yellow oil (49%, 0.086 g). ^{1}H NMR ($CDCl_3$, 500 MHz, 22 °C): δ 7.65 (s, 1H), 4.21 (t, *J* = 7.0 Hz, 2H), 3.61 (s, 3H), 3.42 (s, 3H), 1.97 (t, *J* = 7.0 Hz, 2H), 1.00 (s, 3H). ^{13}C NMR ($CDCl_3$, 500 MHz, 22 °C): δ 155.12, 151.83, 149.42, 141.14, 106.88, 42.29, 36.01, 30.03, 28.23, 23.81, 20.03. ESI-MS: m/z 263.1 ([M+H]+).

2.3.4 3-(2-iodo-ethyl)-3-methyl-3H-diazirine

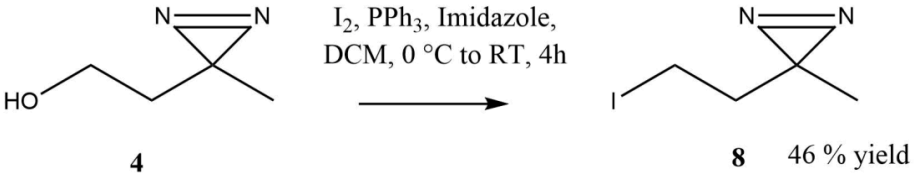

4 **8** 46 % yield

Triphenylphosphine (1.2 eq, 1.19 mmol) and imidazole (2.4 eq, 2.38 mmol) were placed under nitrogen at 0 °C and dissolved in anhydrous DCM. I_2 (1.2 eq, 1.19 mmol) was then added to the flask. 3-(2-hydroxyethyl)-3-methyl-3H-diazirine (1 eq, 0.99 mmol) was dissolved in anhydrous DCM and added dropwise to the mixture. The reaction was stirred for 4 hours, allowing it to come to room temperature. Water (6 mL) was added to the mixture before extracting with 2 x 10 mL DCM. The organic phases were combined and dried ($MgSO_4$) before concentration *in vacuo*. Column chromatography (10:1 Hexanes:Et_2O) resulted in a lightly yellow oil (46% yield, 0.098 g). ^{1}H NMR ($CDCl_3$, 500 MHz, 22 °C): δ 2.95 (t, *J* = 7.6 Hz, 2H), 2.02 (t, *J* = 7.6 Hz, 2H), 1.08 (s, 3H).

2.3.5 1-aminoindan diazirine

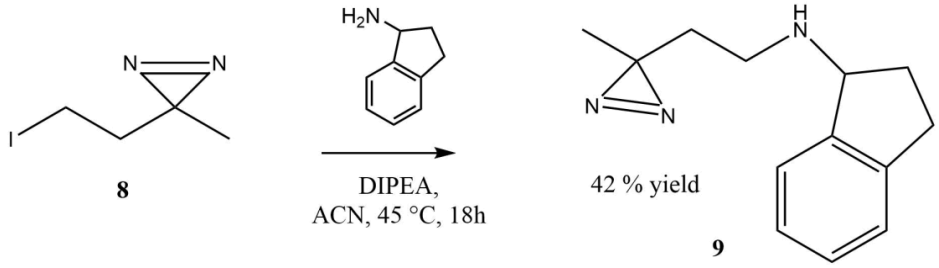

8 42 % yield **9**

1-aminoindan (1.5 eq, 0.698 mmol) was dissolved in anhydrous acetonitrile under nitrogen. DIPEA (3 eq, 1.395 mmol) was added to the mixture and stirred for 1 hour. 3-(2-iodo-ethyl)-3-methyl-3H-diazirine (1 eq, 0.465 mmol) was dissolved in anhydrous acetonitrile then slowly added to the reaction mixture. The solution was heated to 45 °C and stirred overnight. Water (10 mL) was added and the reaction was extracted with 3 x 20 mL DCM. The organic layers were combined and dried over $MgSO_4$ before drying *in vacuo*. The crude product was purified using column

chromatography (EtOAc:Hexanes 2:8) resulting in a yellow oil (42 %, 0.108 g). ^{1}H NMR ($CDCl_3$, 500 MHz, 22 °C): δ 7.34 (bt, *J* = 8.3 Hz, 1H), 7.24-7.18 (m, 3H), 4.18 (t, *J* = 6.6 Hz, 1H), 3.02-2.96 (m, 1H), 2.81 (p, *J* = 15.9, 15.6 Hz, 1H), 2.54 (dt, *J* = 13.9, 7.3 Hz, 2H), 2.40-2.34 (m, 1H), 1.82-1.75 (m, 1H) , 1.68-1.58 (m, 2H), 1.26 (bs, 0.5H), 1.04 (s, 3H). ^{13}C NMR ($CDCl_3$, 500 MHz, 22 °C): δ 145.06, 143.75, 127.67, 126.47, 124.97, 124.29, 63.43, 42.05, 34.94, 33.53, 30.54, 25.00, 20.40. ESI-MS: m/z 215.9 ($[M+H]^+$).

2.3.6 Nicotine diazirine

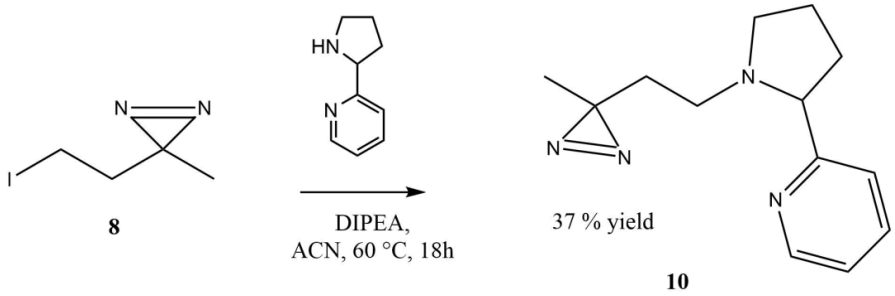

(+/-)-nornicotine (1.1 eq, 0.75 mmol) was placed under nitrogen and dissolved in anhydrous acetonitrile. DIPEA (1.5 eq, 1.02 mmol) was added to the (+/-)-nornicotine solution and allowed to stir for 1 hour before adding 3-(2-iodo-ethyl)-3-methyl-3H-diazirine (1 eq, 0.68 mmol) also dissolved in anhydrous acetonitrile. The mixture was heated to 60 °C and stirred overnight. The reaction was cooled to room temperature before adding 30 mL saturated $NaHCO_3$ and extracting 3 x 40 mL DCM. The organic layers were combined and dried ($MgSO_4$) then concentrated under *in vacuo*. The crude oil was purified by column chromatography (8:2 Hexanes:EtOAc) yielding an amber coloured oil (37%, 0.058 g). ^{1}H NMR ($CDCl_3$, 500 MHz, 22 °C): δ 8.54 (d, *J* = 1.6 Hz, 1H), 8.50 (d, *J* = 3.5 Hz, 1H), 7.74 (bs, 1H), 7.28-7.26 (m, 1H), 3.26 (d, *J* = 7.5 Hz, 2H), 2.41 (dt, *J* = 11.9, 5.0 Hz, 1H), 2.22-2.12 (m, 2H), 2.02-1.90 (m, 2H), 1.87-1.77 (m, 1H), 1.69 (bs, 1.5H), 1.51-1.35 (m, 2H), 0.90 (s, 3H). ^{13}C NMR ($CDCl_3$, 500 MHz, 22 °C): δ 149.70, 148.90, 135.20, 123.77, 67.89, 53.58, 49.19, 35.39, 33.86, 25.02, 22.81, 20.01. ESI-MS: m/z 231.1 ($[M+H]^+$).

2.3.7 C_8-6-C_8 Diazirine

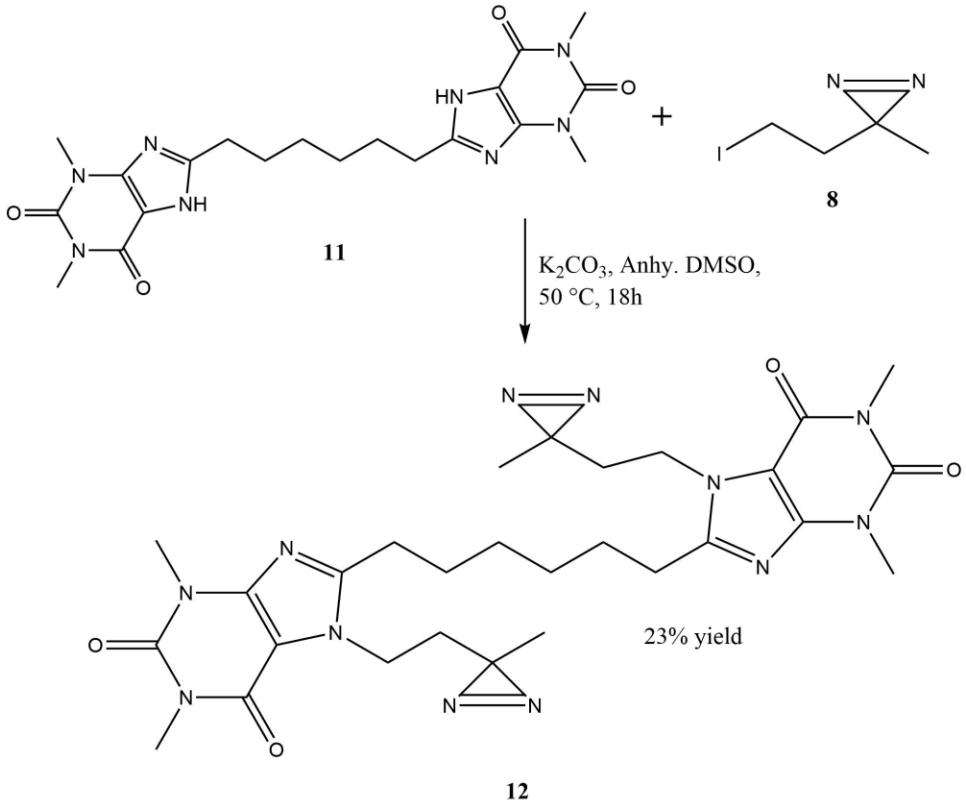

Theophylline six-carbon linked theophylline was synthesized as previously described. One equivalent (0.232 mmol) was then solubilized in 5 mL DMSO under nitrogen. Potassium carbonate (6 eq, 1.391) was added to the solution before 3-(2-iodo-ethyl)-3-methyl-3H-diazirine (10 eq, 2.318 mmol) solubilized in DMSO was added to the reaction flask. The flask was sealed and heated to 50 °C to react overnight. The following morning, the flask was cooled to room temperature and 10 mL water was added. The solution was extracted three times with 20 mL DCM. The organic phases were combined and dried as much as possible before the addition of 25 mL DCM. The DCM was extracted three times with 15 mL water. The water layers were combined and extracted three times with 15 mL DCM. The new DCM washes were extracted twice with 15 mL water. Both sets of DCM layers were combined and dried over magnesium sulfate and under reduced pressure to produce a brown oil and precipitate mixture. Silica column chromatography was completed using a 9.75: 0.25 ratio of ethyl acetate to methanol. The product from the column (orange precipitate) was finally rinsed with acetone to produce the final product, a white precipitate at a 23% yield. ^{1}H NMR ($CDCl_3$, 500 MHz, 22 °C): δ 4.20 (t, *J* = 15.2 Hz, 2H), 3.57 (s, 3H), 3.40 (s, 3H), 2.74 (t, *J* = 15.5 Hz, 2H), 1.84 (t, *J* = 15.2 Hz, 2H), 1.81-1.73 (m, 2H), 1.49-1.44 (m, 2H), 1.06 (s, 3H). ^{13}C

NMR ($CDCl_3$, 500 MHz, 22 °C): δ 155.1, 153.9, 151.8, 148.7, 106.6, 40.5, 36.5, 29.9, 29.1, 28.1, 27.9, 26.9, 24.0, 19.8.

2.4 Isothermal Titration Calorimetry

Both the protein and the drug were dissolved in phosphate-buffered saline (PBS) (0.01 M phosphate buffer, 0.0027 M potassium chloride and 0.137 M sodium chloride, pH 7.4, at 25 °C) to the desired concentration. The samples were degassed and then loaded into a NanoITC calorimeter. The more concentrated sample was added to the syringe, and the more dilute sample was added to the well. The temperature was held at 20 °C, and the well was mixed at 300 rpm. For each experiment, twenty aliquots of 2.5 μL of the sample were injected into the well at 250 s intervals except for the first injection which was 0.48 μL. NanoAnalyze software was used to process the data.

2.5 Thioflavin T Assay Conditions

First, 56.25 μL of 2 mg/ml AS and 18.75 μL of PBS at physiological pH (7.4) were pipetted into a 0.25 mL microcentrifuge tube to produce a 1.5 mg/mL solution of AS. Next, 3.75 μL of 10 mM drug or buffer were added to the microcentrifuge tube to obtain 500 μM of the drug in the assay. All components were mixed and settled at the bottom of the microcentrifuge tube by flicking the tube. The tubes were placed in large vials that could be held by the thermomixer. Some sand was added in the vials to fill the space between the tubes and vials to facilitate heat transfer. The tubes and sand were held in place by wrapping parafilm around the top of the vials. Each experiment was run in triplicate. The vials were added to the thermomixer at 37 °C and 1400 rpm for 5 days. Working in the dark, a 26 μM working solution of ThT was made. From each tube, 10 μL AS mixture was pipetted in triplicate onto a 96-well plate to which 144 μL ThT working solution was added. Fluorescence of the wells was measured by excitation at 444 nm and emission at 484 nm with a plate reader. The data was treated by first averaging the readings coming from a single tube. The resulting averages from tubes of the same drug were compared with the control using a t-test assuming equal variances.

2.6 Photoaffinity Labelling Protocol

To each quartz tube used in the assay, AS protein was added from a stock solution of 69.15 μM to the final required concentration of protein. The buffer (TRIS•HCl 20 mM, NaCl 100 mM, pH 7.4) was added to dilute AS to the appropriate concentration for labelling. To the control, both

the buffer and DMSO were added for a total of 200 µL solution in the vial and 1% DMSO. To the experimental vial, the drug was added to the appropriate final concentration of probe in a 200 µL vial with a final concentration of 1% DMSO. The vials were mixed so that all the fluid was at the bottom of the vial. Next, the vials were capped and incubated at 37 °C and 220 rpm for 30 minutes. Finally, the vials were incubated for a total of 30 minutes under two F20T12/BL/HO UVA lamps (National Biological Corp. Beachwood, OH) filtered to remove UVC. The strength of the light during this incubation was held at approximately 1500 $\mu W \bullet cm^{-2}$ in the UVA range, as measured with a UVP UVX-36 sensor (Ultraviolet Products Ltd, Upland, CA). After UVA exposure, the samples were transferred to microcentrifuge tubes and stored at -80 °C until analysis.

2.7 Protein Digestion Protocol

To each microcentrifuge tube containing 50 µL protein sample dissolved in 100 mM ammonium bicarbonate (ABC) buffer, an equal volume of trifluoroethanol (TFE; 50 µL) was added. Following this, the samples were placed in a speedvac for 25 minutes in order to remove TFE. Cold acetone (1 mL) was then added, samples mixed gently and stored at -80°C for 1 hour. Most of the acetone was then removed by centrifugation at 13,000 rpm for 30 minutes, leaving behind 50-100 µL solvent. This was repeated once more to remove unwanted material and prepare proteins for digestion. After the second time, acetone was removed completely in the speedvac, and samples were then reconstituted in 300 µL of 100 mM ABC buffer. Trypsin was added to the protein sample in a trypsin/protein ratio of 1:40 and samples were incubated in a shaker at 300 RPM (Eppendorf Thermomixer, Eppendorf, Mississauga, ON, Canada) overnight at 37°C to digest proteins. Trypsin was added again in the morning and incubated in a shaker at 300 RPM for 2 hrs at 37°C to complete the protein digestion. The samples were then completely dried and stored at -80°C until mass spectrometric analysis (LC-MS/MS). The digested protein samples were reconstituted in 97:3 water: acetonitrile, containing 0.1% formic acid, to a concentration range of 1-5 µg/µL prior to LC-MS/MS.

2.8 LC-MS/MS Analysis

The mass spectral analyses were performed on an Agilent 6550 iFunnel quadrupole time-of-flight (QTOF) mass spectrometer equipped with an Agilent 1260 series liquid chromatography instrument and an Agilent Chip Cube LC-MS interface (Agilent Technologies Canada Ltd., Mississauga, ON, CA). Peptide samples of 1 to 5 µg were injected and chromatographic separation was carried out on a high-capacity Agilent HPLC-Chip II: G4240-62030 Polaris-HR-Chip_3C18

consisting of a 360 nL enrichment column and a 75 µm × 150 mm analytical column, both packed with Polaris C18-A, 180Å, 3 µm stationary phase. Initially, injected samples were loaded onto the enrichment column with solvent A (0.1% formic acid in water) at a flow rate of 2.0 µL/min. Samples loaded to enrichment column were transferred onto the analytical column and peptides were separated with a linear gradient solvent system, consisting of solvent A and solvent B (0.1% formic acid in acetonitrile). The linear gradient was 3–25% solvent B for 50 min and then 25–90% solvent B for 10 min at a flow rate of 0.3 µL/min. Positive-ion electrospray mass spectral data was acquired using a capillary voltage set at 1850 V, the ion fragmentor set at 360 V, and the drying gas (nitrogen) set at 225 ºC with a flow rate of 12 L/min. Spectral results were collected over a mass range of 250–1700 (mass/charge; m/z) at a scan rate of 8 spectra/s. MS/MS data were collected over a range of 100–1700 m/z and a set isolation width of 1.3 atomic mass units. The top 20 most intense precursor ions for each MS scan were selected for tandem MS with active exclusion for 0.25 minutes. Data were analyzed using Agilent MassHunter Qualitative Analysis Software (Agilent Technologies Canada Ltd., Mississauga, ON, CA). The BioConfirm molecular feature tool was used to extract compounds from the collected data and the incorporation of labeling agent (caffeine diazirine, $C_{11}H_{14}O_2N_6$) was identified using BioConfirm define and match sequences tool.

RESULTS AND DISCUSSION

3.1 Synthesis

3.1.1 Caffeine Diazirine (CD) Probe

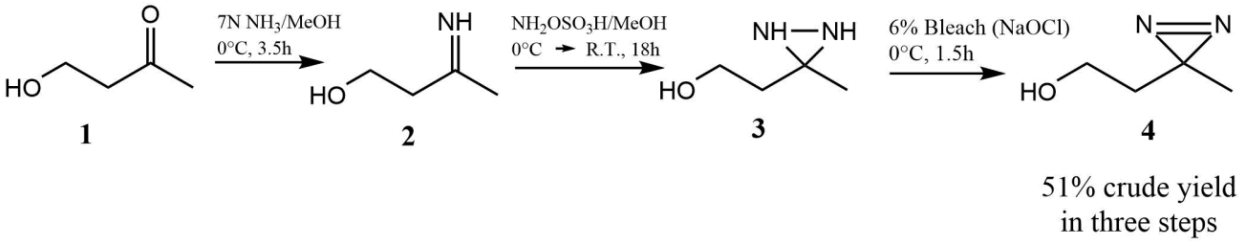

Figure 3.1 Synthetic pathway used for diazirine synthesis from 4-hydroxy-2-butanone (far left, 1) to create the diazirine linker (far right, 4).

3-(2-hydroxyethyl)-3-methyl-3H-diazirine (**4**) was obtained though the route outlined in Figure 3.1. This begins with 4-hydroxy-2-butanone (**1)** in which the ketone is converted to an imine (**2**) using ammonia in methanol. Hydroxylamine-*O*-sulfonic acid is then used to convert the imine to into a diaziridine (**3**). Finally, the diaziridine is converted into a diazirine (**4**) using a 6% bleach solution. The overall yield in three steps is 51% crude yield.

Initially, the yield for these three steps was a 6% crude yield. A variety of conditions were employed to improve the yield of diazirine. For the first step, the length of time, the temperature, and the reagents were all changed successively to improve the yield. The oxidizing agent in the third step was changed from bleach to potassium hydroxide as well. None of these conditions improved the yield.

The scale of the reaction was increased to 500 mg of starting material in hopes that the reaction works better at a larger scale where small impurities (water, etc.) have less influence on the reaction. The larger scale reaction improved the yield to 28% crude. The NMR spectrum showed the presence of residual solvent from the extraction step; however, attempts to remove residual solvent under high vacuum also led to loss of product (11% crude yield after two hours on the high vacuum). The NMR spectrum was free of solvent at this point, and the sample was returned to the high vacuum to monitor for further product loss. A decrease in the mass of product from 65 mg to 19 mg occurred over 5 hours, confirming that the diazirine was volatile under high vacuum. To confirm that removing the high vacuum step would improve the yield, the reaction was repeated on a 2 g scale. The reaction yielded 24% crude product when dried and confirmed the volatility of the diazirine.

One patented literature procedure for the synthesis of **4** made use of the same reagents and isolated product via vacuum distillation at 90 °C and 2 mbar. [85] In agreement with the results in this work, it only obtained a 3% yield of **4**, providing further support for the volatility of **4**. The use of vacuum distillation should not be ruled out for the isolation of **4** though as it has been used in the past for high yielding reactions, but the precise conditions were not listed. [88]

Regarding the sensitivity of the synthesized diazirine compound to ambient light, two samples of crude diazirine compound were left out on the bench top for three consecutive days. One sample was covered in foil and the other was not. There were no significant changes in NMR spectra observed between the two samples over the three days, suggesting little sensitivity to ambient visible light.

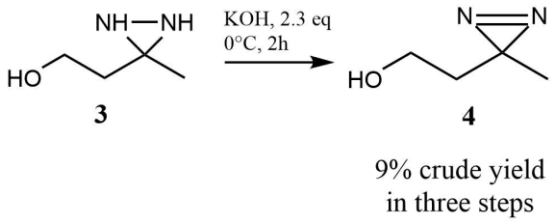

Figure 3.2 Alternate synthetic conditions for the conversion of the diaziridine to a diazirine. The yield corresponds to the yield when converting from the ketone to the final diazirine.

To further increase the amount of diazirine produced, the same procedure was repeated, substituting potassium hydroxide for bleach (Figure 3.2). [89] This reaction only yielded 9% crude diazirine. It was concluded that using bleach is more efficient for conversion from diaziridine to diazirine, and these conditions were used to move on to the next step.

When returning to synthesize more diazirine for other monomer compounds, the reaction began yielding lower quantities of product again akin to the 9% seen in the reaction with potassium hydroxide. The only obvious change made in the preparation of the diazirine was that the drying of the diaziridine was not as thorough as it was when originally trying to synthesize the compound. Therefore, the amount of time the diaziridine spent on the high vacuum was extended until the compound was as dry as possible before the oxidation step. This drying appeared to improve the yield to approximately 40% crude product. When repeated another time, the yield had dropped back to 9%. Absorption of water by hydroxylamine-*O*-sulfonic acid (HOSA) was suspected to cause this issue. HOSA was dried using diethyl ether and reduced pressure before being used to repeat the reaction. There was no observable improvement in the yield. The ammonia in methanol solution was replaced following this with a resultant increase to 51% crude yield. Upon further

investigation, a second bottle of ammonia in methanol was found in storage which had become yellow in colour. It was concluded that alternating between bottles of ammonia in methanol was the cause of the changes in yields. While this solves the question of why the yield was poor, it also calls into question whether the yield from potassium hydroxide was a result of the quality of the ammonia in methanol solution or KOH not being as effective as bleach.

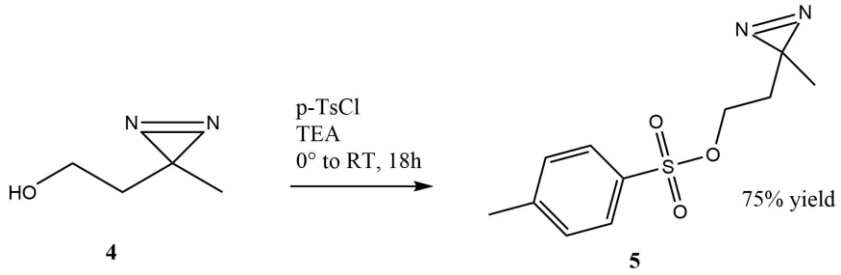

Figure 3.3 Conditions for the tosylation of the alcohol diazirine linker (4) to produce the tosylated diazirine linker (5).

The next step in the synthetic scheme, tosylation of the alcohol of the diazirine, used tosyl chloride and trimethylamine to covert the alcohol to the tosylate (Figure 3.3). The reaction yielded the tosylated diazirine (**5)** at a 125% crude yield. NMR indicated the major product was the tosylated diazirine linker, so the product was used without further purification. Figure 3.4 shows the final step in synthesizing the caffeine diazirine photoaffinity label **6**. In this step, theophylline is dissolved in DMSO with K_2CO_3 to enable alkylation at the N7 position when the tosylated diazirine compound is added, producing **6** at a 49% yield.

A functional mobile phase to isolate **5** has been developed which may allow for higher yields in the alkylation step. Silica gel column flash chromatography was used to purify **5** with 1:1 DCM: hexanes as a mobile phase. The yield resulting from the 1:1 DCM:hexanes column was 75%. It should be noted that the use of ethyl acetate in place of DCM to isolate **5** results in coelution of spots and should be avoided.

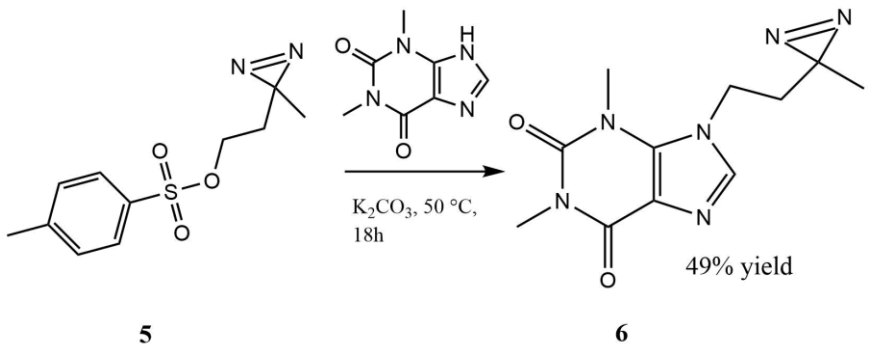

Figure 3.4 Conditions for alkylation of theophylline by the tosylated diazirine (5) to produce the caffeine diazirine probe (6).

3.1.2 1-aminoindan Diazirine (AD) Probe

Synthesis of the 1-aminoindan diazirine probe using the same tosylated linker and potassium carbonate conditions from the alkylation of theophylline was unsuccessful. Similarly, alkylation utilizing the tosylated linker with potassium carbonate and THF at 50 °C substituted for DIPEA and acetonitrile at 45 °C (Figure 3.5) also did not produce the desired product.

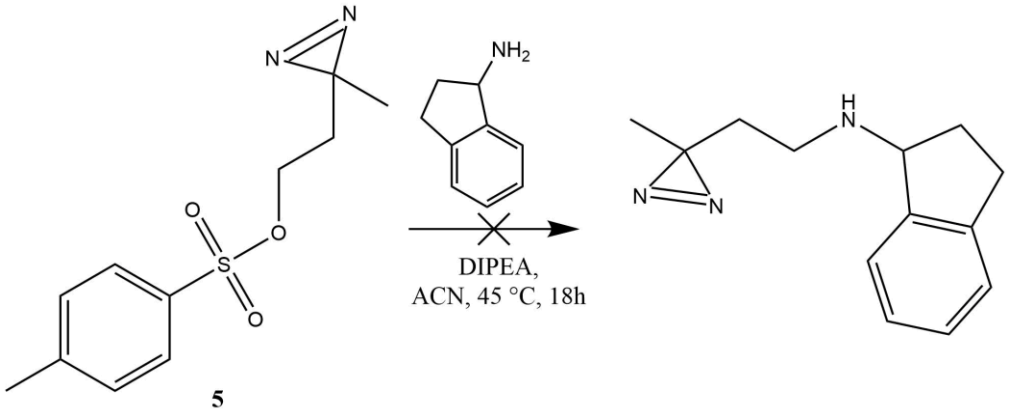

Figure 3.5 Conditions for the second attempt at the synthesis of 1-aminoindan diazirine probe.

At this point, the leaving group was hypothesized to be the issue, as our lab had determined that different leaving groups were required in the functionalization of caffeine, nicotine, and 1-aminoindan (O. Aigbogun, personal communication). Consequently, the preparation of halogenated linkers was proposed instead of tosylated linkers. To do so, the crude tosylated diazirine **5** was converted to a brominated diazirine **7** (Figure 3.6) via reflux of **5** with lithium bromide in anhydrous THF. The NMR of the crude product was an unidentifiable crude mixture.

To remove some of the impurities from the reaction, **5** was purified before repeating the bromination. The resulting NMR from the repeated reaction was modestly cleaner than its predecessor, allowing identification of the signals corresponding to **7**. Column chromatography was not successful at isolating the compound of interest in any subsequent attempts, so the crude brominated linker was used in the alkylation step without further purification. The conditions for the alkylation with the brominated linker were the same as used in figure 3.4. Unfortunately, the reaction was unsuccessful again.

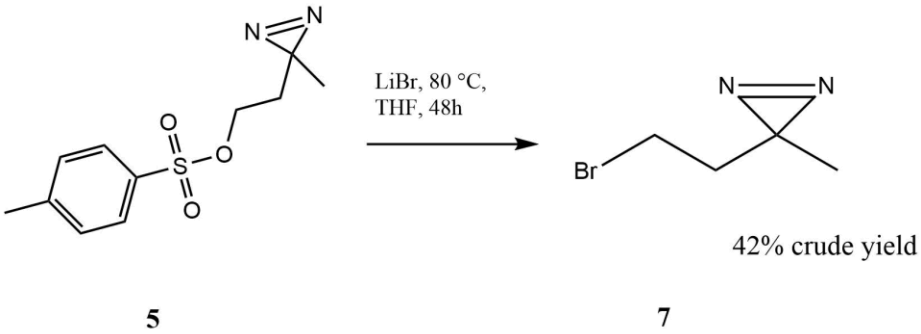

5 **7**

Figure 3.6 Conditions for bromination of the tosylated diazirine linker (left, 5) to form the brominated diazirine (right, 7).

In response to the previous failure to alkylate 1-aminoindan, iodination of the linker was proposed. Iodination has been reported as problematic to reproduce. [93] However, careful selection of solvents has improved this, with speculation that volatility of **8** may be a contributing factor. [81] Iodination of **4** uses iodine, triphenylphosphine, and imidazole to perform an Appel-like reaction in anhydrous dichloromethane over four hours (Figure 3.7). The reaction is purified by flash column chromatography using a 10:1, hexanes: diethyl ether mobile phase resulting in a 46 % yield of **8**. The low yield of this reaction is thought to be a result of either the column chromatography conditions being suboptimal or the compound being too volatile during the removal of solvent. Unfortunately, experimentation was never performed to confirm this observation, so it is possible the yield may have been affected by other mechanisms such as the generation of iodine radicals during the reaction due to exposure to ambient light.

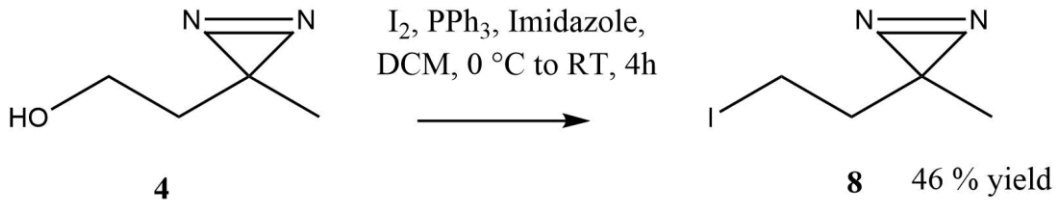

Figure 3.7 Conditions for the conversion of the diazirine linker an alcohol (left, 4) directly to the iodinated diazirine linker (right, 8).

Alkylation was repeated with similar conditions to figure 3.5. **8** was used to alkylate 1-aminoindan with DIPEA in acetonitrile overnight (Figure 3.8). Flash column chromatography was used to purify **9** using a 8:2 hexanes: ethyl acetate mobile phase for a 42% yield.

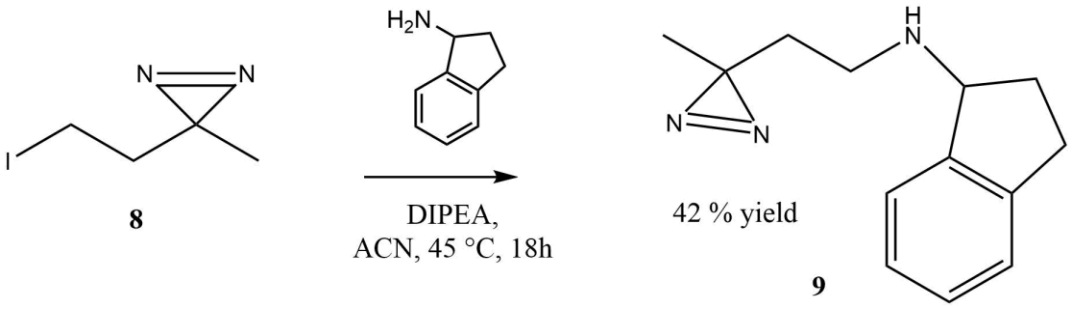

Figure 3.8 Alkylation of 1-aminoindan with 8 using DIPEA, ACN and heat to produce the 1-aminoindan probe (right, 9).

3.1.3 Nicotine Diazirine (ND) Probe

The nicotine-diazirine probe was synthesized easily using a similar procedure as was used for 1-aminoindan. Iodinated diazirine **8** was produced as described previously before being combined with nornicotine and DIPEA to produce **10** (Figure 3.9). Flash column chromatography with a 8:2 hexanes: ethyl acetate mobile phase isolated **10** at a 37 % yield.

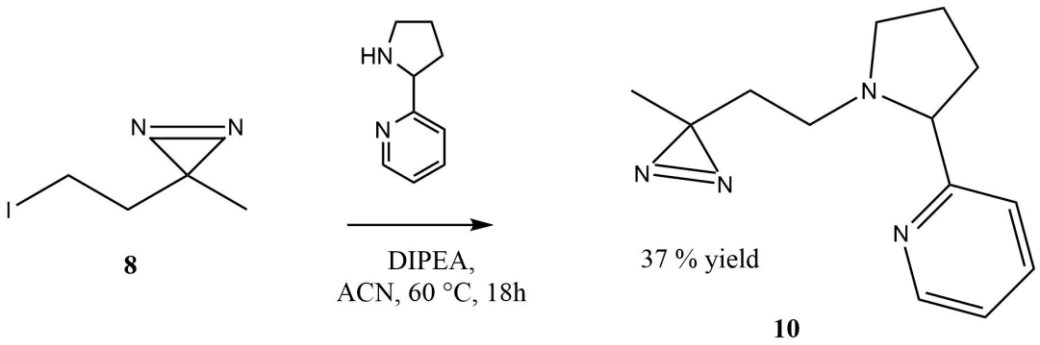

Figure 3.9 Alkylation of nornicotine using 8 to produce the nicotine diazirine probe (right, 10).

3.1.4 C_8-6-C_8 Diazirine Probe (C_2D_2)

Alkylation of 1-aminoindan and nornicotine were more responsive to the iodinated diazirine linker (**8**), and the original synthetic pathway used iodomethane to produce C_8-6-C_8. [10] For these reasons, theophylline six carbon linked theophylline (**11**) was alkylated at the N7 position with ten equivalents of **8** and six equivalents of potassium carbonate in DMSO (Figure 3.10). The product, C_2D_2 (**12**), was purified by column chromatography after extraction with a 9.75:0.25 ethyl acetate: methanol mobile phase. Compound **12** was originally isolated at a 43% yield, but the product was tinted orange and NMR had a peak at 1.22 ppm that did not correspond to the compound. In the original synthesis of C_8-6-C_8, the final step is to wash the product with acetone following alkylation. [10] As column chromatography was not enough for purification of **12**, a rinse of the product with acetone was proposed for this reaction as well. Fortunately, C_2D_2 was also insoluble in acetone while the impurity appeared to be soluble. **12** was rinsed with acetone, which removed the orange colour as well as decreasing the peak height of the NMR impurity at 1.22 ppm. The final product **12** was a white precipitate obtained at a 23% yield.

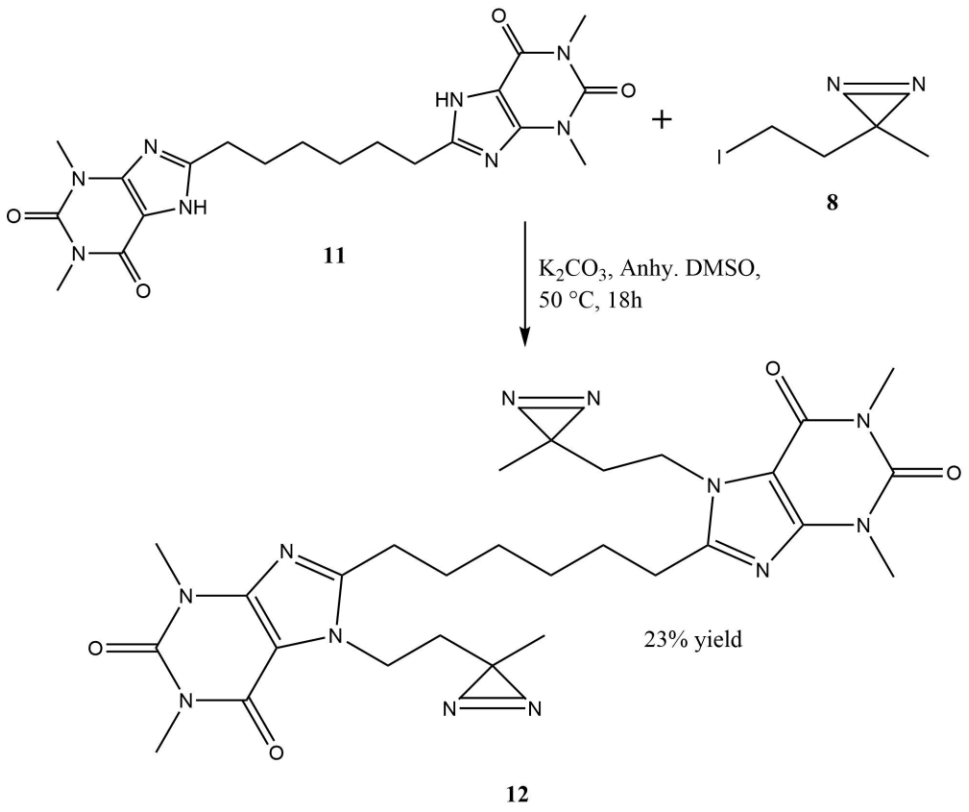

Figure 3.10 Alkylation of theophylline six-carbon linked theophylline (top left, 11) using potassium carbonate, DMSO, and heat to produce C2D2 (12).

3.1.5 C_8-6-I Diazirine Probe

The initial idea for the synthesis of the C_8-6-I diazirine probe was to alkylate both the N7 position and the amine of the 1-aminoindan simultaneously. In order to accomplish this, the theophylline six-carbon linked 1-aminoindan would have to react with the iodinated diazirine **8** in the presence of DIPEA. Before doing so, the ability of theophylline to react with **8** was uncertain when using DIPEA as a base, therefore a reaction was run doing just that (Figure 3.11). The reaction resulted in a 20% yield, which was relatively low; however, the reaction worked.

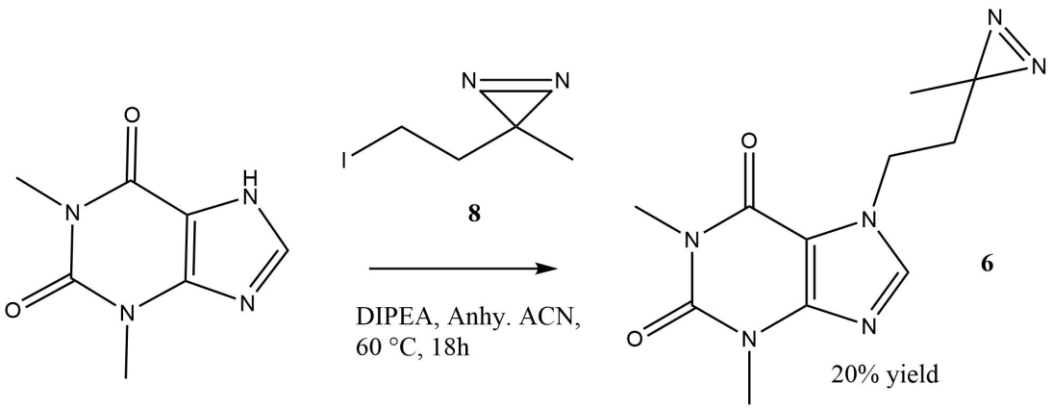

Figure 3.11 Alkylation of theophylline (left) using DIPEA as a base for alkylation of the N7 position to make the caffeine diazirine probe (right, 6).

To begin synthesis of the bifunctional probe, boc-protected theophylline six-carbon linked 1-aminoindan was synthesized by O. Aigbogun as described previously. [10] The molecule was first deprotected using an excess of 4 M HCl in dioxane and anhydrous dichloromethane as solvent. The reaction ran overnight with stirring at room temperature. The reaction was quenched by adding saturated $NaHCO_3$ to the flask and the mixture was extracted three times with DCM. Column chromatography using an 8:2 ethyl acetate: methanol mobile phase obtained deprotected theophylline six-carbon linked 1-aminoindan (**13**) at a 68% yield.

The resulting compound (**13**) was used in combination with **8** (13.5 equivalents) and DIPEA (3 equivalents) in tetrahydrofuran at 50 °C overnight (Figure 3.12). New spots appeared on thin layer chromatography monitoring of the reaction, but when the spots were subjected to TLC-MS, none of them corresponded to masses indicative of either mono- or di-alkylated T-6-I (**14)**. Unfortunately, the focus had to be shifted to completing ThT analyses and photoaffinity labelling, as such continued attempts at alkylation of **13** were ceased. Substitution of DIPEA with potassium carbonate is proposed as a modification to complete the alkylation.

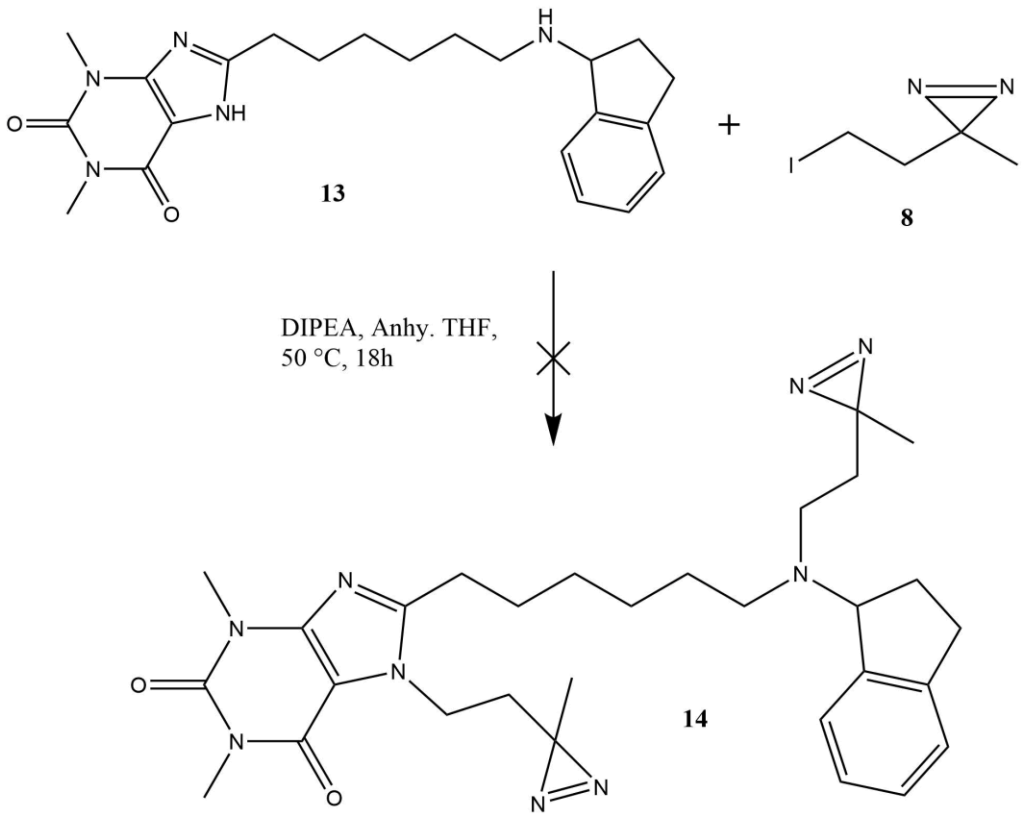

Figure 3.12 Conditions used for the attempted alkylation of theophylline six-carbon linked 1-aminoindan (13) when attempting to produce the doubly alkylated C_8-6-I diazirine (14).

3.2 Isothermal Titration Calorimetry

The goal of using ITC was to determine the binding affinity of all compounds to AS, both with and without the diazirine groups, to compare the diazirine linker's effects on binding affinity. Unfortunately, we were unable to collect any usable data. The following describes my attempts at ITC data collection.

Seven key experiments were run prior to termination of ITC experiments, listed in table 1. In these experiments, modifications were made as follows.

1. The drug may be placed in the syringe of the ITC instrument and AS placed in the well, i.e. the drug is then injected into the well (i.e. trial #1, #4 in table 3.1).

2. The concentration of drug being injected into the protein can be increased (trial #2, #7 table 3.1). This would be attempted if experimental approach 1 does not result in saturation of binding sites.

3. AS is placed in the syringe of the ITC instrument and drug placed in the well, i.e. the AS is injected into the well. (trial #3, #5, #6 table 3.1).

4. The solvents used in dilution of both the protein and the drug are identical, i.e. NaOH was not used to solubilize AS prior to dilution as it was not being used to solubilize the drug prior to its dilution (trial #7 table 3.1).

First, trial #1 from table 3.1 was completed along with its corresponding control. The result of subtracting the control data from the experimental data is shown in Figure 3.13 which suggested that the titration of drug into protein was not able to saturate all potential binding sites to produce a sigmoidal curve. Therefore, trial #2 made use of a higher concentration of drug (table 3.1). The results (data not shown) were the same as for trial #1, indicating that there may be an issue other than the inability to saturate binding sites.

Table 3.1 Key ITC experiments run.

Trial #	Syringe	Syringe [	Well	Well [ ]	Notes
1	**6**	50 μM	AS	5 μM	See figure 3.13 for data
2	**6**	200 μM	AS	5 μM	Data similar to figure 3.13
3	AS	50 μM	**6**	5 μM	See figure 3.14 for data
4	Caffeine	50 μM	AS	5 μM	See figure 3.15
5	AS	50 μM	Caffeine	5 μM	See figure 3.16
6	AS	50 μM	**6**	5 μM	Data similar to figure 3.16
7	Caffeine	500 μM	AS	5 μM	No NaOH used

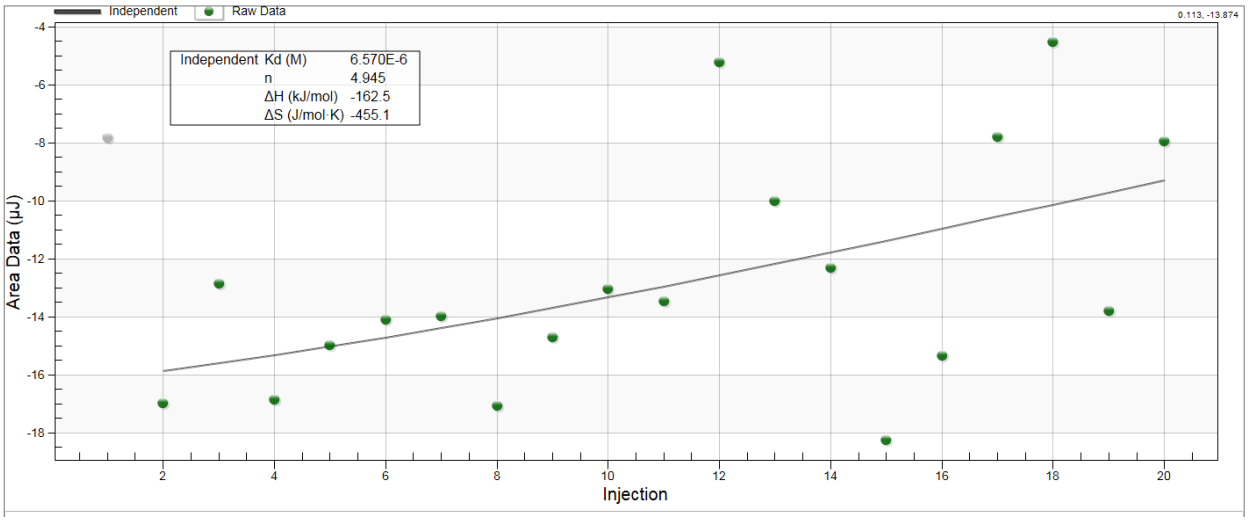

Figure 3.13 Processed data for 50 µM of 6 into 5 µM AS is inconsistent and does not produce the desired curve.

Following this, trial #3 from table 3.1 was performed. The resulting graph has an apparent sigmoidal shape (Figure 3.14), following subtraction of the control. The K_d was comparable to previously reported data for caffeine (K_d = 1.31x10^{-6} M), although the number of bindings sites was 1 and not 2. [10]

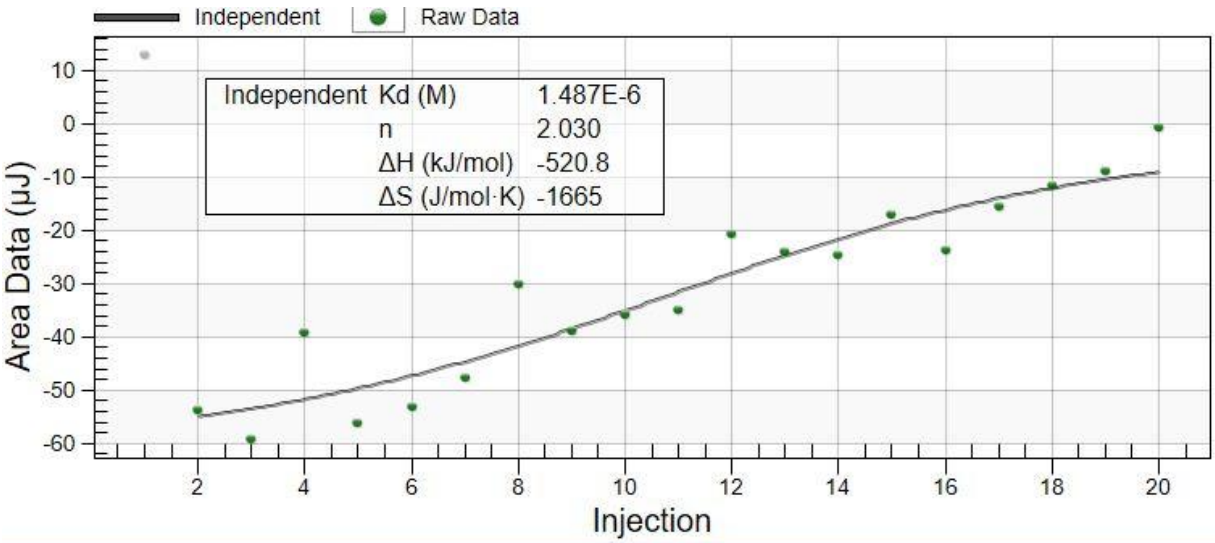

Figure 3.14 Trial #3: processed ITC data for 50 µM of AS injected into 5 µM compound 6 (caffeine-diazirine).

Next, trial #4 from table 3.1 was completed, injecting caffeine into AS. In the literature, caffeine was titrated into AS, so this was the procedure used to produce Figure 3.15. [10] However, the data was comparable to the data from Figure 3.13 for **6**, rather than what had been expected.

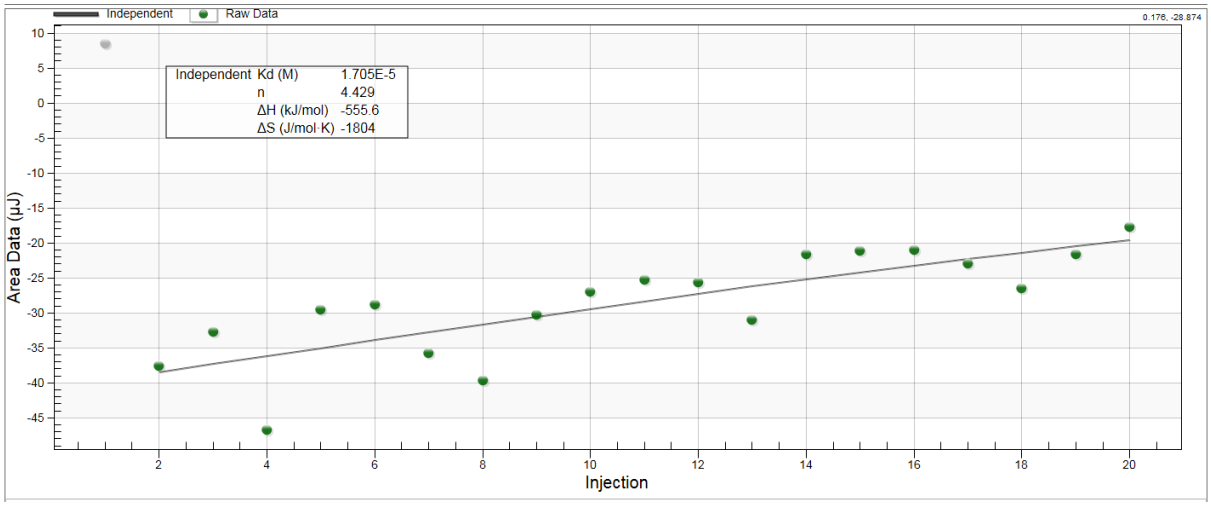

Figure 3.15 Trial #4: Processed ITC data for 50 µM of caffeine into 5 µM AS.

Given that interchanging the location of the protein and the drug had worked well in the case of **6**, this was applied to the caffeine-AS titration (trial #5 table 3.1). In addition to this, titration of AS into caffeine-diazirine was repeated again to confirm the results of the first titration (trial #6 table 3.1). Unfortunately, trial #5 from table 3.1 resulted in a horizontal linear line as seen in Figure 3.16, with trial #6 having similar results (data not shown). The difference in results between trial #3 and trial #5 led to the hypothesis that there may have been buffer mismatch in trial #3 (AS injected into compound **6**, Figure 3.14) between the control and the experimental runs. Whereas the control and experimental runs were prepared and completed on the same day and in the same way for trial #5, this was not the case for trial #3. The control for trial #3 was completed previously (several months prior) and it is unknown if their preparation of the AS stock made use of 1 mM NaOH initially to solubilize the protein before its dilution (refer to the ThT experimental section for further information on the use of 1 mM NaOH with AS) or if the concentration of NaOH may have varied in previous work. Therefore, it is possible that the changes in heat seen in Figure 3.14 (trial #3) were a result of NaOH dilution and not drug-protein interaction.

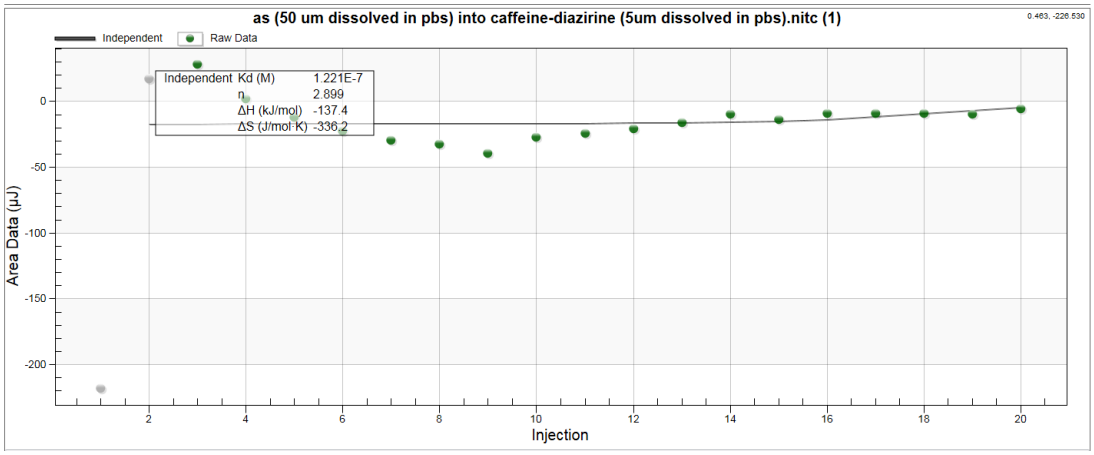

Figure 3.16 Trial #5: Processed ITC data for 50 µM of AS into 5 µM compound 6 (caffeine-diazirine).

To test the most recent hypothesis, trial #7 from table 3.1 was performed which eliminated the use of other solvents in the preparation and dilution of AS (i.e. 1 mM NaOH). Again, the data from this final experiment was a horizontal, linear line (data not shown) as observed for trial #5 (Figure 3.16), indicating that buffer mismatch likely produced the angled linear line from earlier experiments (trials # 1 and #4, Figures 3.13 and 3.15 respectively). This is reasonable because there would have been a minimal amount of NaOH in the well containing AS for the experimental run in the samples for trials #1 and #4, but NaOH would not have been present in the control. Unfortunately, these results also indicate that the interaction between the drug and AS is either not occurring or not observable through ITC.

Previous work has demonstrated binding of AS to caffeine though ITC. [10] However, the studies performed herein have isolated a potential issue that may have caused confusion in previous work. Generally, the literature recommends the use of NaOH for the storage of proteins used in ThT assays, and AS has been prepared in this way as well. [12,94] NaOH was used for storage of AS in early work in this study which led to buffer mismatch in some ITC runs. This work was based upon work done by others within the same lab, meaning that NaOH may have been used in previous ITC studies. There is no way of knowing when the use of sodium hydroxide was adopted; however, this may have contributed to the confusing ITC results in the past.[10] Whether these issues can be resolved with the current set up is unknown, however it may be useful to investigate alternative methods of measuring ligand-AS binding.

3.3 Thioflavin T Assay

ThT assays, commonly used to observe the effects drugs have on aggregation of proteins with beta sheet character, were chosen to observe for the effect that the drugs have on AS aggregation.

3.3.1 Development of a Time-Course ThT Method

The original ThT assay protocol (J. Garcias, personal communication) employed in this work was one that was developed to monitor AS aggregation over time. This approach was taken as there was interest in developing an assay which monitored the changes in fibrillation over time in a quick and reproducible manner. This meant the ideal protocol would be finished in a single workday. The other purpose in performing the assay over time was to reduce the amount of protein over the course of this work, consequently saving on cost. Also due to the cost of AS, AS was not manipulated as a variable. However, the initial concentration of AS chosen for the assay was based upon correspondence with other researchers in the field of PD who have made use of the ThT assay in the past (M. J. Daniels, personal communication).

The assay initially took place by aggregating AS in a 96-well plate with a cover and a small polystyrene bead. The plate was then heated and shaken at 300 rpm over the course of seven hours to test the effects of a drug. Readings were to be done hourly to obtain the data. Otherwise, the experimental conditions are listed in table 3.2, along with all subsequent time-course ThT modifications made in the order they were completed.

Table 3.2 Experiments run to develop a time-course ThT method. AS concentration and ThT concentration refer to the stock concentration for each (50 µL of each was added to the wells). The heparin stock concentration was 75 µg/mL for experiments 1-4 and 1 mg/mL for 5 onward.

Experiment #	Drug	Drug [ ]	AS [ ]	AS Solvent	ThT [ ]	ThT Sovent	Heparin (µL)	Spike	Temperature (°C)	Time (hours)	Figure	Notes
1	Fluorinated caffeine	0 to 200 µM	2 mg/mL	NaOH	40 µM	2X PBS	7	No	30	5		Drug was not added
2	Fluorinated caffeine	0 to 200 µM	2 mg/mL	NaOH	40 µM	2X PBS	7	No	30	7		Drug was added at 5h
3	None	N/A	2 mg/mL	NaOH	40 µM	2X PBS	7	No	30	7		Technique was observed
4	Fluorinated caffeine	0 to 100 µM	2 mg/mL	NaOH	40 µM	2X PBS	7	No	30	24	3.17	Drug was added at 5h; 100 µM was repeated with 7 µL from 1 mg/mL heparin
5	None	N/A	2 mg/mL	NaOH	40 µM	2X PBS	0 to 20	No	30	22	3.18	
6	None	N/A	2 mg/mL	NaOH	40 µM	2X PBS	0 to 20	No	30	22		Equimolar HCl to NaOH added
7	None	N/A	2 mg/mL	NaOH	40 µM	2X PBS	20	No	30	20	3.20	Repeated in quadruplet
8	None	N/A	2 mg/mL	NaOH	40 µM	2X PBS	20	No	30	24		6.3 µL of 20 mM EDTA added
9	None	N/A	2 mg/mL	NaOH	40 µM	2X PBS	20	No	30	24		Equimolar HCl to NaOH added and mixed before pipetting into wells
10	None	N/A	2 mg/mL	NaOH	40 µM	2X PBS	20	No	30	24		Beads rinsed with water
11	None	N/A	2 mg/mL	1X PBS	40 µM	1X PBS	0 to 20	No	37	24	3.19	
12	None	N/A	2 mg/mL	1X PBS	40 µM	1X PBS	15	No	37	7	3.21	
13	None	N/A	2 mg/mL	1X PBS	40 µM	1X PBS	15	Yes	37	7	3.22	
14	1-aminoindan	0 to 200 µM	2 mg/mL	1X PBS	40 µM	1X PBS	15	Yes	37	7	3.23	
15	1-aminoindan	0 to 200 µM	2 mg/mL	1X PBS	40 µM	1X PBS	0	Yes	37	49	3.24	
16	cNDGA	0 to 200 µM	2 mg/mL	1X PBS	40 µM	1X PBS	5	Yes	37	24		
17	1-aminoindan	0 to 200 µM	2 mg/mL	1X PBS	40 µM	1X PBS	5	Yes	37	24	3.27	
18	1-aminoindan	0 to 200 µM	2 mg/mL	1X PBS	40 µM	1X PBS	5	No	37	24	3.28	
19	1-aminoindan	0 to 200 µM	2 mg/mL	1X PBS	40 µM	1X PBS	2	Yes	37	48	3.29	
20	1-aminoindan	0 to 600 µM	2 mg/mL	1X PBS	40 µM	1X PBS	5	Yes	37	24	3.30	
21	cNDGA	0 to 500 µM	2 mg/mL	1X PBS	40 µM	1X PBS	5	Yes	37	24	3.26	
22	None	N/A	None	N/A	40 µM	1X PBS	5	Yes	37	24		Equivalent volume PBS added (50 µL) to AS removed
23	None	N/A	None	N/A	40 µM	1X PBS	5	No	37	24		Equivalent volume PBS added (50 µL) to AS removed
24	C8-6-I	0 to 500 µM	2 mg/mL	1X PBS	40 µM	1X PBS	5	Yes	37	24	3.32	
25	C8-6-N	0 to 500 µM	2 mg/mL	1X PBS	40 µM	1X PBS	5	Yes	37	24	3.33	
26	None	N/A	2 mg/mL	1X PBS	40 µM	1X PBS	0	No	37	96	3.34	
27	cNDGA	100, 500 µM	2 mg/mL	1X PBS	40 µM	1X PBS	0	No	37	96	3.34	
28	C8-6-I	100, 500 µM	2 mg/mL	1X PBS	40 µM	1X PBS	0	No	37	96	3.34	
29	C8-6-N	100, 500 µM	2 mg/mL	1X PBS	40 µM	1X PBS	0	No	37	96	3.34	

Optimization of the experiments in this assay was extensive. Initial experiments carried out by me (Figure 3.17) did not result in aggregation as compared to previous data (J. Garcias, personal communication). Given the ability of the compounds in the study to rescue yeast cell growth in a PD model, the protocol called for the drug of interest to be added at the 5-hour time point

(experiments 2 and 4 from table 3.2).[10] Due to the assay failing, this was abandoned early in the development of the protocols where drugs were being tested.

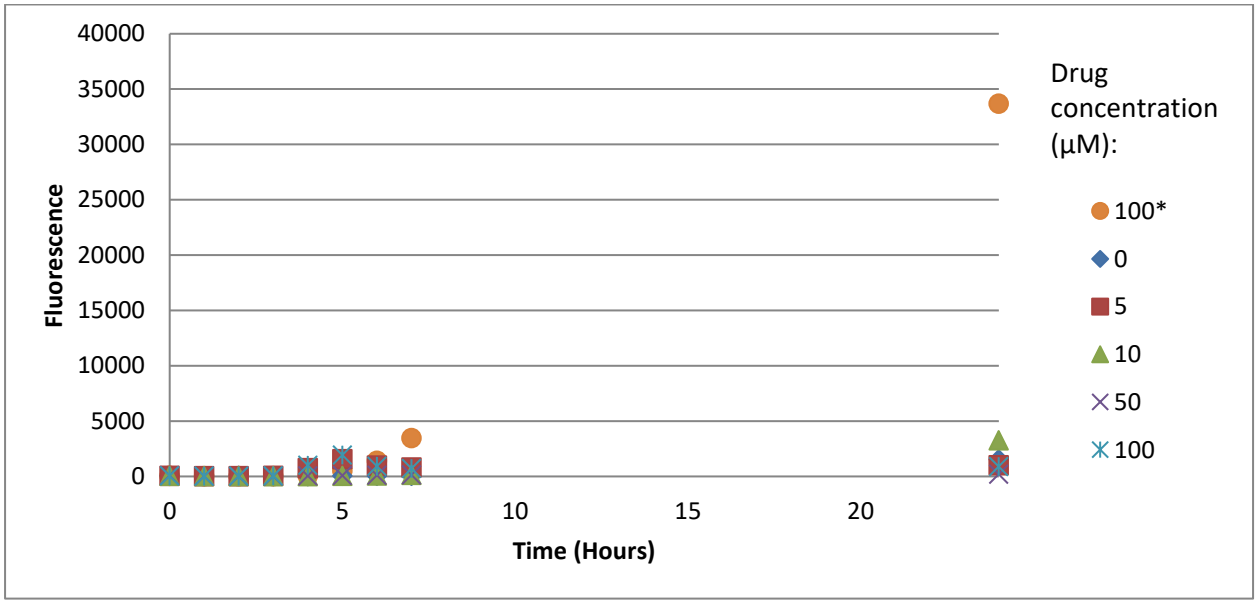

Figure 3.17 There is more aggregation of AS with more heparin. Graph shows changes in ThT fluorescence in the presence of varying quantities of fluorinated caffeine derivative. The * denotes the well using 100 µM fluorinated caffeine with a final heparin concentration of 64 µg/mL, as opposed to the final concentration 5 µg/mL heparin in the other wells. Fluorescence measured with excitation/ emission 444/ 484 nm.

In an effort to improve the assay, several changes were made that had little to no impact on the assay. First, HCl was used in two experiments to try to resolve issues with aggregation (experiments #6 and #9 from table 3.2). The aggregation did not improve because of these experiments though (data not shown). Second, EDTA was used in another attempt at improving the assay (experiment #8 from table 3.2). Again, there was no resulting improvement in aggregation with this experimental manipulation (data not shown). Third, the plastic beads used in the study were rinsed with buffer (experiment #10 from table 3.2). Not surprisingly, there was no improvement in the assay with this modification as well (data not shown).

Both the temperature and the use of NaOH were altered simultaneously as part of optimization (experiment #11 from table 3.2). The time needed to reach maximal aggregation improved as demonstrated by the change from figure 3.18 to figure 3.19. Due to the simultaneous modifications, it is impossible to say to what extent either change helped or if one of the two modifications had no effect.

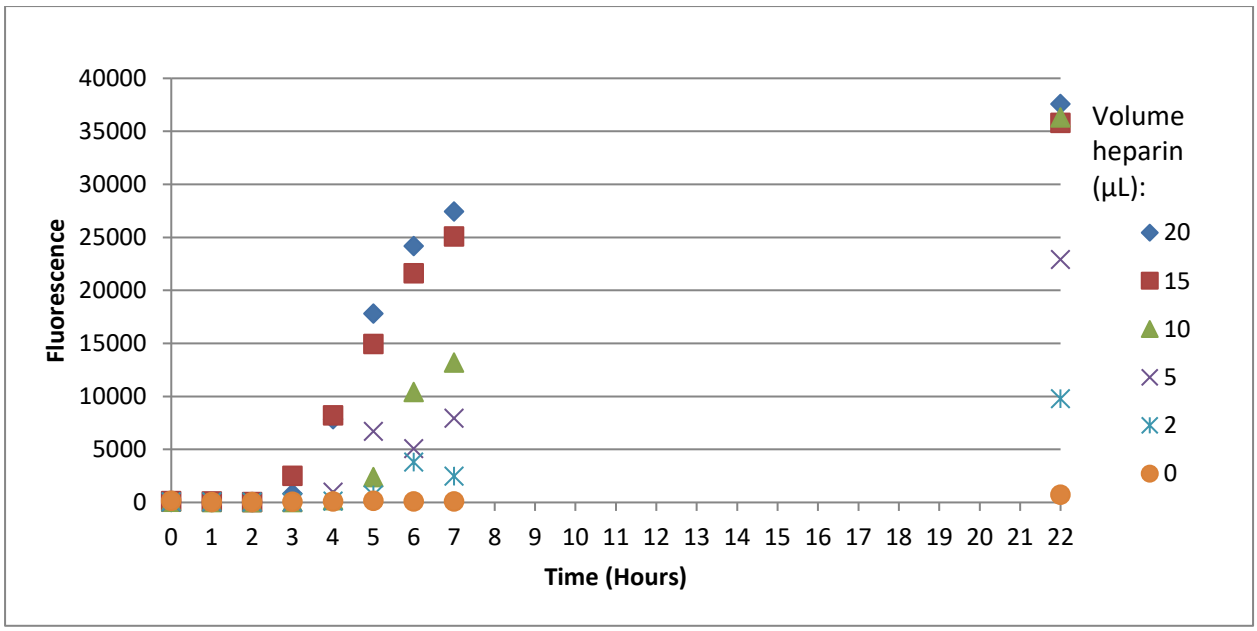

Figure 3.18 Using 20 µL of 1 mg/mL gives the fastest aggregation from varying amounts of heparin. Graph shows changes in ThT fluorescence in response to increasing volumes of heparin added to the assay wells. The legend corresponds to the number of µL of 1 mg/mL heparin used in each well. Fluorescence measured with excitation/ emission 444/ 484 nm.

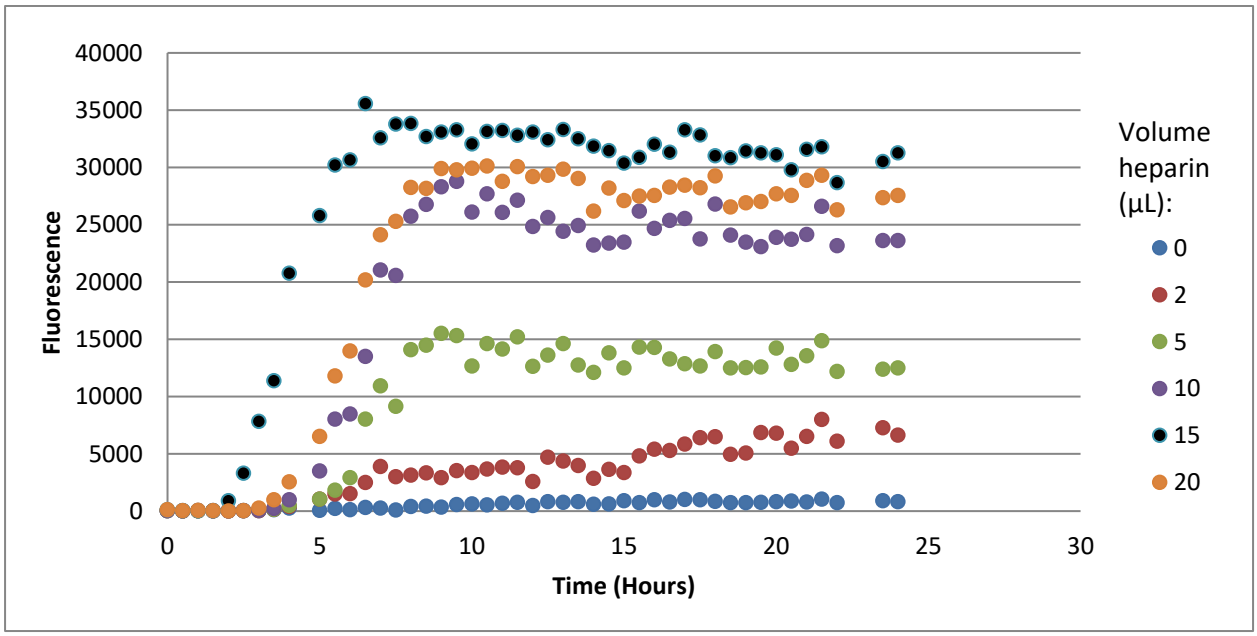

Figure 3.19 Re-optimization of assay with new conditions suggests that 15 µL of 1 mg/mL heparin should be used instead of 20 µL of 1 mg/mL heparin. Graph shows changes in ThT fluorescence in response to varying quantities of 1 mg/mL heparin under new conditions of 37 °C and PBS. The legend is the number of µL of 1 mg/mL heparin used in each well. Fluorescence measured with excitation/ emission 444/ 484 nm.

The change in temperature and buffer also improved another aspect of the assay. Reproducibility between wells improved when the conditions in figure 3.20 are changed to those from figure 3.21. However, these results are not entirely comparable as the quantity of heparin is increased in figure 3.20.

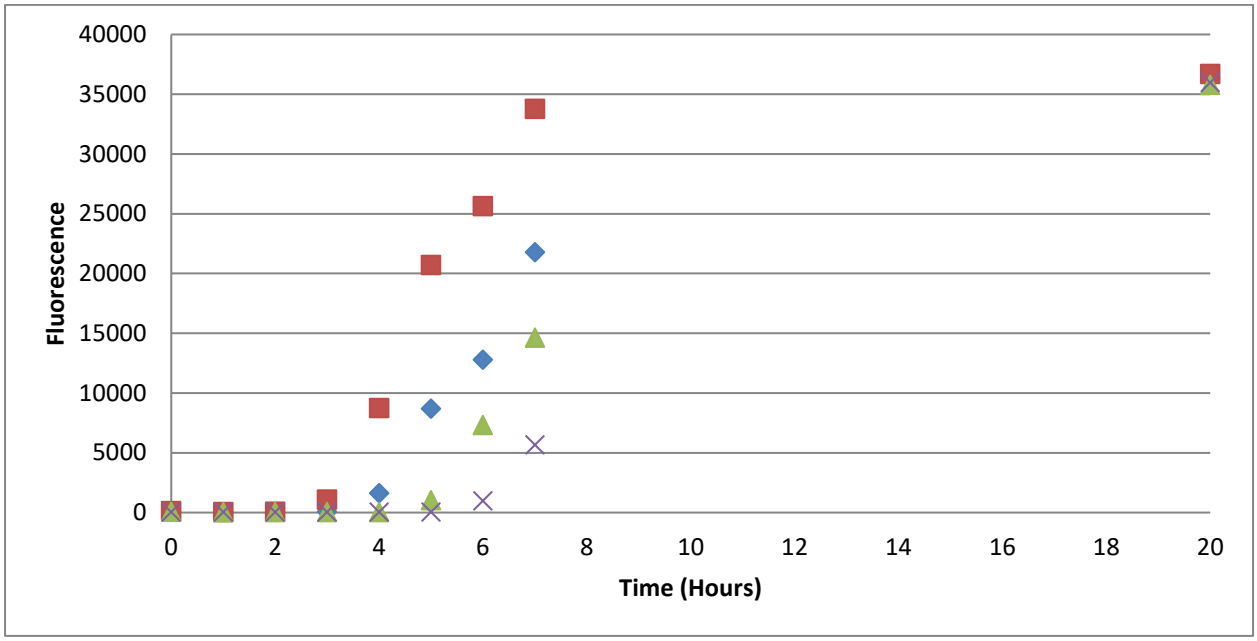

Figure 3.20 Variation is significantly different between identically prepared wells. Graph shows changes in ThT fluorescence over time in four wells prepared the same way with 20 µL of 1 mg/mL heparin. Each symbol (■, ◆, ▲, ×) represents a different well. Fluorescence measured with excitation/ emission 444/ 484 nm.

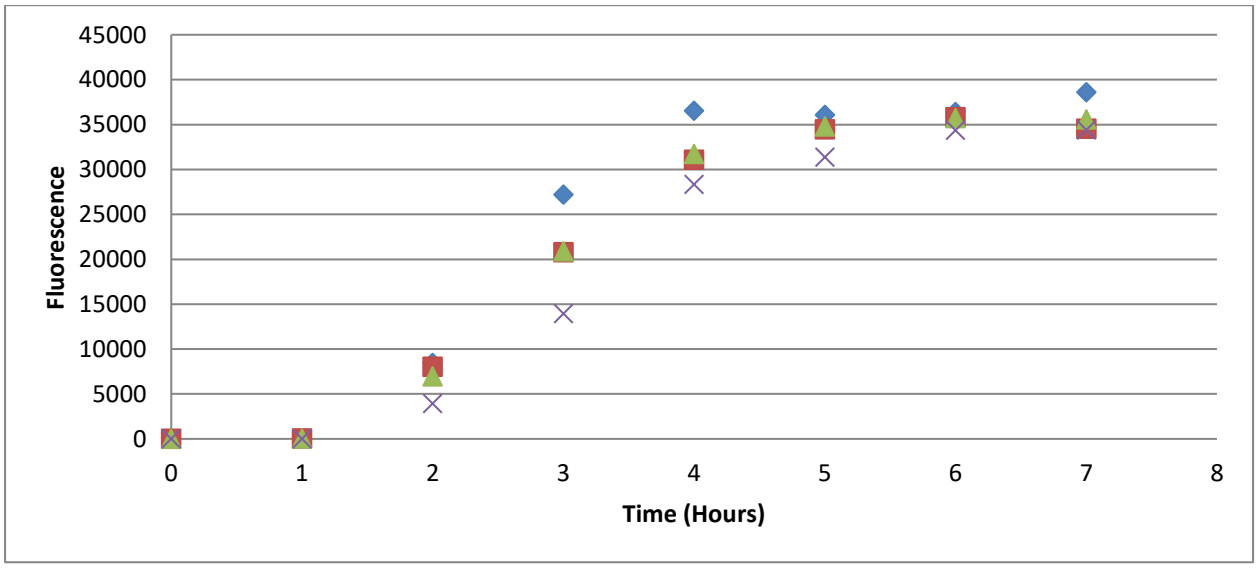

Figure 3.21 The increase in temperature improved assay reproducibility. Graph shows

changes in ThT fluorescence in response to new assay conditions with 15 µL of 1 mg/mL heparin repeated in quadruplet. Each symbol (■, ◆, ▲, ×) represents a different well. Fluorescence measured with excitation/ emission 444/ 484 nm.

Spiking the wells with protein was the first of the two variables to improve the assay the most. This involved pipetting a small volume of some previously aggregated protein into the experimental wells. There was a corresponding improvement in reproducibility during the period in which the fibrils were growing as seen when comparing figures 3.21 to figure 3.22.

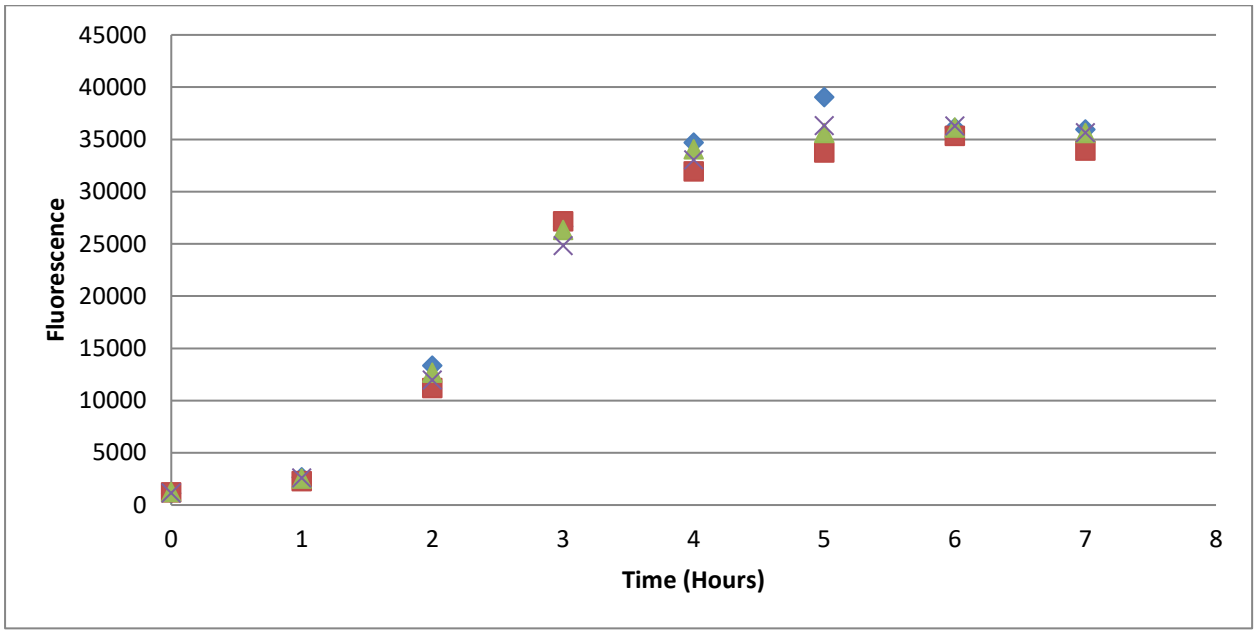

Figure 3.22 The addition of AS aggregate spike improves reproducibility. Graph shows changes in ThT fluorescence when previously aggregated protein is added along with the new conditions which include 15 µL of 1 mg/mL heparin repeated in quadruplet. Each symbol (■, ◆, ▲, ×) represents a different well. Fluorescence measured with excitation/ emission 444/ 484 nm.

Heparin was the second of the two most effective variables at improving the assay. Heparin sped up the rate of aggregation and increased the reproducibility as well. The increase in aggregation rate can be visualized in figure 3.19. Improvement to reproducibility was observed in data from experiments 14 and 15 table 3.2 (figures 3.23 and 3.24).

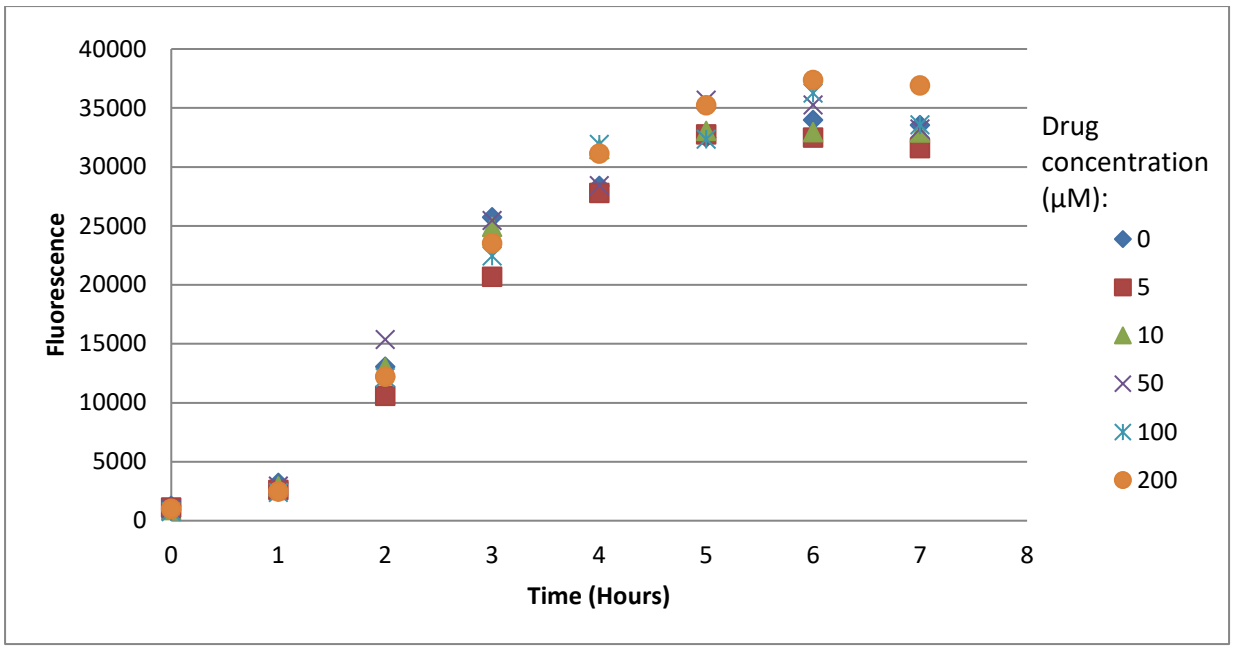

Figure 3.23 Little observable changes in response to the use of 1-aminoindan in the newly designed seven-hour long ThT assay. Graph shows changes in ThT fluorescence in response to the addition of 1-aminoindan. The legend is the concentration of 1-aminoindan in µM used in each well. Fluorescence measured with excitation/ emission 444/ 484 nm.

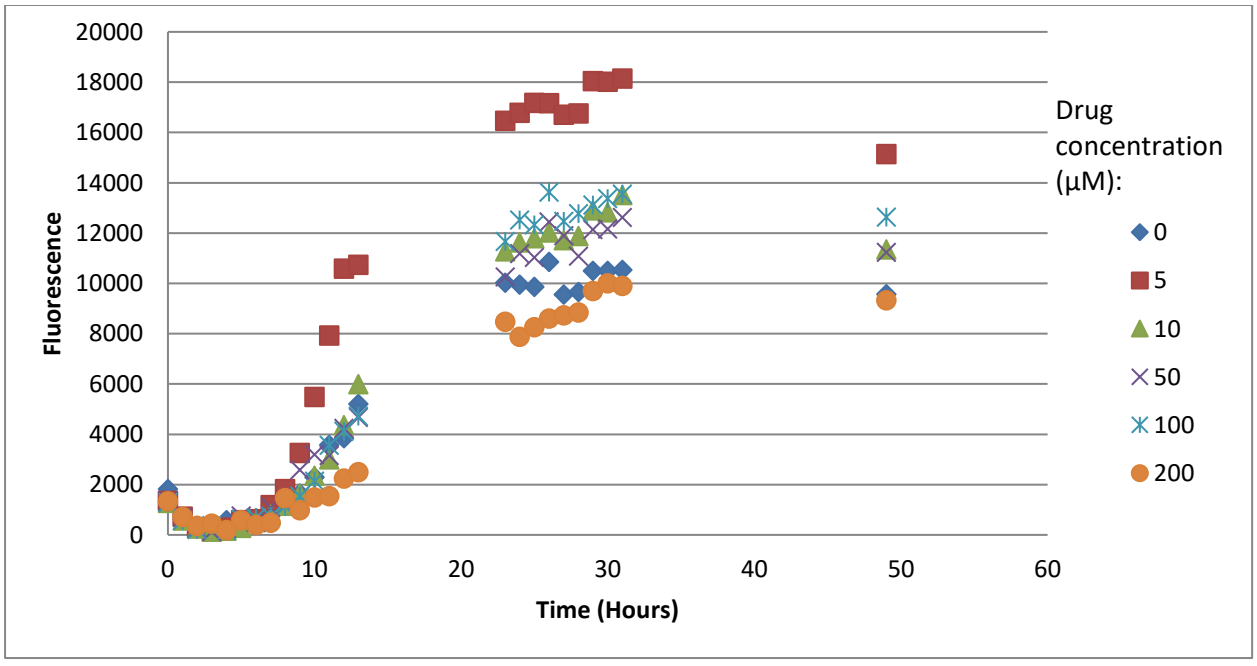

Figure 3.24 The removal of heparin from the seven-hour long ThT assay with 1-aminoindan does not result in dose-dependent effects for 1-aminoindan. Graph shows changes in ThT fluorescence in response to the aforementioned conditions. The legend is the concentration of 1-aminoindan in µM used in each well. Fluorescence detected with excitation/ emission 444/ 484 nm.

Negative controls were run to confirm there was no significant background fluorescence in experiments #22 and #23 from table 3.2. Fluorescence was not significant in either control (data not shown).

Also, a positive control was used for the assay, cyclized nordihydroguaiaretic acid (cNDGA) (Figure 3.25). cNDGA is known for its ability to inhibit the aggregation of AS in ThT assays. [95] cNDGA would result consistently in a dose-dependent reduction of fibril growth in the assays in which it was used. Figure 3.26 best depicts the results; however, cNDGA consistently worked in a variety of other conditions (data not shown).

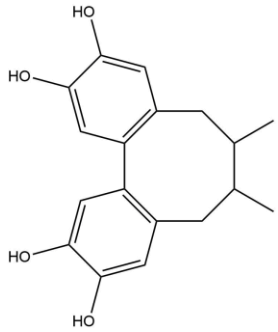

Figure 3.25 Chemical structure of cyclized nordihydroguaiaretic acid (cNDGA).

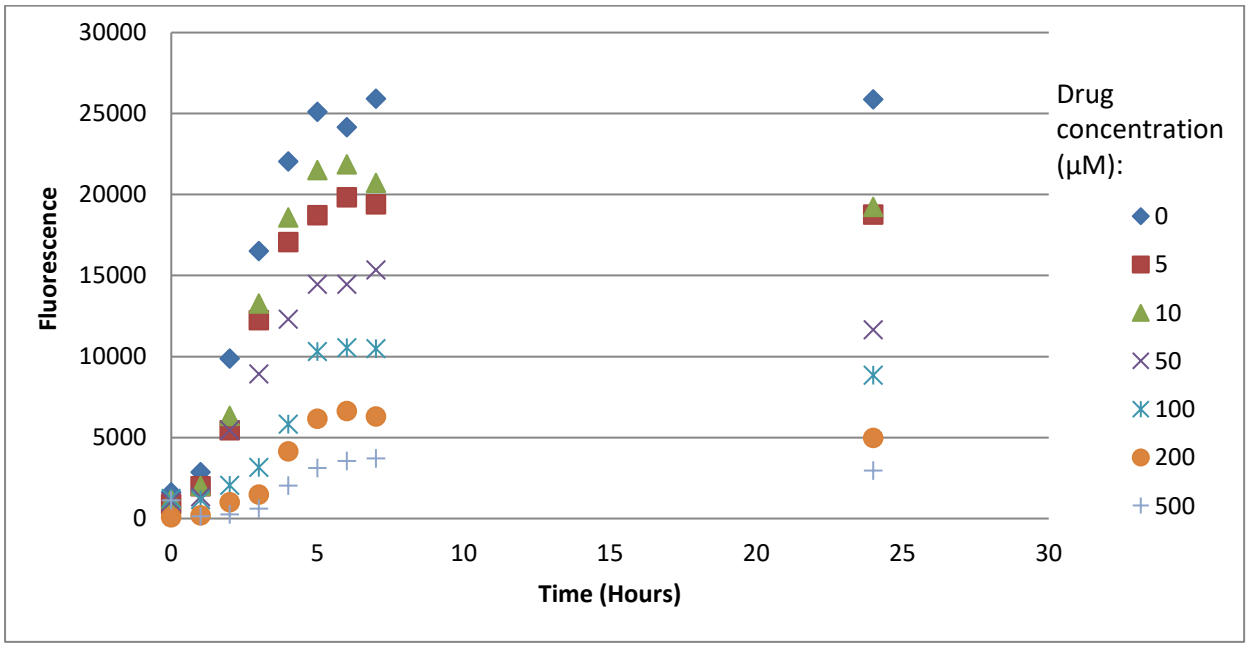

Figure 3.26 Dose-dependent changes in response to cNDGA assay repeated with an additional well at 500 µM cNDGA. Graph shows changes in ThT fluorescence with the same conditions as figure 3.27 in addition to the well with 500 µM cNDGA. The readings were repeated three times

in this assay at each time point and averaged. The legend is the concentration of cNDGA in μM used in each well. Fluorescence detected with excitation/ emission 444/ 484 nm.

Unlike cNDGA, 1-aminoindan did not produce dose-dependent changes in AS aggregation in the same conditions as figure 3.26 (Figure 3.27). The lack of dose-dependent changes was consistent in a variety of other conditions (Figures 3.28-3.30). For example, figure 3.29 shows that 100 μM 1-aminoindan has the most aggregation and 200 μM has the least. The remaining quantities of 1-aminoindan (5, 10, 50 μM) and the control were arbitrarily positioned in between, whereas the data for cNDGA (Figure 3.26) is in the following order: the control, 5 and 10 μM, 50 μM, 100 μM, 200 μM, and 500 μM.

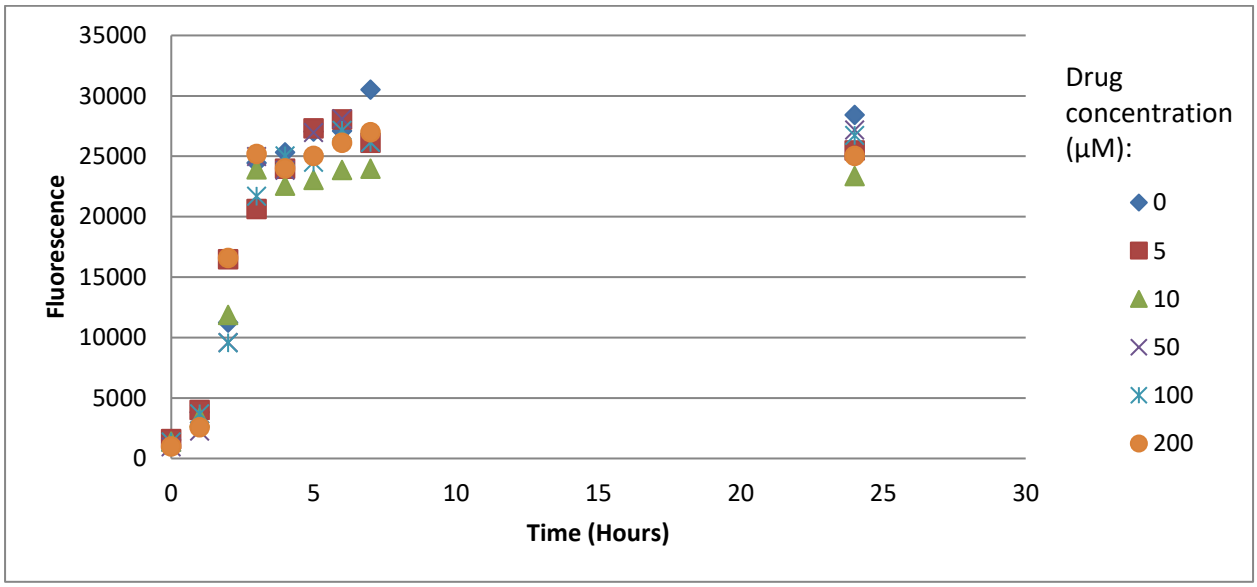

Figure 3.27 No dose-dependent response to the use of 1-aminoindan in the newly modified assay conditions. Graph shows changes in ThT fluorescence resulting from the use of 1-aminoindan, spike, and 5 μL of 1 mg/ml heparin. The legend is the concentration of 1-aminoindan in μM used in each well. Fluorescence detected with excitation/ emission 444/ 484 nm.

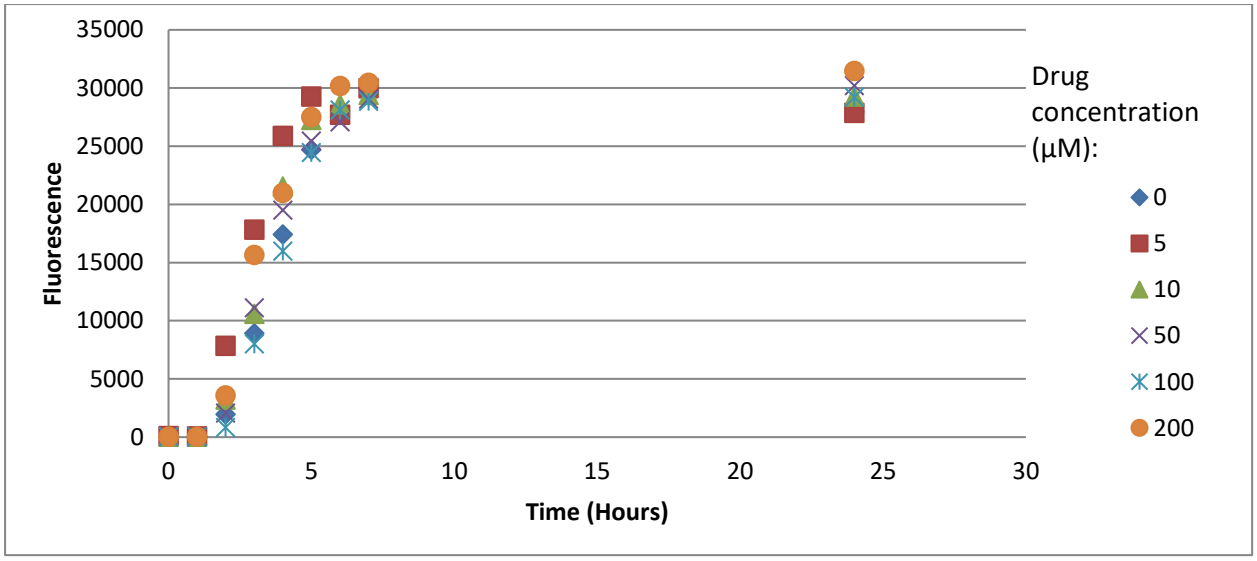

Figure 3.28 Removal of the spike from the same conditions as the previous assay does not result in an observable dose-dependent response. Graph shows changes in ThT fluorescence in response to the use of varying concentrations of 1-aminoindan, no spike, and 5 µL of 1 mg/ml heparin. The legend is the concentration of 1-aminoindan in µM used in each well. Fluorescence detected by excitation/ emission 444/ 484 nm.

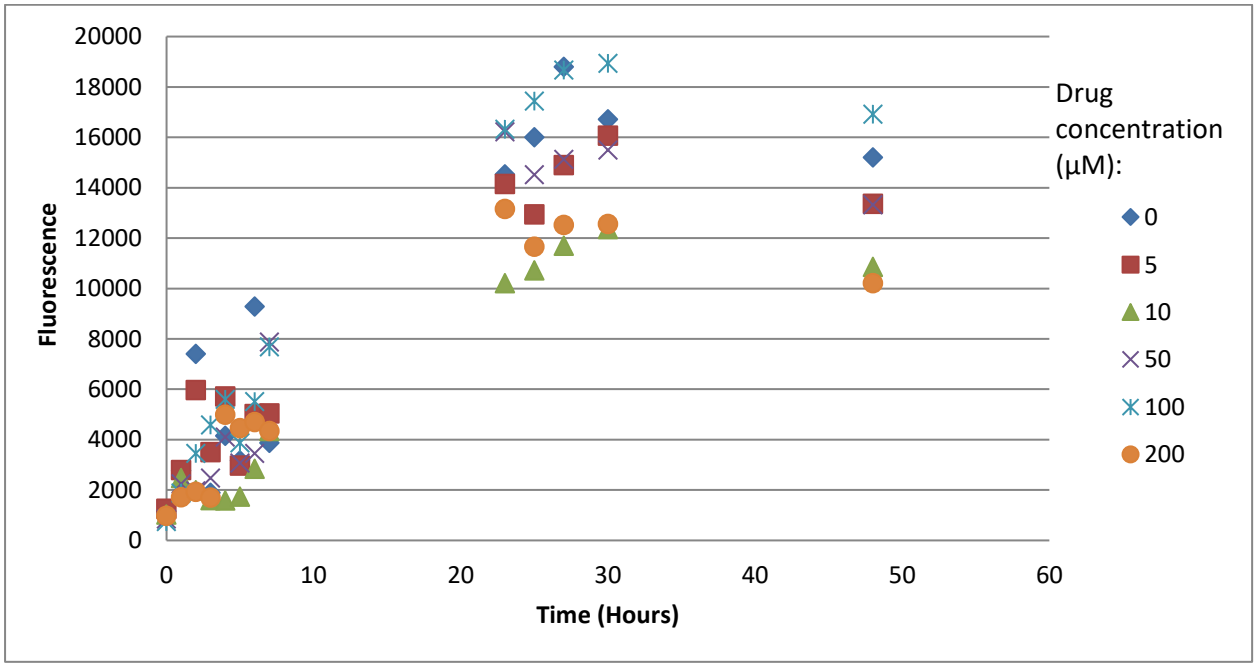

Figure 3.29 The re-introduction of the aggregated protein spike and the reduction of heparin from 5 to 2 µL of 1 mg/ml stock does not produce a dose-dependent response to 1-aminoindan. Graph shows changes in ThT fluorescence over time in response to the new conditions. The readings were repeated three times in this assay at each time point and averaged. The legend is the concentration of 1-aminoindan in µM used in each well. Fluorescence detected by excitation/ emission 444/ 484 nm.

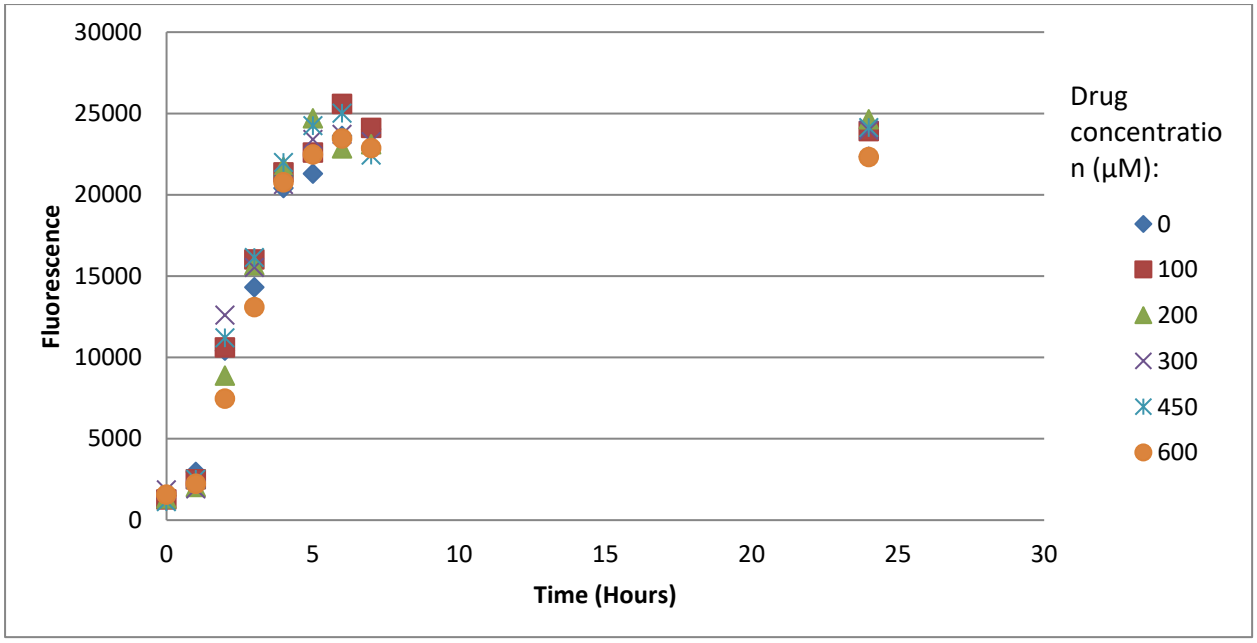

Figure 3.30 The return to previous assay conditions with an increase in the maximum 1-aminoindan concentration used does not produce dose-dependent ThT fluorescence changes. The readings were repeated three times in this assay at each time point and averaged. The legend is the concentration of 1-aminoindan in µM used in each well. Fluorescence detected with excitation/ emission 444/ 484 nm.

Early experiments made use of a fluorinated caffeine derivative (table 3.2 experiments 1-4). Due to its structural similarity to caffeine (Figure 3.31), it was hypothesized to reduce AS aggregation, but none was observed with early experimental conditions (Figure 3.17). The caffeine derivative was not employed in the final time-based assay conditions, as such no certain conclusion is possible.

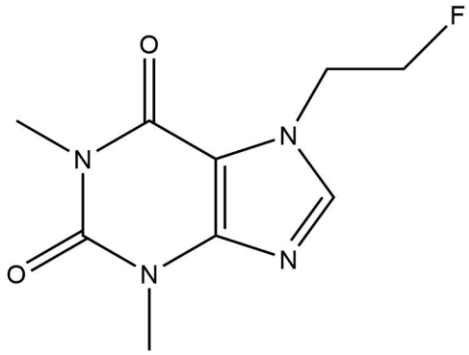

Figure 3.31 Chemical structure of the fluorinated caffeine derivative being used in early ThT studies.

Finally, the compounds C_8-6-I and C_8-6-N were tested for anti-fibrillogenic activity in the finalized conditions. There was no corresponding dose-dependent reduction in fibrils (Figures 3.32 and 3.33). This was consistent without heparin or a protein spike as well, but under the same conditions cNDGA was still effective (Figure 3.34).

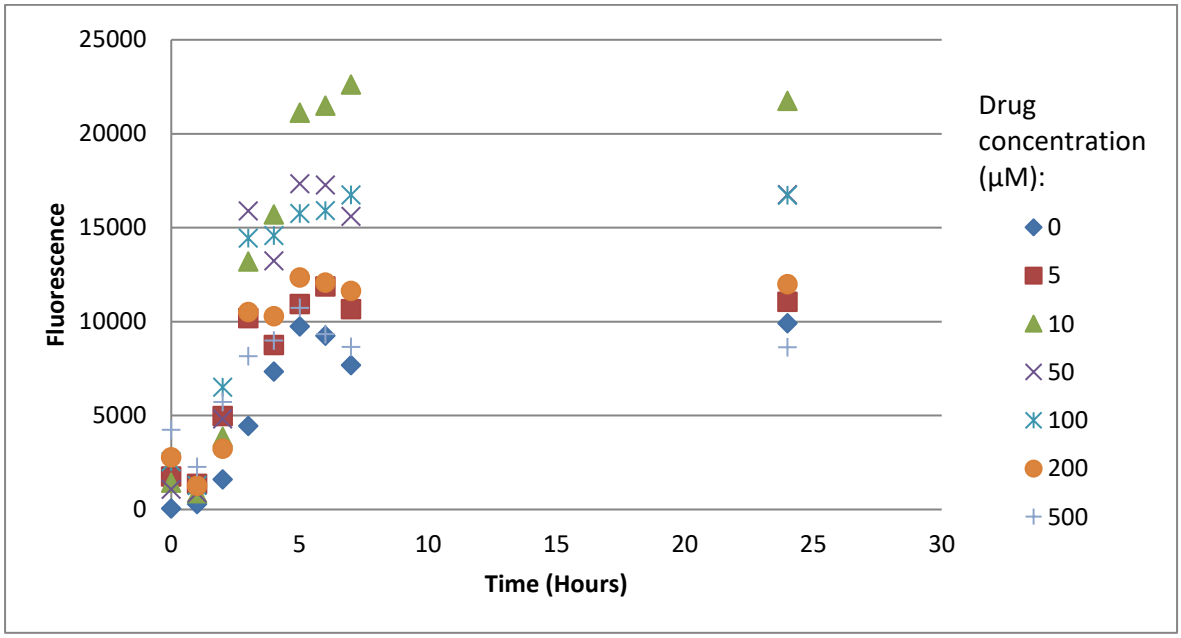

Figure 3.32 No dose-dependent response for C8-6-I with the finalized seven-hour long assay conditions. Graph shows changes in ThT fluorescence in response to the conditions used. The readings were repeated three times in this assay at each time point and averaged. The legend is the concentration of C_8-6-I in μM used in each well. Fluorescence detected with excitation/ emission 444/ 484 nm.

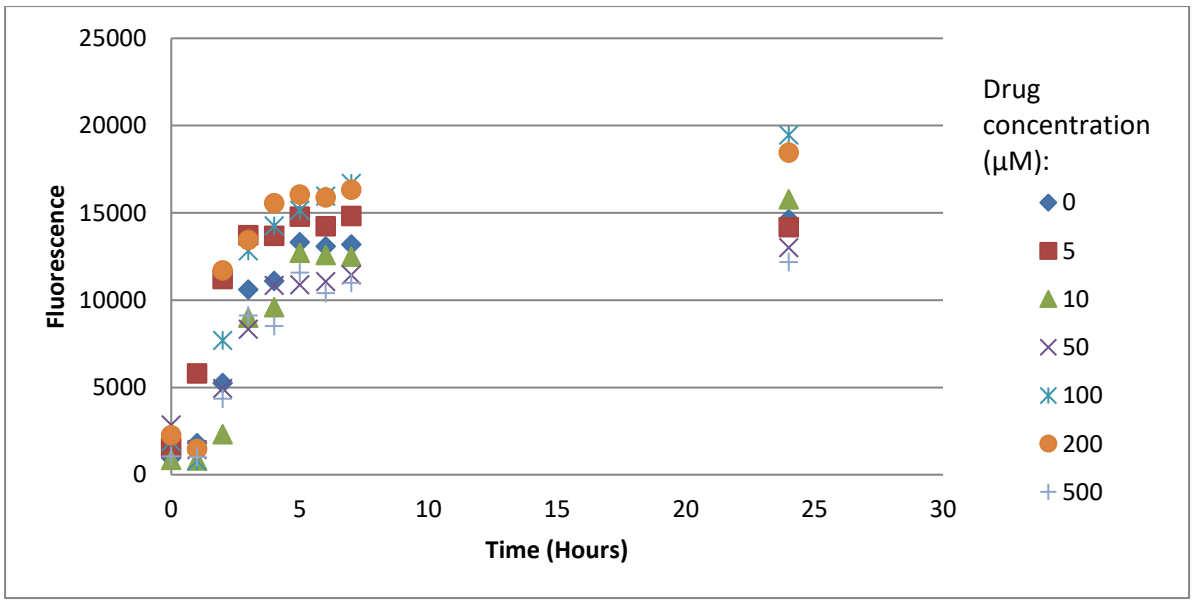

Figure 3.33 No dose dependent response for C8-6-N in the finalized assay conditions. Graph shows changes in ThT fluorescence in response to the conditions used in the assay. The readings were repeated three times in this assay at each time point and averaged. The legend is the concentration of C_8-6-N in µM used in each well. Fluorescence detected with excitation/ emission 444/ 484 nm.

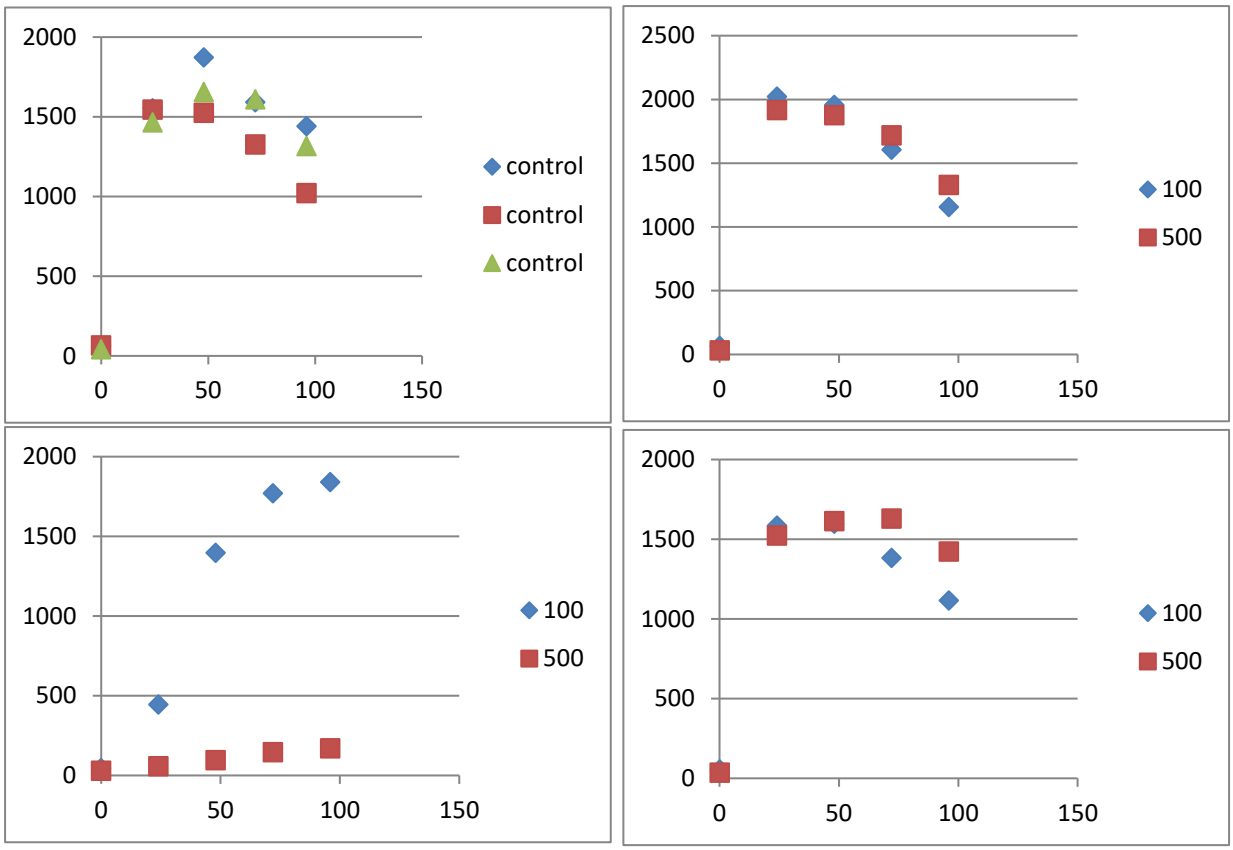

Figure 3.34 Confirmation of results from previous assays without the use of either heparin or a protein spike. No changes observed for C_8-6-I or C_8-6-N in comparison to the control, but the cNDGA positive control still shows changes in fluorescence. Changes in fluorescence for different drugs at 100 and 500 μM as well as a control. The control was run in triplicate. The experimental wells were not. The y-axis corresponds to the fluorescence in arbitrary units. The x-axis corresponds to hours. Top left is the control. Top right is the C_8-6-I. Bottom left is cNDGA. Bottom right is C_8-6-N. Fluorescence measured with excitation/ emission 444/ 484 nm.

It was possible 1-amnioindan might not have had observable effects as the effects resulting from the monomer compounds (i.e. 1-aminoindan, nicotine, caffeine) were not as strong as they were with the bifunctional compounds (i.e. C_8-6-C_8, C_8-6-I, C_8-6-N).[79] However, the bifunctional compounds should have had observable effects in figures 3.32 and 3.33. Thus, it was possible the heparin was impairing the ability to observe any apparent changes to fibrillation. Removal of heparin did not ameliorate the results in figure 3.34, so the transition was made to a single time-point method for the ThT assay to retest the most recent observation. This decision was also supported by some of the limitations of the time-course ThT assay methodology.

The first potential limitation of this experimental design was the addition of fibril seeds to reduce the variation between replicates. This methodology is not new.[48,50] This may be desirable

in some cases, especially ones which monitor aggregate development over time, although it may be a limitation in others as it may remove an essential step in aggregation from the experiment.

The use of heparin was the other potential limitation to the time-course assay developed. Heparin has been tested for pro-aggregation effects on AS previously. [94,96] This is confirmed again in the current work as the addition of heparin results in faster aggregation of AS. Interestingly, an increase in final fluorescence values was also observed in accordance with the addition of increasing amounts of heparin (Figure 3.19). One possible explanation for this phenomenon is that heparin may alter the way AS fibrils form in the assay. Alternatively, heparin may alter the way ThT can interact with the developing AS fibrils. Analyzing the cause for this observation was beyond the scope of the research question. Therefore, it was not pursued any further. However, there is evidence to support the integration of heparin into the fibrils and different fibril morphology with heparin. [94] Thus, the use of heparin may be criticized on the basis of producing a ThT assay that does not accurately represent PD pathology. Another potential criticism for a heparin-based assay is that the effects may only occur in the presence of heparin. Therefore, applying heparin to the ThT assay should be considered carefully in future work.

In summary, the goal of achieving a time-course ThT assay was considered complete due to the success with the positive control (Figure 3.26). Unfortunately, 1-aminoindan, C_8-6-I, and C_8-6-N did not demonstrate the ability to inhibit AS aggregation with the time-course method. Due to the limitations of this time-course method, it was still possible these compounds had an effect, so a final change in methodology was the best option to obtain clearer results.

3.3.2 Development of a Single Time Point ThT Method

The methodology for the following protocol was followed from the literature. [95] This procedure only measured the end point of AS aggregation. Unfortunately, this change meant that the assay requires more protein than the time-course assay. This was done with the goal of reducing the time required for the assay to take place (M. J. Daniels, personal communication). However, the experimental set up was far simpler (i.e. no heparin, spike, or ThT present) and allowed for the use of statistics to compare the control to the drug, thereby making it less qualitative and open to criticism. The methods section details the full, finalized procedure for the single time point ThT method. Switching to the single time point method required some optimization prior to reaching the final procedure.

Early attempts at completing the single time point method had to be optimized on three fronts. The evaporation of solvent was the first problem encountered with the set up. Originally, the vials used were 0.5 mL microcentrifuge tubes as these fit into the thermomixer on their own. Due to evaporation of solvent in the tube, it was decided to transition to smaller tubes (0.25 mL or so) to reduce the surface area. To supplement this modification, parafilm was used to keep the lids shut. The parafilm also served a dual purpose as it was used to anchor the smaller microcentrifuge tubes into larger vials.

Larger vials were required to hold onto the small microcentrifuge tubes as they were not capable of staying in the thermomixer on their own otherwise. This led to the second issue encountered with the new assay: heat transfer. With the small tube seated in the larger vial, there was a large gap between the two. This resulted in slower aggregation for the assay. Therefore, sand (Ottawa sand from fisher scientific) was used to resolve the issue. The sand was used to fill the space between the two vials, resulting in the aggregation returning to approximately 80% of the original value before the transition to the smaller tube.

The final modification to the assay was to extend the duration of the assay in order to achieve maximum aggregation. As seen in the time-based ThT assay, the growth phase of the fibrils could vary significantly between trials (refer to Figure 3.20). This was the same in this assay as well. Three controls were run, and their variation was considered statistically significant as per a one-way ANOVA ($P=0.0017$). However, when the assay was extended to five days, there was no statistically significant differences between the wells (P-value > 0.05). Thus, a five-day incubation time was chosen going forward as it allowed for the assay to reach its end point.

In terms of establishing a single time point based ThT assay, all three of these conditions should be optimized. This work was based upon the work of others, and evidently, there are differences in the performance of the assay. Optimization of the assay is recommended prior to testing of drugs due to these differences. Furthermore, optimization prior to drug testing would save on costs as there will be less protein wasted overall.

Finally, the drugs of interest were tested in two batches. In the first group, every drug (or control) was run in triplicate and then pipetted in triplicate for readings after the five-day incubation period (see methods section for a succinct description of assay conditions). The drugs of interest in this experiment were caffeine, C_8-6-C_8, and C_2D_2. The control wells in this assay were consistent (P-value > 0.05) with the data from the optimization phase of assay development. Comparing the

drugged vials to the control vials with a t-test assuming equal variance suggests no difference between control wells or drug wells (P-value > 0.05). Two controls were run for the single time point ThT assay which measured free AS both in the presence and the absence of ThT. Neither of these two controls had any significant fluorescence.

The same results were obtained with the second set of compounds used in the single time point assay. Caffeine-diazirine, nicotine-diazirine, 1-aminoindan diazirine, C_8-6-I, 1-aminoindan, and (S)-nicotine were not significantly different from the control when comparing with a t-test assuming equal variance (P-value > 0.05). Again, the variation between control vials was not significant when compared with a one-way ANOVA (P-value > 0.05).

All drugs of interest, both monomers and bifunctional agents, were previously shown capable of rescuing yeast cell growth in a yeast cell model overexpressing AS. [10] This was hypothesized to occur though direct interaction with AS protein as ITC demonstrated their ability to interact with AS. Unfortunately, the results from the ThT assays support the null hypothesis.

There was no observed reduction in AS aggregation as shown by ThT in this work, except for cNDGA which was the positive control. The results were consistent in a variety of assay conditions (i.e. both the time-based and single point ThT assays) for both the positive control and the drugs of interest. In contrast to the drugs in this work, cNDGA had been used in previous ThT assays. [95] The results herein support the conclusion that the molecules tested do not inhibit AS aggregation through a direct mechanism. However, this does not eliminate the possibility of the drugs affecting aggregation though alternative cellular pathways that would in turn prevent or reduce aggregation. This was even speculated as a possibility in previous work and may be worth investigating further in the future. [10]

All the tested compounds had been observed to cause conformational changes to AS when analyzed via nanopore. [8,10] It may be that the conformational changes do not affect aggregation but rather some other property of AS in yeast cells that is protective.

In congruence with the results for the monomers and bifunctional agents, all the diazirine probes synthesized in the work did not inhibit AS aggregation in the ThT assay. The implication is that the addition of the diazirine linker does not affect the lack of activity. However, as there was no activity observed for the monomers or bifunctional compounds, it is difficult to say to what extent the linker affects the way the molecules interact with AS.

3.4 Photoaffinity Labelling Studies

After characterizing the compounds of interest, the final step could be taken: photoaffinity labelling (PAL). The labelling protocol was decided upon by surveying the literature for similar photoaffinity labelling studies. As the purpose of this study is to determine the monomers' and bifunctional compounds' interaction to AS, PAL will be performed *in vitro*. Recent *in vitro* studies were used as benchmarks for experimental set up. *In vitro* studies made use of either buffer or water to solubilize protein for labelling. AS protein was lyophilized in TRIS•HCl 20 mM, NaCl 100 mM, pH 7.4 buffer prior to purchase, so this buffer was chosen for the procedure. Other studies have reported using the same buffer with no ill effects. [79,97] DMSO was used in limited amounts to solubilize the drug in similar studies, therefore this strategy was adopted whenever possible. [79,95,97] Concentrations of protein used ranged from 1 μM to 10 μM with the probe generally equimolar or in excess to the protein. [97–100] Given the cost of AS, 1 μM was used as a starting point. Also, a high probe: protein ratio (10:1) was chosen. Most studies had an incubation period prior to irradiation which averaged to half an hour. [97–99,101] UV exposure for diazirine-based photoaffinity labelling was brief. Half an hour was the maximum length of time in such studies. [97–101] Therefore, a 30-minute incubation period followed by a 30-minute irradiation period were used as starting points for labelling experiments. Light intensity from the source was frequently not measured. The few studies that did were far stronger (light flux: 5 mW/cm^2 and 14 mW/cm^2) than what could be achieved with the UVA lamp (light flux: 1.5 mW/cm^2). [97,101] However, this was acceptable as additional experiments at the lower intensity can be used to confirm activation of the diazirine probes by UV light.

3.4.1 PAL and LC-MS Analysis of Intact Protein

For the first attempt at PAL, the assay made use of a final concentration of 1 μM protein. Three controls were run along with the experimental vial. One control had AS but no probe, and it was exposed to UV light for the same duration as the experimental vial. The other two controls were prepared in the same way as the first two with the exception that they were not exposed to UV light. The probe used to test the protocol was the caffeine diazirine probe, added to the mixture in a tenfold excess. The duration of UV exposure was 30 minutes. Following UV exposure, the buffer was removed and the protein was re-suspended in 100 mM ammonium bicarbonate buffer before being subjected to LC-MS. Analysis of the intact protein did not demonstrate any labelling

of either the control or experimental vials with the diazirine probe. The protein exposed to UV light did not show any notable changes, implying the protein held up without injury under the light used.

To pressure the probe to label the protein, the next experiment increased the duration of UV light exposure to six hours. Again, another control was prepared with only AS protein present to confirm there were no negative effects on the protein related to UV exposure. The protein appeared to be intact following mass spectrometric analysis, but again, there was no labelling of the protein.

The following PAL experiment modified the ratio of probe and protein. This time, a one-hundred-fold excess of drug was used (100 μM CD). All other experimental parameters were kept consistent as the previous PAL experiment. Once mass spectrometry was performed, no labelling of the protein by the caffeine-diazirine was observed with the increase in probe concentration.

Given that the strength of the UV light used in PAL experiments in literature was largely ignored as a parameter measured, confirmation was desired that the probe was reacting with UV light. The following experiment run was two vials of only 100 μM CD in buffer, either exposed or not exposed to UV light. When analyzed with HPLC-MS, there was a peak on the DAD which corresponded to a compound with a m/z of 253. This peak was not present in the control; therefore, it was thought to be the probe that had reacted with water from the solvent, indicating that the probe was activated by UV light at the intensity it was applied during all previous experiments. Unfortunately, this also indicates that the issue with the labelling lies elsewhere.

3.4.2 PAL and LC-MS Analysis of Digested Protein

As options were limited to optimize the conditions further, the following attempt did not make any changes to the protocol. Instead, digestion was performed prior to HPLC-MS so that the proteins would be broken down into peptides, and hopefully, this could help with detection of the label on the peptides. This approach resulted in observation of a labelled peptide fragment. HPLC-MS/MS was used to determine the precise location of the labelling. Labelling was observed on the tyrosine 39 position of the protein, which is in the N-terminal region of AS. It is interesting to note that tyrosine 39 is located in a potential binding region in AS *fibrils*.[79] This may indicate the importance of this region in both aggregated AS and free AS interactions with small molecules.

Given the positive results from the previous PAL experiment, there was the desire to confirm the results a second time and perhaps even identify additional binding sites. The experiment was repeated on two separate days with two sets of modifications. The first modification was that the concentration of protein was increased tenfold, maintaining the same

concentration of probe. The second experiment used the changes from the first experiment as well, but the length of UV exposure was shortened to 30 minutes. These experiments both yielded labelling of tyrosine 39, like the previous labeling study. Two new modifications were identified in the six-hour incubation period at amino acids 28 and 136 which correspond to glutamic acid and tyrosine, respectively. Unfortunately, the modification to the 136 position was not fully validated due to missing ions in the spectra. The 30-minute labelling period was able to identify the modification to glutamic acid 28, but it did not identify modification at tyrosine 136. It remains possible that tyrosine 136 was labelled, but further optimization would be required such as using alternative proteins for digestion. However, it can be stated confidently that glutamic acid was labelled.

These findings partially support the hypothesis that caffeine binds in both the N- and C-terminal regions of AS, assuming CD is an appropriate substitute for caffeine. Taking the ThT and ITC data into consideration, one must wonder whether the binding events are specific. PAL in the presence of both CD and caffeine may be able to allow further insight into the issue.

One *in silico* study supports some of the results from the CD PAL studies.[102] This study reports potential interactions of caffeine near the tyrosine 39 position, but it does not report interactions occurring close to either glutamic acid 28 or tyrosine 136. A major limitation of the *in silico* study was that AS was kept rigid whereas the inherent conformational flexibility is a known challenge for modelling AS *in silico*.[103] Second, this PDB file was of micelle bound AS, a form which may not accurately mimic the conformation of AS when bound to small molecules. In spite of these limitations, it is interesting to note that the proposed N-terminal binding region (approximately Lys 32 to Lys 45) and the binding poses shown could place the diazirine adjacent to either Glu 28 or Tyr 39.[102]

Following establishment of the PAL protocol, PAL with digestion prior to MS/MS was performed with the remaining probes: AD, ND, and C_2D_2. The labelling step made use of the 30-minute UV exposure time. Unfortunately, none of the probes labelled AS in the given conditions. No labelling from any of these probes was not entirely unexpected due to the difficulties with the ThT assay. Another possibility is that once activated the carbenes may preferentially react with solvent, other molecules of AD, ND or C_2D_2. An additional possibility for C_2D_2, which possesses a great deal of conformational flexibility, is an intramolecular reaction due to pi-stacking of the caffeine moieties, although there is no evidence that such an interaction predominates in solution.

Therefore, these results support the null hypothesis in that they do not bind preferentially to either the N- or C terminal domains.

3.5 Conclusion

In summary, diazirine probes were synthesized for caffeine, 1-aminoindan, nicotine, and C_8-6-C_8. Due to time constraints and a global pandemic, synthesis of diazirine probes for C_8-6-I and C_8-6-N was not completed. ITC was unable to demonstrate binding of caffeine and CD to AS. ThT assays for caffeine, 1-aminoindan, nicotine, C_8-6-C_8, C_8-6-I, CD, ND, AD, and C_2D_2 did not demonstrate direct AS fibrillization inhibition. PAL with CD identified three potential binding sites for caffeine on AS: tyrosine 39, glutamic acid 28, and tyrosine 136. The remaining PAL compounds – ND, AD, and C_2D_2 – did not label AS protein under our experimental conditions.

Taken together, the results support the first study hypothesis (The diazirine functionalized probes will interact with AS the same way that the drugs they are derived from interact with AS) in that the probes and the drugs from which they were designed behave the same way toward AS. However, all compounds did not behave in the way in which they were expected, meaning no direct anti-fibrillization activity. The PAL data for CD partially supports the second hypothesis (The diazirine-functionalized probes will preferentially label the N- and C- terminal regions of AS), but the results from ThT and ITC call into question whether the sites are specifically or non-specifically labelled. AD, ND, and C_2D_2 PAL studies do not support the second hypothesis, but due to the limited attempts, labelling may still be possible under different conditions.

3.6 Future work

Given the inability to reproduce the results in previous ITC studies, it would be prudent to replicate other studies done in the past. Therefore, the replication of yeast studies is proposed in future work, assuming this would be feasible for someone with the necessary background.[10] This could serve two purposes. First, the results from the yeast study could be reconfirmed. Second, the yeast cells may serve as a system for in-cell PAL.

Again, given the issues faced with the ThT assay, it may be useful to develop an assay or a protocol for testing the quality of AS. Perhaps gel electrophoresis or some variation of mass spectrometry may be helpful toward verifying the protein is in the correct state prior to its use in biological assays and that there are not contaminants that may affect the outcome of those biological assays. While it is unlikely that this was a major issue given the success with cNDGA positive controls, it may again be prudent nonetheless.

More biological assays may be beneficial toward our understanding of the mechanisms of the bifunctional agents and monomers. For instance, gel electrophoresis could be run following aggregation to identify changes in aggregation profiles.[95] Circular dichroism may also be used to identify the secondary structure of the protein aggregates. Even transmission electron microscopy may be beneficial toward understanding the changes in aggregation.

Many PAL experiments could be performed following this work. First, there could be experiments which vary the stoichiometry of AS to probe. This would allow a qualitative measure of the strength of interaction between AS and probe. It would also serve to fine tune the ratio for future PAL studies with the probes developed in this work.

Second, PAL should be performed in the presence of the original drugs. Other studies have successfully completed PAL competition studies *in vitro* to identify the sites that are specific for the drug versus those that are non-specific. [100]

Third, PAL of AS fibrils could also be performed. This would allow a better comparison between the study done by Hsieh et al. and the probes in this work.[79] Also, *in silico* methods could be used in comparison to the results from such a study.

As was previously mentioned, in-cell PAL could be performed. This would require the development of new probes capable of click chemistry with terminal alkynes for isolation (Figure 3.35), and validation of the newly developed probes.[69] However, doing so may provide a more complete picture of the binding profile of these small molecules, and potentially offer insight into the cellular mechanisms of PD.

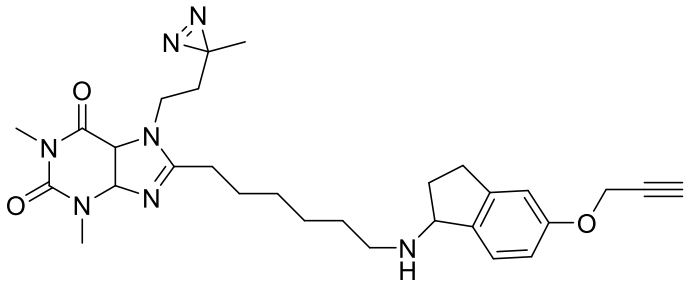

Figure 3.35 Proposed PAL click chemistry probe for yeast cell studies.

Fifth, bifunctional probes could be synthesized that contain only one diazirine functional group (Figure 3.36). There are two potential benefits from experiments of this variety. First, the synthesis may be easier to complete. Second, only one linker would cause fewer alterations to the

overall structure of the bifunctional molecules, which may contribute to the lack of protein labelling observed.

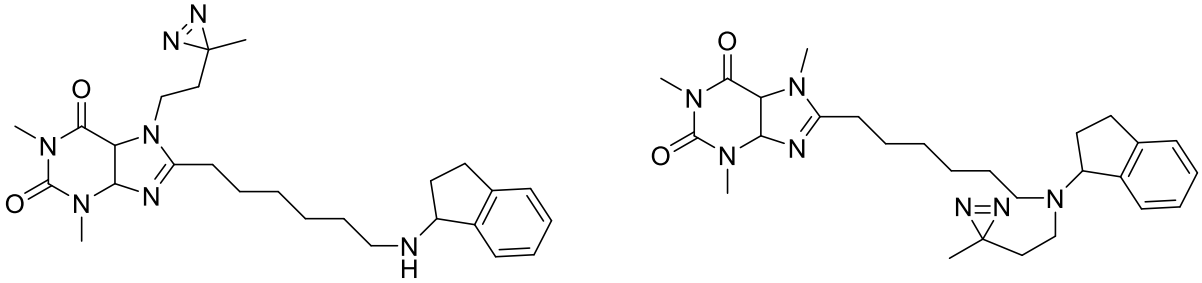

Figure 3.36 Proposed single diazirine functionalized probes for AS binding studies.

Finally, more work can be done to optimize the labelling with CD, ND, and C_2D_2. DMSO was used to solubilize these compounds as it had been used in previous work with ThT assays.[95] However, DMSO is known to influence protein conformation with proteins other than AS.[104,105] By making use of another solvent to solubilize these compounds for PAL, we may observe changes to labelling. Therefore, a control using methanol to solubilize may be useful.

APPENDICES

Representative MS data from PAL and MS.

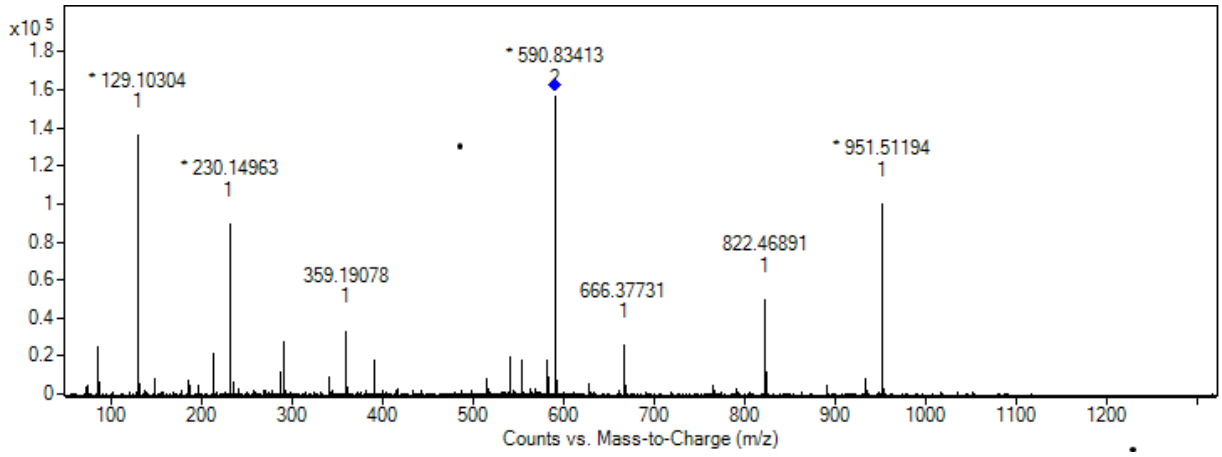

Figure 4.1 MS/MS spectrum of a representative tryptic peptide (TKEGVLYVGSK).

Table 4.1 Signature peptides (*y* and *b* ions) resulting from the fragmentation of TKEGVLYVGSK peptide.

FRAGMENT ION	Calculated m/z	Measured m/z	FRAGMENT ION	Calculated m/z	Measured m/z
y_1	147.1128	147.1121	b_1	102.0550	84.0530
y_2	234.1448	234.1434	b_2	230.1499	230.1496
y_3	291.1663	291.1645	b_3	359.1925	359.1907
y_4	390.2347	390.2320	b_4	416.2140	416.2082
y_5	553.2980	553.2943	b_5	515.2824	515.2799
y_6	666.3821	666.3773	b_6	628.3665	628.3656
y_7	765.4505	765.4478	b_7	791.4298	791.4260
y_8	822.4720	822.4689	b_8	890.4982	890.4927
y_9	951.5146	951.5119	b_9	947.5197	947.5122
y_{10}	1079.6095	1079.5991	b_{10}	1034.5514	1034.5390

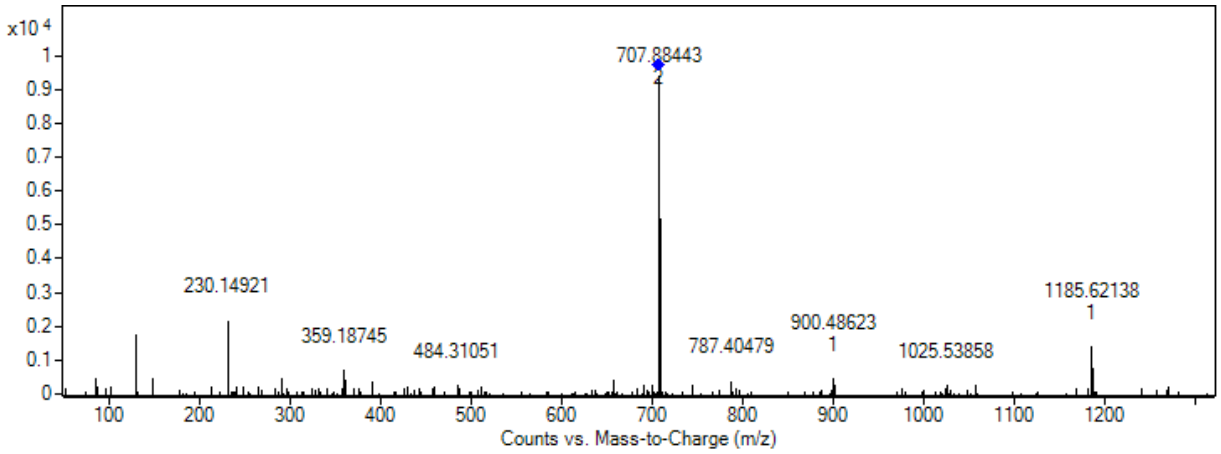

Figure 4.2 MS/MS spectrum of TKEGVLyVGSK peptide modified at tyrosine (y) amino acid with caffeine diazirine.

Table 4.2 Signature peptides (*y* and *b* ions) resulting from the fragmentation of the modified TKEGVLyVGSK peptide.

FRAGMENT ION	Calculated m/z	Measured m/z	FRAGMENT ION	Calculated m/z	Measured m/z
y_1	147.1128	147.1097	b_1-H_2O	84.0444	84.0413
y_2	234.1448	234.1374	b_2	230.1499	230.1492
y_3	291.1663	291.1650	b_3	359.1925	359.1874
y_4	390.2347	390.2326	b_4	416.2140	416.2453
y_5	787.4097	787.4047	b_5	515.2824	515.2872
y_6	900.4938	900.4862	b_6	628.3665	628.3739
y_7	999.5622	999.5399	b_7	1025.5415	1025.5385
y_8	1056.5837	1056.5679	b_8	1124.6099	1124.6053
y_9	1185.6262	1185.6213	b_9	1181.6313	1181.5929
y_{10}	1313.7212	1313.7141	b_{10}	1268.6634	1268.6453

REFERENCES

(1) Obeso, J. A.; Stamelou, M.; Goetz, C. G.; Poewe, W.; Lang, A. E.; Weintraub, D.; Burn, D.; Halliday, G. M.; Bezard, E.; Przedborski, S.; Lehericy, S.; Brooks, D. J.; Rothwell, J. C.; Hallett, M.; DeLong, M. R.; Marras, C.; Tanner, C. M.; Ross, G. W.; Langston, J. W.; Klein, C.; Bonifati, V.; Jankovic, J.; Lozano, A. M.; Deuschl, G.; Bergman, H.; Tolosa, E.; Rodriguez-Violante, M.; Fahn, S.; Postuma, R. B.; Berg, D.; Marek, K.; Standaert, D. G.; Surmeier, D. J.; Olanow, C. W.; Kordower, J. H.; Calabresi, P.; Schapira, A. H. V.; Stoessl, A. J. Past, Present, and Future of Parkinson's Disease: A Special Essay on the 200th Anniversary of the Shaking Palsy. *Movement Disorders*. John Wiley and Sons Inc. September 1, 2017, pp 1264–1310. https://doi.org/10.1002/mds.27115.

(2) Dickson, D. W.; Braak, H.; Duda, J. E.; Duyckaerts, C.; Gasser, T.; Halliday, G. M.; Hardy, J.; Leverenz, J. B.; del Tredici, K.; Wszolek, Z. K.; Litvan, I. Neuropathological Assessment of Parkinson's Disease: Refining the Diagnostic Criteria. *The Lancet Neurology*. Lancet Publishing Group December 1, 2009, pp 1150–1157. https://doi.org/10.1016/S1474-4422(09)70238-8.

(3) Spillantini, M. G.; Crowther, R. A.; Jakes, R.; Hasegawa, M.; Goedert, M. α-Synuclein in Filamentous Inclusions of Lewy Bodies from Parkinson's Disease and Dementia with Lewy Bodies. *Proceedings of the National Academy of Sciences of the United States of America* **1998**, *95* (11), 6469–6473. https://doi.org/10.1073/pnas.95.11.6469.

(4) Fauvet, B.; Mbefo, M. K.; Fares, M. B.; Desobry, C.; Michael, S.; Ardah, M. T.; Tsika, E.; Coune, P.; Prudent, M.; Lion, N.; Eliezer, D.; Moore, D. J.; Schneider, B.; Aebischer, P.; El-Agnaf, O. M.; Masliah, E.; Lashuel, H. A. α-Synuclein in Central Nervous System and from Erythrocytes, Mammalian Cells, and Escherichia Coli Exists Predominantly as Disordered Monomer. *Journal of Biological Chemistry* **2012**, *287* (19), 15345–15364. https://doi.org/10.1074/jbc.M111.318949.

(5) Iwai, A.; Masliah, E.; Yoshimoto, M.; Ge, N.; Flanagan, L.; Rohan de Silva, H. A.; Kittel, A.; Saitoh, T. The Precursor Protein of Non-Aβ Component of Alzheimer's Disease Amyloid Is a Presynaptic Protein of the Central Nervous System. *Neuron* **1995**, *14* (2), 467–475. https://doi.org/10.1016/0896-6273(95)90302-X.

(6) Serpell, L. C.; Berriman, J.; Jakes, R.; Goedert, M.; Crowther, R. A. Fiber Diffraction of Synthetic α-Synuclein Filaments Shows Amyloid-like Cross-β Conformation. *Proceedings of the National Academy of Sciences of the United States of America* **2000**, *97* (9), 4897–4902. https://doi.org/10.1073/pnas.97.9.4897.

(7) Goedert, M.; Spillantini, M. G.; del Tredici, K.; Braak, H. 100 Years of Lewy Pathology. *Nature Reviews Neurology*. Nature Publishing Group January 27, 2013, pp 13–24. https://doi.org/10.1038/nrneurol.2012.242.

(8) Tavassoly, O.; Kakish, J.; Nokhrin, S.; Dmitriev, O.; Lee, J. S. The Use of Nanopore Analysis for Discovering Drugs Which Bind to α-Synuclein for Treatment of Parkinson's Disease. *European Journal of Medicinal Chemistry* **2014**, *88*, 42–54. https://doi.org/10.1016/J.EJMECH.2014.07.090.

(9) Kakish, J.; Tavassoly, O.; Lee, J. S. Rasagiline, a Suicide Inhibitor of Monoamine Oxidases, Binds Reversibly to α-Synuclein. *ACS Chemical Neuroscience* **2015**, *6* (2), 347–355. https://doi.org/10.1021/cn5002914.

(10) Kakish, J.; Allen, K. J. H.; Harkness, T. A.; Krol, E. S.; Lee, J. S. Novel Dimer Compounds That Bind α-Synuclein Can Rescue Cell Growth in a Yeast Model Overexpressing α-Synuclein. A Possible Prevention Strategy for Parkinson's Disease. *ACS Chemical Neuroscience* **2016**, *7* (12), 1671–1680. https://doi.org/10.1021/acschemneuro.6b00209.

(11) Murale, D. P.; Hong, S. C.; Haque, M. M.; Lee, J. S. Photo-Affinity Labeling (PAL) in Chemical Proteomics: A Handy Tool to Investigate Protein-Protein Interactions (PPIs). *Proteome Science*. BioMed Central Ltd. June 24, 2017. https://doi.org/10.1186/s12953-017-0123-3.

(12) Gade Malmos, K.; Blancas-Mejia, L. M.; Weber, B.; Buchner, J.; Ramirez-Alvarado, M.; Naiki, H.; Otzen, D. ThT 101: A Primer on the Use of Thioflavin T to Investigate Amyloid Formation. *Amyloid* **2017**, *24* (1), 1–16. https://doi.org/10.1080/13506129.2017.1304905.

(13) Marras, C.; Beck, J. C.; Bower, J. H.; Roberts, E.; Ritz, B.; Ross, G. W.; Abbott, R. D.; Savica, R.; van den Eeden, S. K.; Willis, A. W.; Tanner, C. Prevalence of Parkinson's Disease across North America. *npj Parkinson's Disease* **2018**, *4* (1). https://doi.org/10.1038/s41531-018-0058-0.

(14) Poewe, W.; Seppi, K.; Tanner, C.; Halliday, G. M.; Brundin, P.; Volkmann, J.; Eleonore Schrag, A.; Lang, A. E. Parkinson Disease. *Nature Reviews Disease Primers* **2017**, *3* (17013).

(15) Tysnes, O. B.; Storstein, A. Epidemiology of Parkinson's Disease. *Journal of Neural Transmission*. Springer-Verlag Wien August 1, 2017, pp 901–905. https://doi.org/10.1007/s00702-017-1686-y.

(16) Postuma, R. B.; Berg, D.; Stern, M.; Poewe, W.; Olanow, C. W.; Oertel, W.; Obeso, J.; Marek, K.; Litvan, I.; Lang, A. E.; Halliday, G.; Goetz, C. G.; Gasser, T.; Dubois, B.; Chan, P.; Bloem, B. R.; Adler, C. H.; Deuschl, G. MDS Clinical Diagnostic Criteria for Parkinson's Disease. *Movement Disorders*. John Wiley and Sons Inc. October 1, 2015, pp 1591–1601. https://doi.org/10.1002/mds.26424.

(17) Köllensperger, M.; Geser, F.; Seppi, K.; Stampfer-Kountchev, M.; Sawires, M.; Scherfler, C.; Boesch, S.; Mueller, J.; Koukouni, V.; Quinn, N.; Pellecchia, M. T.; Barone, P.; Schimke, N.; Dodel, R.; Oertel, W.; Dupont, E.; Østergaard, K.; Daniels, C.; Deuschl, G.; Gurevich, T.; Giladi, N.; Coelho, M.; Sampaio, C.; Nilsson, C.; Widner, H.; del Sorbo, F.; Albanese, A.; Cardozo, A.; Tolosa, E.; Abele, M.; Klockgether, T.; Kamm, C.; Gasser, T.; Djaldetti, R.; Colosimo, C.; Meco, G.; Schrag, A.; Poewe, W.; Wenning, G. K. Red Flags for Multiple System Atrophy. *Movement Disorders* **2008**, *23* (8), 1093–1099. https://doi.org/10.1002/mds.21992.

(18) Postuma, R. B.; Berg, D. Prodromal Parkinson's Disease: The Decade Past, the Decade to Come. *Movement Disorders* **2019**, *34* (5), 665–675. https://doi.org/10.1002/mds.27670.

(19) Postuma, R. B.; Aarsland, D.; Barone, P.; Burn, D. J.; Hawkes, C. H.; Oertel, W.; Ziemssen, T. Identifying Prodromal Parkinson's Disease: Pre-Motor Disorders in Parkinson's Disease. *Movement Disorders* **2012**, *27* (5), 617–626. https://doi.org/10.1002/mds.24996.

(20) Berg, D.; Postuma, R. B.; Adler, C. H.; Bloem, B. R.; Chan, P.; Dubois, B.; Gasser, T.; Goetz, C. G.; Halliday, G.; Joseph, L.; Lang, A. E.; Liepelt-Scarfone, I.; Litvan, I.; Marek, K.; Obeso, J.; Oertel, W.; Olanow, C. W.; Poewe, W.; Stern, M.; Deuschl, G. MDS Research Criteria for Prodromal Parkinson's Disease. *Movement Disorders* **2015**, *30* (12), 1600–1611. https://doi.org/10.1002/mds.26431.

(21) Dickson, D. W. Neuropathology of Parkinson Disease. *Parkinsonism & Related Disorders* **2018**, *46*, S30–S33. https://doi.org/10.1016/j.parkreldis.2017.07.033.

(22) Fearnley, J. M.; Lees, A. J. Ageing and Parkinson's Disease: Substantia Nigra Regional Selectivity. *Brain* **1991**, *114* (5), 2283–2301.

(23) Barbeau, A. L-Dopa Therapy in Parkinson's Disease: A Critical Review of Nine Years' Experience. *Canadian Medical Association journal*. Canadian Medical Association December 27, 1969, pp 59–68.

(24) Sarkar, S.; Raymick, J.; Imam, S. Neuroprotective and Therapeutic Strategies against Parkinson's Disease: Recent Perspectives. *International Journal of Molecular Sciences*. MDPI AG June 8, 2016. https://doi.org/10.3390/ijms17060904.

(25) Fox, S. H.; Katzenschlager, R.; Lim, S. Y.; Barton, B.; de Bie, R. M. A.; Seppi, K.; Coelho, M.; Sampaio, C. International Parkinson and Movement Disorder Society Evidence-Based Medicine Review: Update on Treatments for the Motor Symptoms of Parkinson's Disease. *Movement Disorders*. John Wiley and Sons Inc. August 1, 2018, pp 1248–1266. https://doi.org/10.1002/mds.27372.

(26) Seppi, K.; Ray Chaudhuri, K.; Coelho, M.; Fox, S. H.; Katzenschlager, R.; Perez Lloret, S.; Weintraub, D.; Sampaio, C.; Chahine, L.; Hametner, E. M.; Heim, B.; Lim, S. Y.; Poewe, W.; Djamshidian-Tehrani, A. Update on Treatments for Nonmotor Symptoms of Parkinson's Disease—an Evidence-Based Medicine Review. *Movement Disorders*. John Wiley and Sons Inc. February 1, 2019, pp 180–198. https://doi.org/10.1002/mds.27602.

(27) Polymeropoulos, M. H.; Lavedan, C.; Leroy, E.; Ide, S. E.; Dehejia, A.; Dutra, A.; Pike, B.; Root, H.; Rubenstein, J.; Boyer, R.; Stenroos, E. S.; Chandrasekharappa, S.; Athanassiadou, A.; Papapetropoulos, T.; Johnson, W. G.; Lazzarini, A. M.; Duvoisin, R. C.; di Iorio, G.; Golbe, L. I.; Nussbaum, R. L. Mutation in the α-Synuclein Gene Identified in Families with Parkinson's Disease. *Science* **1997**, *276* (5321), 2045–2047. https://doi.org/10.1126/science.276.5321.2045.

(28) Deng, H.; Wang, P.; Jankovic, J. The Genetics of Parkinson Disease. *Ageing Research Reviews*. Elsevier Ireland Ltd March 1, 2018, pp 72–85. https://doi.org/10.1016/j.arr.2017.12.007.

(29) Blauwendraat, C.; Nalls, M. A.; Singleton, A. B. The Genetic Architecture of Parkinson's Disease. *The Lancet Neurology*. Lancet Publishing Group February 1, 2020, pp 170–178. https://doi.org/10.1016/S1474-4422(19)30287-X.

(30) Weinreb, P. H.; Zhen, W.; Poon, A. W.; Conway, K. A.; Lansbury, P. T. NACP, a Protein Implicated in Alzheimer's Disease and Learning, Is Natively Unfolded. *Biochemistry* **1996**, *35* (43), 13709–13715. https://doi.org/10.1021/bi961799n.

(31) Bartels, T.; Choi, J. G.; Selkoe, D. J. α-Synuclein Occurs Physiologically as a Helically Folded Tetramer That Resists Aggregation. *Nature* **2011**, *477* (7362), 107–111. https://doi.org/10.1038/nature10324.

(32) Davidson, W. S.; Jonas, A.; Clayton, D. F.; George, J. M. Stabilization of α-Synuclein Secondary Structure upon Binding to Synthetic Membranes. *Journal of Biological Chemistry* **1998**, *273* (16), 9443–9449. https://doi.org/10.1074/jbc.273.16.9443.

(33) Nakai, M.; Fujita, M.; Waragai, M.; Sugama, S.; Wei, J.; Akatsu, H.; Ohtaka-Maruyama, C.; Okado, H.; Hashimoto, M. Expression of α-Synuclein, a Presynaptic Protein Implicated in Parkinson's Disease, in Erythropoietic Lineage. *Biochemical and Biophysical Research Communications* **2007**, *358* (1), 104–110. https://doi.org/10.1016/j.bbrc.2007.04.108.

(34) Barbour, R.; Kling, K.; Anderson, J. P.; Banducci, K.; Cole, T.; Diep, L.; Fox, M.; Goldstein, J. M.; Soriano, F.; Seubert, P.; Chilcote, T. J. Red Blood Cells Are the Major Source of Alpha-Synuclein in Blood. *Neurodegenerative Diseases* **2008**, *5* (2), 55–59. https://doi.org/10.1159/000112832.

(35) Pranke, I. M.; Morello, V.; Bigay, J.; Gibson, K.; Verbavatz, J. M.; Antonny, B.; Jackson, C. L. α-Synuclein and ALPS Motifs Are Membrane Curvature Sensors Whose Contrasting Chemistry Mediates Selective Vesicle Binding. *Journal of Cell Biology* **2011**, *194* (1), 89–103. https://doi.org/10.1083/jcb.201011118.

(36) Burré, J. The Synaptic Function of α-Synuclein. *Journal of Parkinson's Disease*. IOS Press November 21, 2015, pp 699–713. https://doi.org/10.3233/JPD-150642.

(37) Bernal-Conde, L. D.; Ramos-Acevedo, R.; Reyes-Hernández, M. A.; Balbuena-Olvera, A. J.; Morales-Moreno, I. D.; Argüero-Sánchez, R.; Schüle, B.; Guerra-Crespo, M. Alpha-Synuclein Physiology and Pathology: A Perspective on Cellular Structures and Organelles. *Frontiers in Neuroscience*. Frontiers Media S.A. January 23, 2020, p 1399. https://doi.org/10.3389/fnins.2019.01399.

(38) Ueda, K.; Fukushima, H.; Masliah, E.; Xia, Y.; Iwai, A.; Yoshimoto, M.; Otero, D. A. C.; Kondo, J.; Ihara, Y.; Saitoh, T. Molecular Cloning of CDNA Encoding an Unrecognized Component of Amyloid in Alzheimer Disease. *Proceedings of the National Academy of Sciences of the United States of America* **1993**, *90* (23), 11282–11286. https://doi.org/10.1073/pnas.90.23.11282.

(39) Ulmer, T. S.; Bax, A.; Cole, N. B.; Nussbaum, R. L. Structure and Dynamics of Micelle-Bound Human α-Synuclein. *Journal of Biological Chemistry* **2005**, *280* (10), 9595–9603. https://doi.org/10.1074/jbc.M411805200.

(40) Fernández, C. O.; Hoyer, W.; Zweckstetter, M.; Jares-Erijman, E. A.; Subramaniam, V.; Griesinger, C.; Jovin, T. M. NMR of α-Synuclein-Polyamine Complexes Elucidates the Mechanism and Kinetics of Induced Aggregation. *EMBO Journal* **2004**, *23* (10), 2039–2046. https://doi.org/10.1038/sj.emboj.7600211.

(41) Cuervo, A. M.; Stafanis, L.; Fredenburg, R.; Lansbury, P. T.; Sulzer, D. Impaired Degradation of Mutant α-Synuclein by Chaperone-Mediated Autophagy. *Science* **2004**, *305* (5688), 1292–1295. https://doi.org/10.1126/science.1101738.

(42) Melki, R. Role of Different Alpha-Synuclein Strains in Synucleinopathies, Similarities with Other Neurodegenerative Diseases. *Journal of Parkinson's Disease*. IOS Press June 1, 2015, pp 217–227. https://doi.org/10.3233/JPD-150543.

(43) Emmanouilidou, E.; Stefanis, L.; Vekrellis, K. Cell-Produced α-Synuclein Oligomers Are Targeted to, and Impair, the 26S Proteasome. *Neurobiology of Aging* **2010**, *31* (6), 953–968. https://doi.org/10.1016/j.neurobiolaging.2008.07.008.

(44) Winner, B.; Jappelli, R.; Maji, S. K.; Desplats, P. A.; Boyer, L.; Aigner, S.; Hetzer, C.; Loher, T.; Vilar, M.; Campioni, S.; Tzitzilonis, C.; Soragni, A.; Jessberger, S.; Mira, H.; Consiglio, A.; Pham, E.; Masliah, E.; Gage, F. H.; Riek, R. In Vivo Demonstration That α-

Synuclein Oligomers Are Toxic. *Proceedings of the National Academy of Sciences of the United States of America* **2011**, *108* (10), 4194–4199. https://doi.org/10.1073/pnas.1100976108.

(45) Choi, B. K.; Choi, M. G.; Kim, J. Y.; Yang, Y.; Lai, Y.; Kweon, D. H.; Lee, N. K.; Shin, Y. K. Large α-Synuclein Oligomers Inhibit Neuronal SNARE-Mediated Vesicle Docking. *Proceedings of the National Academy of Sciences of the United States of America* **2013**, *110* (10), 4087–4092. https://doi.org/10.1073/pnas.1218424110.

(46) Anderson, J. P.; Walker, D. E.; Goldstein, J. M.; de Laat, R.; Banducci, K.; Caccavello, R. J.; Barbour, R.; Huang, J.; Kling, K.; Lee, M.; Diep, L.; Keim, P. S.; Shen, X.; Chataway, T.; Schlossmacher, M. G.; Seubert, P.; Schenk, D.; Sinha, S.; Gai, W. P.; Chilcote, T. J. Phosphorylation of Ser-129 Is the Dominant Pathological Modification of α-Synuclein in Familial and Sporadic Lewy Body Disease. *Journal of Biological Chemistry* **2006**, *281* (40), 29739–29752. https://doi.org/10.1074/jbc.M600933200.

(47) Smith, W. W.; Margolis, R. L.; Li, X.; Troncoso, J. C.; Lee, M. K.; Dawson, V. L.; Dawson, T. M.; Iwatsubo, T.; Ross, C. A. α-Synuclein Phosphorylation Enhances Eosinophilic Cytoplasmic Inclusion Formation in SH-SY5Y Cells. *Journal of Neuroscience* **2005**, *25* (23), 5544–5552. https://doi.org/10.1523/JNEUROSCI.0482-05.2005.

(48) Flagmeier, P.; Meisl, G.; Vendruscolo, M.; Knowles, T. P. J.; Dobson, C. M.; Buell, A. K.; Galvagnion, C. Mutations Associated with Familial Parkinson's Disease Alter the Initiation and Amplification Steps of α-Synuclein Aggregation. *Proceedings of the National Academy of Sciences of the United States of America* **2016**, *113* (37), 10328–10333. https://doi.org/10.1073/pnas.1604645113.

(49) Jucker, M.; Walker, L. C. Propagation and Spread of Pathogenic Protein Assemblies in Neurodegenerative Diseases. *Nature Neuroscience*. Nature Publishing Group October 1, 2018, pp 1341–1349. https://doi.org/10.1038/s41593-018-0238-6.

(50) Buell, A. K.; Galvagnion, C.; Gaspar, R.; Sparr, E.; Vendruscolo, M.; Knowles, T. P. J.; Linse, S.; Dobson, C. M. Solution Conditions Determine the Relative Importance of Nucleation and Growth Processes in α-Synuclein Aggregation. *Proceedings of the National Academy of Sciences of the United States of America* **2014**, *111* (21), 7671–7676. https://doi.org/10.1073/pnas.1315346111.

(51) Li, J. Y.; Englund, E.; Holton, J. L.; Soulet, D.; Hagell, P.; Lees, A. J.; Lashley, T.; Quinn, N. P.; Rehncrona, S.; Björklund, A.; Widner, H.; Revesz, T.; Lindvall, O.; Brundin, P. Lewy Bodies in Grafted Neurons in Subjects with Parkinson's Disease Suggest Host-to-Graft Disease Propagation. *Nature Medicine* **2008**, *14* (5), 501–503. https://doi.org/10.1038/nm1746.

(52) Sacino, A. N.; Brooks, M.; Thomas, M. A.; McKinney, A. B.; Lee, S.; Regenhardt, R. W.; McGarvey, N. H.; Ayers, J. I.; Notterpek, L.; Borchelt, D. R.; Golde, T. E.; Giasson, B. I. Intramuscular Injection of α-Synuclein Induces CNS α-Synuclein Pathology and a Rapid-Onset Motor Phenotype in Transgenic Mice. *Proceedings of the National Academy of Sciences of the United States of America* **2014**, *111* (29), 10732–10737. https://doi.org/10.1073/pnas.1321785111.

(53) Ayers, J. I.; Brooks, M. M.; Rutherford, N. J.; Howard, J. K.; Sorrentino, Z. A.; Riffe, C. J.; Giasson, B. I. Robust Central Nervous System Pathology in Transgenic Mice Following Peripheral Injection of α-Synuclein Fibrils. *Journal of Virology* **2017**, *91* (2). https://doi.org/10.1128/jvi.02095-16.

(54) Biancardi, A.; Biver, T.; Burgalassi, A.; Mattonai, M.; Secco, F.; Venturini, M. Mechanistic Aspects of Thioflavin-T Self-Aggregation and DNA Binding: Evidence for Dimer Attack on DNA Grooves. *Physical Chemistry Chemical Physics* **2014**, *16* (37), 20061–20072. https://doi.org/10.1039/c4cp02838d.

(55) Naiki, H.; Higuchi, K.; Hosokawa, M.; Takeda, T. Fluorometric Determination of Amyloid Fibrils in Vitro Using the Fluorescent Dye, Thioflavine T. *Analytical Biochemistry* **1989**, *177* (2), 244–249. https://doi.org/10.1016/0003-2697(89)90046-8.

(56) Biancalana, M.; Koide, S. Molecular Mechanism of Thioflavin-T Binding to Amyloid Fibrils. *Biochimica et Biophysica Acta - Proteins and Proteomics*. NIH Public Access July 2010, pp 1405–1412. https://doi.org/10.1016/j.bbapap.2010.04.001.

(57) Jellinger, K. A. Dementia with Lewy Bodies and Parkinson's Disease-Dementia: Current Concepts and Controversies. *Journal of Neural Transmission*. Springer-Verlag Wien April 1, 2018, pp 615–650. https://doi.org/10.1007/s00702-017-1821-9.

(58) Jellinger, K. A.; Korczyn, A. D. Are Dementia with Lewy Bodies and Parkinson's Disease Dementia the Same Disease? *BMC Medicine* **2018**, *16* (1), 1–16. https://doi.org/10.1186/s12916-018-1016-8.

(59) Outeiro, T. F.; Koss, D. J.; Erskine, D.; Walker, L.; Kurzawa-Akanbi, M.; Burn, D.; Donaghy, P.; Morris, C.; Taylor, J. P.; Thomas, A.; Attems, J.; McKeith, I. Dementia with Lewy Bodies: An Update and Outlook. *Molecular Neurodegeneration*. BioMed Central Ltd. January 21, 2019, pp 1–18. https://doi.org/10.1186/s13024-019-0306-8.

(60) Goedert, M.; Jakes, R.; Spillantini, M. G. The Synucleinopathies: Twenty Years On. *Journal of Parkinson's Disease*. IOS Press 2017, pp S53–S71. https://doi.org/10.3233/JPD-179005.

(61) Fanciulli, A.; Wenning, G. K. Multiple-System Atrophy. *New England Journal of Medicine* **2015**, *372* (3), 249–263. https://doi.org/10.1056/NEJMra1311488.

(62) Chen, H.; Huang, X.; Guo, X.; Mailman, R. B.; Park, Y.; Kamel, F.; Umbach, D. M.; Xu, Q.; Hollenbeck, A.; Schatzkin, A.; Blair, A. Smoking Duration, Intensity, and Risk of Parkinson Disease. *Neurology* **2010**, *74* (11), 878. https://doi.org/10.1212/WNL.0B013E3181D55F38.

(63) Ritz, B.; Lee, P.-C.; Lassen, C. F.; Arah, O. A. Parkinson Disease and Smoking Revisited: Ease of Quitting Is an Early Sign of the Disease. *Neurology* **2014**, *83* (16), 1396–1402. https://doi.org/10.1212/WNL.0000000000000879.

(64) Weisskopf, M. G.; Knekt, P.; O'Reilly, E. J.; Lyytinen, J.; Reunanen, A.; Laden, F.; Altshul, L.; Ascherio, A. Persistent Organochlorine Pesticides in Serum and Risk of Parkinson Disease. *Neurology* **2010**, *74* (13), 1055. https://doi.org/10.1212/WNL.0B013E3181D76A93.

(65) Prediger, R. D. S. Effects of Caffeine in Parkinson's Disease: From Neuroprotection to the Management of Motor and Non-Motor Symptoms. *Journal of Alzheimer's Disease* **2010**, *20* (s1), S205–S220. https://doi.org/10.3233/JAD-2010-091459.

(66) Postuma, R. B.; Lang, A. E.; Munhoz, R. P.; Charland, K.; Pelletier, A.; Moscovich, M.; Filla, L.; Zanatta, D.; Romenets, S. R.; Altman, R.; Chuang, R.; Shah, B. Caffeine for Treatment of Parkinson Disease: A Randomized Controlled Trial. *Neurology* **2012**, *79* (7), 651. https://doi.org/10.1212/WNL.0B013E318263570D.

(67) Bar-Am, O.; Weinreb, O.; Amit, T.; Youdim, M. B. H. The Neuroprotective Mechanism of 1-R-Aminoindan, the Major Metabolite of the Anti-Parkinsonian Drug Rasagiline. *Journal of Neurochemistry* **2010**, *112* (5), 1131–1137. https://doi.org/10.1111/j.1471-4159.2009.06542.x.

(68) Am, O. B.; Amit, T.; Youdim, M. B. H. Contrasting Neuroprotective and Neurotoxic Actions of Respective Metabolites of Anti-Parkinson Drugs Rasagiline and Selegiline. *Neuroscience Letters* **2004**, *355* (3), 169–172. https://doi.org/10.1016/J.NEULET.2003.10.067.

(69) Geurink, P. P.; Prely, L. M.; van der Marel, G. A.; Bischoff, R.; Overkleeft, H. S. Photoaffinity Labeling in Activity-Based Protein Profiling. *Topics in Current Chemistry*. Springer, Berlin, Heidelberg 2012, pp 85–113. https://doi.org/10.1007/128_2011_286.

(70) Blencowe, A.; Hayes, W. Development and Application of Diazirines in Biological and Synthetic Macromolecular Systems. *Soft Matter*. August 28, 2005, pp 178–205. https://doi.org/10.1039/b501989c.

(71) Pan, S.; Zhang, H.; Wang, C.; Yao, S. C. L.; Yao, S. Q. Target Identification of Natural Products and Bioactive Compounds Using Affinity-Based Probes. *Natural Product*

Reports. Royal Society of Chemistry May 1, 2016, pp 612–620. https://doi.org/10.1039/c5np00101c.

(72) Smith, E.; Collins, I. Photoaffinity Labeling in Target- and Binding-Site Identification. *Future Medicinal Chemistry* **2015**, *7* (2), 159–183. https://doi.org/10.4155/fmc.14.152.

(73) Wilson, R. Sensitivity and Specificity: Twin Goals of Proteomics Assays. Can They Be Combined? *Expert Review of Proteomics*. Expert Rev Proteomics April 2013, pp 135–149. https://doi.org/10.1586/epr.13.7.

(74) Halloran, M. W.; Lumb, J. Recent Applications of Diazirines in Chemical Proteomics. *Chemistry – A European Journal* **2019**, *25* (19), 4885–4898. https://doi.org/10.1002/chem.201805004.

(75) and, Q. L.; Tor*, Y. Simple Conversion of Aromatic Amines into Azides. **2003**. https://doi.org/10.1021/OL034919+.

(76) Shields, C. J.; Falvey, D. E.; Schuster, G. B.; Buchardt, O.; Nielsen, P. E. Competitive Singlet-Singlet Energy Transfer and Electron Transfer Activation of Aryl Azides: Application to Photo-Cross-Linking Experiments. *Journal of Organic Chemistry* **1988**, *53* (15), 3501–3507.

(77) A. Fleming, S. Chemical Reagents in Photoaffinity Labeling. *Tetrahedron* **1995**, *51* (46), 12479–12520. https://doi.org/10.1016/0040-4020(95)00598-3.

(78) Kakish, J.; Lee, D.; Lee, J. S. Drugs That Bind to α-Synuclein: Neuroprotective or Neurotoxic? *ACS Chemical Neuroscience* **2015**, *6* (12), 1930–1940. https://doi.org/10.1021/acschemneuro.5b00172.

(79) Hsieh, C.-J.; Ferrie, J. J.; Xu, K.; Lee, I.; Graham, T. J. A.; Tu, Z.; Yu, J.; Dhavale, D.; Kotzbauer, P.; Petersson, E. J.; Mach, R. H. Alpha Synuclein Fibrils Contain Multiple Binding Sites for Small Molecules. *ACS Chemical Neuroscience* **2018**, *9* (11), 2521–2527. https://doi.org/10.1021/acschemneuro.8b00177.

(80) Walko, M.; Hewitt, E.; Radford, S. E.; Wilson, A. J. Design and Synthesis of Cysteine-Specific Labels for Photo-Crosslinking Studies. *RSC Advances* **2019**, *9* (14), 7610–7614. https://doi.org/10.1039/C8RA10436K.

(81) Horne, J. E.; Walko, M.; Calabrese, A. N.; Levenstein, M. A.; Brockwell, D. J.; Kapur, N.; Wilson, A. J.; Radford, S. E. Rapid Mapping of Protein Interactions Using Tag-Transfer Photocrosslinkers. *Angewandte Chemie International Edition* **2018**, *57* (51), 16688–16692. https://doi.org/10.1002/anie.201809149.

(82) Tian, Y.; Jacinto, M. P.; Zeng, Y.; Yu, Z.; Qu, J.; Liu, W. R.; Lin, Q. Genetically Encoded 2-Aryl-5-Carboxytetrazoles for Site-Selective Protein Photo-Cross-Linking.

Journal of the American Chemical Society **2017**, *139* (17), 6078–6081. https://doi.org/10.1021/jacs.7b02615.

(83) Morieux, P.; Salomé, C.; Park, K. D.; Stables, J. P.; Kohn, H. The Structure-Activity Relationship of the 3-Oxy Site in the Anticonvulsant (R)- N -Benzyl 2-Acetamido-3-Methoxypropionamide. *Journal of Medicinal Chemistry* **2010**, *53* (15), 5716–5726. https://doi.org/10.1021/jm100508m.

(84) Shigdel, U. K.; Zhang, J.; He, C. Diazirine-Based DNA Photo-Cross-Linking Probes for the Study of Protein–DNA Interactions. *Angewandte Chemie International Edition* **2008**, *47* (1), 90–93. https://doi.org/10.1002/anie.200703625.

(85) Inflazome Ltd; Cooper, M.; Miller, D.; MacLeod, A.; van Wiltenburg, J.; Thom, S.; St-Gallay, S.; Shannon, J. Novel Sulfonamide Carboxamide Compounds, 2019.

(86) Kambe, T.; Correia, B. E.; Niphakis, M. J.; Cravatt, B. F. Mapping the Protein Interaction Landscape for Fully Functionalized Small-Molecule Probes in Human Cells. *Journal of the American Chemical Society* **2014**, *136* (30), 10777–10782. https://doi.org/10.1021/ja505517t.

(87) Längle, D.; Wesseler, F.; Flötgen, D.; Leek, H.; Plowright, A. T.; Schade, D. Unique Photoaffinity Probes to Study TGFβ Signaling and Receptor Fates. *Chemical Communications* **2019**, *55* (30), 4323–4326. https://doi.org/10.1039/c9cc00929a.

(88) Wang, L.; Ishida, A.; Hashidoko, Y.; Hashimoto, M. Dehydrogenation of the NH−NH Bond Triggered by Potassium *Tert* -Butoxide in Liquid Ammonia. *Angewandte Chemie International Edition* **2017**, *56* (3), 870–873. https://doi.org/10.1002/anie.201610371.

(89) Wang, L.; Tachrim, Z. P.; Kurokawa, N.; Ohashi, F.; Sakihama, Y.; Hashidoko, Y.; Hashimoto, M. Base-Mediated One-Pot Synthesis of Aliphatic Diazirines for Photoaffinity Labeling. *Molecules* **2017**, *22* (8), 1389. https://doi.org/10.3390/molecules22081389.

(90) Modarelli, D. A.; Morgan, S.; Platz, M. S. Carbene Formation, Hydrogen Migration, and Fluorescence in the Excited States of Dialkyldiazirines. *Journal of the American Chemical Society* **1992**, *114* (18), 7034–7041. https://doi.org/10.1021/ja00044a013.

(91) Zhao, X.; Wu, G.; Yan, C.; Lu, K.; Li, H.; Zhang, Y.; Wang, J. Microwave-Assisted, Pd(0)-Catalyzed Cross-Coupling of Diazirines with Aryl Halides. *Organic Letters* **2010**, *12* (23), 5580–5583. https://doi.org/10.1021/ol102434v.

(92) Schneider, Y.; Prévost, J.; Gobin, M.; Legault, C. Y. Diazirines as Potent Electrophilic Nitrogen Sources: Application to the Synthesis of Pyrazoles. *Organic Letters* **2014**, *16* (2), 596–599. https://doi.org/10.1021/ol403495e.

(93) Fanning, K. N. New Approaches for the Synthesis of Unusual Amino Acids, 2008.

(94) Cohlberg, J. A.; Li, J.; Uversky, V. N.; Fink, A. L. Heparin and Other Glycosaminoglycans Stimulate the Formation of Amyloid Fibrils from α-Synuclein in Vitro. *Biochemistry* **2002**, *41* (5), 1502–1511. https://doi.org/10.1021/bi011711s.

(95) Daniels, M. J.; Nourse, J. B.; Kim, H.; Sainati, V.; Schiavina, M.; Murrali, M. G.; Pan, B.; Ferrie, J. J.; Haney, C. M.; Moons, R.; Gould, N. S.; Natalello, A.; Grandori, R.; Sobott, F.; Petersson, E. J.; Rhoades, E.; Pierattelli, R.; Felli, I.; Uversky, V. N.; Caldwell, K. A.; Caldwell, G. A.; Krol, E. S.; Ischiropoulos, H.; Ischiropoulos, H. Cyclized NDGA Modifies Dynamic α-Synuclein Monomers Preventing Aggregation and Toxicity. *Scientific reports* **2019**, *9* (1), 2937. https://doi.org/10.1038/s41598-019-39480-z.

(96) Uversky, V. N.; Li, J.; Souillac, P.; Millett, I. S.; Doniach, S.; Jakes, R.; Goedert, M.; Fink, A. L. Biophysical Properties of the Synucleins and Their Propensities to Fibrillate. *Journal of Biological Chemistry* **2002**, *277* (14), 11970–11978. https://doi.org/10.1074/jbc.M109541200.

(97) Muranaka, H.; Momose, T.; Handa, C.; Ozawa, T. Photoaffinity Labeling of the Human A_{2A} Adenosine Receptor and Cross-Link Position Analysis by Mass Spectrometry. *ACS Medicinal Chemistry Letters* **2017**, *8* (6), 660–665. https://doi.org/10.1021/acsmedchemlett.7b00138.

(98) Morimoto, S.; Tomohiro, T.; Maruyama, N.; Hatanaka, Y. Photoaffinity Casting of a Coumarin Flag for Rapid Identification of Ligand-Binding Sites within Protein. *Chemical Communications* **2013**, *49* (18), 1811–1813. https://doi.org/10.1039/c3cc38594a.

(99) Das, J. Identification of Alcohol-Binding Site(s) in Proteins Using Diazirine-Based Photoaffinity Labeling and Mass Spectrometry. *Chemical Biology & Drug Design* **2019**, *93* (6), 1158–1165. https://doi.org/10.1111/cbdd.13403.

(100) Hamilton, C. M.; Hung, M.; Chen, G.; Qureshi, Z.; Thompson, J. R.; Sun, B.; Bear, C. E.; Young, R. N. Synthesis and Characterization of a Photoaffinity Labelling Probe Based on the Structure of the Cystic Fibrosis Drug Ivacaftor. *Tetrahedron* **2018**, *74* (38), 5528–5538. https://doi.org/10.1016/j.tet.2018.06.016.

(101) Seifert, T.; Malo, M.; Lengqvist, J.; Sihlbom, C.; Jarho, E. M.; Luthman, K. Identification of the Binding Site of Chroman-4-One-Based Sirtuin 2-Selective Inhibitors Using Photoaffinity Labeling in Combination with Tandem Mass Spectrometry. *Journal of Medicinal Chemistry* **2016**, *59* (23), 10794–10799. https://doi.org/10.1021/acs.jmedchem.6b01117.

(102) Rondón-Villarreal, P.; López, W. O. C. Identification of Potential Natural Neuroprotective Molecules for Parkinson's Disease by Using Chemoinformatics and Molecular Docking. *Journal of Molecular Graphics and Modelling* **2020**, *97*, 107547. https://doi.org/10.1016/j.jmgm.2020.107547.

(103) Churchill, C. D. M.; Healey, M. A.; Preto, J.; Tuszynski, J. A.; Woodside, M. T. Probing the Basis of α-Synuclein Aggregation by Comparing Simulations to Single-Molecule Experiments. *Biophysical Journal* **2019**, *117* (6), 1125–1135. https://doi.org/10.1016/j.bpj.2019.08.013.

(104) Arakawa, T.; Kita, Y.; Timasheff, S. N. Protein Precipitation and Denaturation by Dimethyl Sulfoxide. *Biophysical Chemistry* **2007**, *131* (1–3), 62–70. https://doi.org/10.1016/j.bpc.2007.09.004.

(105) Chan, D. S. H.; Kavanagh, M. E.; McLean, K. J.; Munro, A. W.; Matak-Vinković, D.; Coyne, A. G.; Abell, C. Effect of DMSO on Protein Structure and Interactions Assessed by Collision-Induced Dissociation and Unfolding. *Analytical Chemistry* **2017**, *89* (18), 9976–9983. https://doi.org/10.1021/acs.analchem.7b02329.